RELATIVE PERMEABILITY OF SMART WATER FOR CARBONATE RESERVOIRS: EXPERIMENTAL AND MODELING INVESTIGATION

BY

BRAMASTO CINDE ADAM

A Thesis Presented to the
DEANSHIP OF GRADUATE STUDIES

KING FAHD UNIVERSITY OF PETROLEUM & MINERALS

DHAHRAN, SAUDI ARABIA

In Partial Fulfillment of the
Requirements for the Degree of

MASTER OF SCIENCE

In

PETROLEUM ENGINEERING

MAY 2016

KING FAHD UNIVERSITY OF PETROLEUM & MINERALS

DHAHRAN- 31261, SAUDI ARABIA

DEANSHIP OF GRADUATE STUDIES

This thesis, written by **BRAMASTO CINDE ADAM** under the direction his thesis advisor and approved by his thesis committee, has been presented and accepted by the Dean of Graduate Studies, in partial fulfillment of the requirements for the degree of **MASTER OF SCIENCE IN PETROLEUM ENGINEERING.**

Dr. Hasan Salman Al-Hashim
(Advisor)

Dr. Abdullah S. Sultan
Department Chairman

Dr. Hasan Y. Al-Yousef
(Member)

Dr. Salam A. Zummo
Dean of Graduate Studies

Dr. Mohamed A. Mahmoud
(Member)

30/5/16
Date

Love you as always,

My Dear Family & Cecilia.

ACKNOWLEDGMENTS

Alhamdulillah, all praises to Allah S.W.T., The Most Greatest and The Most Merciful for His guidance, blessing, and all energies He bestowed on me to finish my thesis.

I would like to thank King Fahd University of Petroleum and Minerals that gave me a chance to continue my Master degree. Also College of Petroleum and Geosciences, mainly Petroleum Engineering Department, which provided me facilities to gain experiences and useful knowledge.

I would like to express my deep gratitude to my thesis advisor, Dr. Hasan Salman Al-Hashim, for his guidance, encouragement, and patience which allowed me to experience many detail processes of thesis works as well as teaching experience during his class assistance and tons of knowledge during his course in my first semester.

I would like to express my very great appreciation to all of my committee members, Dr. Hasan Y. Al-Yousef and Dr. Mohamed Mahmoud, for their kindness, constructive suggestions and criticisms during the development of this thesis work. Without these, my thesis might way more far from perfection. Also Dr. Abdullah Sultan that helped and allowed me to settle many procedures just before Thesis Defense.

I wish to sincerely thank Dr. Aboulghasem Kazemi for his advices and assistances during valuable discussions about geochemical modelling. Also, I wish to thank Dr. Ungtae Kim and Mr. David L. Parkhurst for their advice in handling geochemical simulator.

I would like to sincerely thanks to all technicians that help me a lot during each process of my thesis work especially Mr. Abdulrahim Muhammadain, head of Petroleum laboratory,

that spared a lot of his time even beyond his working hour. Sincerely thanks to the other technicians; Mr. Mousa, Mr. Abu Samad, Mr. Tajudeen, Dr. Abdulrauf, Mr. Lui, Mr. Wasef, Mr. Darwin, Mr. Hassan, Mr. Rizwan, Mr. Zaid, Ali, Mr. Assad, Mr. Bader and Mr. Wahbi. My deep appreciation also extended to all academic and nonacademic member of the Department of Petroleum Engineering for their kindness and cooperation during my study.

I also would like to thank to all my friends, especially my brothers Amjed Hassan, Mohammad Hassan, Ahmad Abdulazeem, Anas Alsiddig Yousif, Fahim Djatmiko, Lutfi Mulyadi, Adi Kurniawan and Indonesian and KFUPM friends, that gave me supports and helped me during my thesis works.

I wish to thank my beloved mother, my deceased father, my family and Cecilia for their loves, their continuous supplications and encouragement throughout my study. They have become my strength during my struggles of this thesis.

Finally, My deepest gratitude to each and every person, who assisted me in many ways and made this thesis a reality.

TABLE OF CONTENTS

LIST OF TABLES

LIST OF FIGURES

LIST OF ABBREVIATIONS

BL : Buckley-Leverett Equation

EDL : Electrical-double-layer.

EOR : Enhanced Oil Recovery

IC : Ion Chromatograph

ICP : Inductively Coupled Plasma

IFT : Interfacial Tension

JBN : Johnson, Bossler, and Naumann Method

MIE : Multiple Ion Exchange

NMR : Nuclear Magnetic Resonance

PPM : Parts Per Million

TDS : Total Dissolved Solids

UTMN : Uthmania Crude Oil

XRD : X-Ray Diffraction

ABSTRACT

Full Name : BRAMASTO CINDE ADAM

Thesis Title : RELATIVE PERMEABILITY OF SMART WATER FOR CARBONATE RESERVOIRS: EXPERIMENTAL AND MODELING INVESTIGATION

Major Field : PETROLEUM

Date of Degree : May 2016

Petroleum Industries are putting numerous efforts to enhance the oil recovery in the middle of oil price instability. Smart water-flooding offers an opportunity to gain extra oil recovery that requires less costly operations. By means of modifying salinity or certain level of potential determining ions in the injection brine, it gives varying incremental oil recovery from nil up to 30% in the laboratory scale. This variation is attributed to lack of understanding the mechanisms behind Smart water-flooding, affecting the variation of results from both experimental interpretation and simulation models. This study takes a closer look at this contradictive issue by ensuring the successive injection of unsteady state core-flooding experiment to get reliable relative permeabilities data of Smart water flooding using Indiana limestone cores. Accordingly, 1-D Buckley-Leverett transport flow is coupled with IPhreeqc geochemical simulator. The importance of geochemical processes during Smart water flooding such as aqueous-mineral equilibrium (dissolution and precipitation) and surface adsorption model have shown during history matching of the designed smart water flooding experiments. These factors are most likely one of the mechanisms behind smart water flooding benefit in carbonate rock.

ملخص الرسالة

الاسم الكامل : براماستو سيندي آدم

عنوان الرسالة : حقن الماء الذكي في المكامن الكربونية.

التخصص : هندسة النفط

تاريخ الدرجة العلمية : مايو 2016

تبذل الصناعة النفطية جهودا كبيرة لتحسين انتاج النفط في ظل عدم استقرار أسعاره. حقن الماء الذكي يوفر فرصة للحصول على كمية إضافية من النفط بعمليات قليلة التكلفة. يمكن الحصول على نسب إضافية من النفط تتراوح بين الصفر إلى 30 % عن طريق تعديل الملوحة أو تغيير مدى محدد من الأيونات عند حقن الماء المالح في التجارب المعملية. هذه التغييرات في النسبة الإضافية المتحصل عليها مرتبطة بنقص فهم آليات عمل حقن الماء الذكي مما يؤثر على تفسير النتائج المعملية و نتائج نماذج المحاكاة. تهدف هذه الدراسة للنظر عن قرب لهذه الظاهرة المتناقضة عن طريق تأكيد فوائد تطبيق الحقن المتتابع غير المستقر لعينات صخرية اسطوانية من الحجر الجيري الكربوني. يهدف التصميم التجريبي للحصول على مجموعة بيانات للنفاذية النسبية للماء الذكي في الصخور الكربونية لاستخدامها في نموذج محاكاة لغمر هذه المكامن بالماء الذكي. بالإضافة إلى ذلك ، تأخذ الدراسة في اعتباراها أيضا أهمية تحليل عينات السوائل الناتجة من عملية الحقن لتتبع النموذج الجيوكيميائي. بناء على ذلك ، تم دمج نموذج بكلي-ليفرت للسريان الآحادي مع نموذج محاكاة إيفريك الجيوكيميائي. تم توضيح أهمية العمليات الجيولوجية أثناء عملية حقن الماء الذكي مثل التوازن بين الماء – المعدن (الإذابة – الترسب) ونموذج الامتصاص السطحي عن طريق عملية المطابقة التاريخية لتجارب عمليات الحقن الذكي التي تم تصميمها. هذه العوامل على الأرجح هي واحدة من الآليات المفيدة أثناء عمليات الحقن المائي الذكي في الصخور الكربونية.

CHAPTER 1

INTRODUCTION

Petroleum products remain an attractive commodity for mankind through years. In energy supply chain, the petroleum products especially crude oil still dominates total world energy consumption which is reflected by its high energy demand. This phenomenon pushes petroleum industries, including academic researchers, to sustain the world oil supply chain. Some advancements have been emerged to boost oil production into certain level of improvement by enhanced oil recovery (EOR) projects which utilize chemical, microbial, heat combustion and other cutting edge technologies. Unfortunately, conducting most of these EOR needs financial assessment in depth, since some of the projects are high cost and high risk, due to its immaturity in application. Instability in oil price also affects the EOR project to be very selective. Thus, researchers and petroleum industries carry out many means to enhanced oil production reliably. One of the emerging technologies to enhanced oil production is Smart water flooding which is also called low salinity water flooding or modified ion water flooding. Although this approach still immature in application but the benefits in terms of low expense in operational cost, availability of injection resource and recovery gain, give promising opportunity in EOR projects.

1.1 Smart Water Flooding

Smart water flooding recently became popular among researchers due to its benefit and simplicity. The general definition of this term varied among researchers, but, roughly meaning is enhanced oil recovery by means of water flooding injection with modification of its predetermined ions and level of its salinity.

Smart water injection has been experimentally found in improving waterflood performance by up to 38% [49]. In 1990s, Yildiz and Morrow [51] reported brine composition's effect on oil recovery, which identified a possibility to improve waterflood with optimized injection brine composition. Numerous laboratory experiments [33, 36] have confirmed that EOR can be obtained in tertiary Smart water flooding in this case low salinity brine. The salinity in these tests was in the range of 1000-2000 ppm. On the other hand, only limited numbers of field that apply this approach, even though it gives benefits in operational cost and promising oil recovery. This is because the mechanism behind low salinity, is not yet solid. There are many uncertainties that come from the formation rocks, crude oil properties, and also brines (injection and formation brine) that affect the unique result of its application.

These days, the uncertainties in coreflooding experiments are extensively reviewed with different points of view among researchers, which imply in different treatments and benefits. These different thoughts are important as lessons learned to understand the underlying mechanisms that is still immature. Comprehensive understanding will lead to strong theoretical background of the observed mechanisms.

As a new challenge, this study has aimed to carefully design representative coreflooding experiments to investigate the underlying mechanisms of smart water flooding of limestone carbonate rock where most of the experiments and simulations highlight in sandstone formation. The design of experimental coreflooding is based on current discussions, contradictions and approaches in proposed mechanisms of smart water flooding. Eventually with regard to simulation model, a fact of lacking relative permeability data for history matching Smart water / low salinity flooding become one of the concern here.

1.2 Objectives

The main objective of this study is to achieve more confidence in the results of core flooding experiment of Smart water flooding specifically in carbonate reservoir rock. In addition, simulation model is built based on the revealed profiles which lead to its mechanisms. The following are the specific objectives:

1. Investigate the advantages and demerits of the current approaches in experimental and modelling investigation of smart water flooding.
2. Perform unsteady state core flooding experiments with some specific criteria and measurements to emphasize Smart water flooding mechanism, based on the discussions and contradictions of current approaches specifically in carbonate reservoir rock.
3. Obtain reliable relative permeability of Smart water brines data from designed unsteady state core flooding tests that can be used as constraint of transport flow simulation.

4. Build a simulation model that can generate relative permeability of Smart water based on predetermined parameters from the core flooding experiment. This simulation model is based on coupling of transport flow and geochemical model to represent Smart water behavior. In addition, the simulation model is expected to have capability or flexibility to model relative permeability for any modifications of Smart water flooding.

CHAPTER 2

LITERATURE REVIEW

Smart water flooding have been investigated in several studies thoroughly by researchers. In general there are two major parts to be highlighted: coreflooding experiments and simulation models. In core flooding experiments, although the procedure vary from one researcher to others, they share common objective to find predetermined parameters. It's usually done by isolating one parameter from other parameters that might affect smart water flooding. The parameters might be the reservoir rock properties (S_{wi}, porosity, permeability, surface area, clay content), crude oil properties (composition, acid-basse number), brines (salinity and ionic composition of formation brine and injection brine), and environment/condition (injection rate, injection pressure and temperature). In summary, experimental works yield some plausible mechanisms during Smart water flooding. First section in this chapter talks about these proposed mechanisms.

Meanwhile in the simulation model section; an increase of interest by researchers to model these mechanisms are shown in this last decade. Researchers attempt to formulate mathematical models to represent the mechanisms starting from general phenomenon into detail variables of history matching such as ionic profiles and pH of the effluent. Furthermore, most recent approaches, utilize geochemical model to formulate these complex reactions during Smart water injection. This section also provides those attempts in simulation models and highlight the merit and demerit of the applications.

Last section will focus on critical review of current approaches both in experimental and simulation works. It is important to pay attention to the objectives, basic definition, and methodologies of these works. Some technical laboratory procedures need to be defined to ensure that the incremental oil recovery is specific due to Smart water flooding benefit; and whether the assumptions to build the relative permeability model are sufficient enough in practices.

2.1 Smart Water flooding Mechanisms

Researchers attempt to establish proposed Smart water flooding mechanisms from several points of view. The proposed mechanisms apply for any rock Formation but most of them address in sandstone reservoir rock and few for carbonate. Summary of proposed mechanism based on experimental core flooding of Smart water flooding are highlighted below.

2.1.1 Interfacial Tension (IFT) Reduction

During injection of Smart water brine, the effluent pH has tendency to increase. This increase is attributed to carbonic acid buffering process which lead the system becoming less acidic by forming weakly dissociating acid such as carbonic acid. The pH rises are claimed as high enough to saponicate certain components of the oil. As a result, similar to alkaline flooding, smart water flooding is able to lower interfacial tension between water and oil. Another contribution of IFT reduction is due to in-situ surfactant generation of high acid number of crude oil that encounter alkaline type injection. Accordingly, these will result in increased capillary numbers and correspondingly, low residual oil saturations.

This concept is proposed by Buckley [8]. Similarly, proposed idea by Aladasani [1] also showed that appreciable decrease in interfacial tension (IFT) occurs at the breakthrough recovery.

On the other hand, Morrow and Zang [36] stated that not all experiments showed an increase in pH and even if it increases, the value is not as high as criteria of alkaline flooding; pH of 11 – 13. Typical pH profiles of low salinity flooding may increase up to 9 – 10. Moreover, Cissokho [11] showed that increase in pH and pressure drop do not correspond with incremental oil production in their experiment. They found that during stepwise low salinity brine injection, although the pH showed increasing trend during core flooding but the incremental oil recovery behaved different way as shown in figure 2.1.

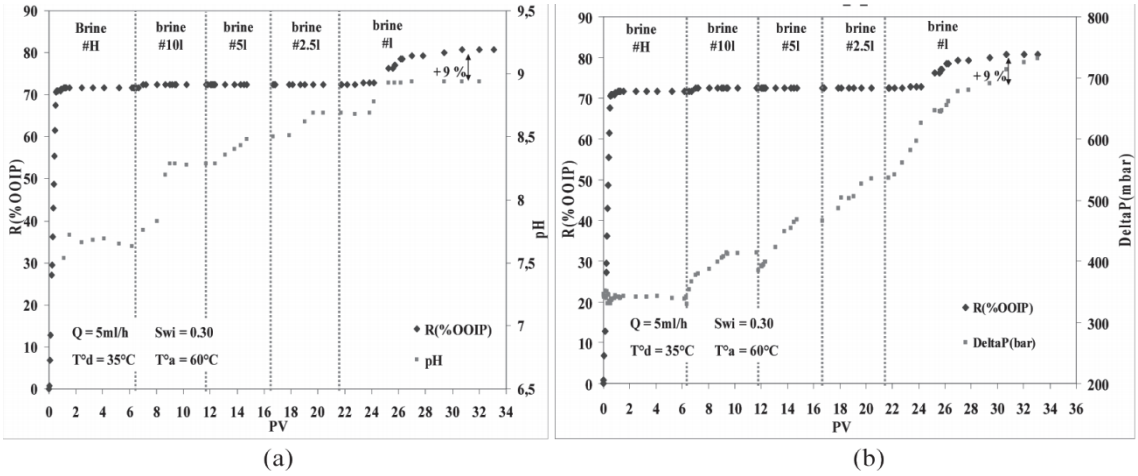

Figure 2.1 Oil Recovery, pH and Pressure drop evolution during tertiary recovery experiment with successive dilution (after Chissoko [11])

Yousef et al. [52] performed composite carbonate core flooding which resulted in insignificant IFT reduction (40 – 32 dyne/cm). Generally, the candidate of in-situ surfactant generation is having high acid number value. Crude oil which has acid number

value higher than 0.5 mg KOH/g indicates that enough hydrocarbon acid is contained in the crude oil; which did not happened in all experimental cases of Smart water flooding. Figure 2.2 shows the typical reduction of IFT in surfactant against Smart water flooding. As can be seen in the following figure, the magnitude of IFT reduction in Smart water brine (diluted brine) is not as high as surfactant which implies that IFT reduction is not main contributor to Smart water flooding mechanism.

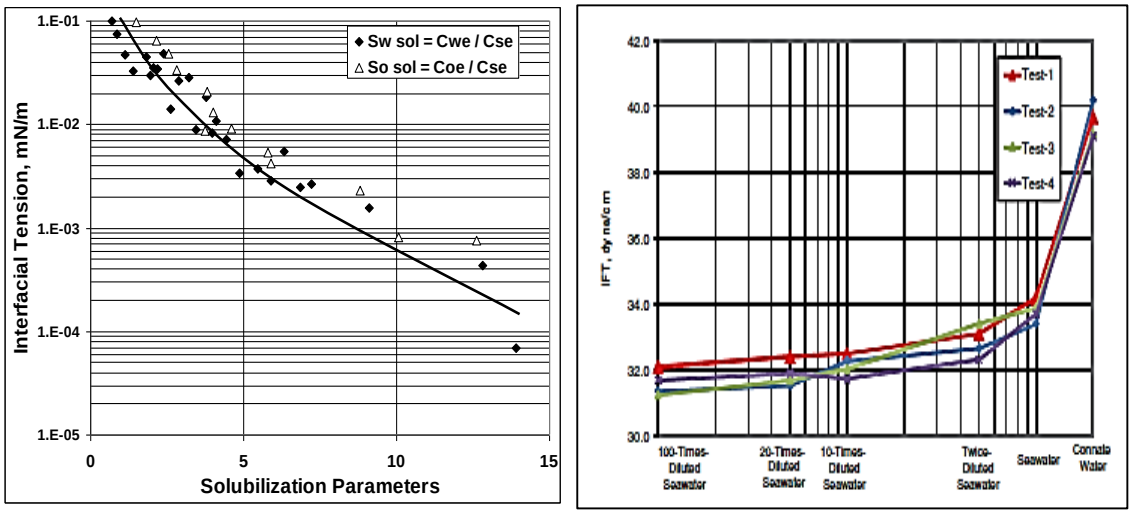

Figure 2.2 Typical IFT reduction in surfactant (left, after Gomaa [19]) and Insignificant IFT reduction in low salinity flooding in composite carbonate rock (right, after Yousef 2010 [52])

Al Attar et al. [2] also performed IFT measurements of carbonate reef limestone core flooding from Bu-Hasa field in Middle East area. They found that there was not a direct relation of the IFT with low salinity brines since an absence of trend between each parameter to IFT such as concentration and type of injection water.

2.1.2 Permeability Change

When low salinity brine is injected, the electric double layer of clay or fine particles might expands. The expansions make these fines partially removed from the rock surface leaving a water-wet area in the rock surface. These fines might divert the path of injected water by blocking certain pore throats. This concept is reported by Tang and Morrow [45]. They showed a decrease in permeability during core flooding experiments but did not observe severe clay mobilization also stated that for both monovalent and multivalent low salinity brine injection, oil recovery still can increase. Figure 2.3 shows a schematic overview of the clay mobilization concept. As mixed-wet fines both interact with the oil and water, they tend to group at the oil-water interface acting as interface stabilizing surfactant. After high salinity water flooding, some oil attached to mixed-wet fines will remain in reservoir. Whereas, during low salinity water injection, the electrical double layer of the particles is expanded. As a result, there are partial mobilization of mixed-wet fines of previous immobile oil will be achieved during low salinity water flooding condition. The incremental oil production are elaborated as follow:

• Direct mobilization of otherwise immobile oil due to mobilization of the clay particles to which the oil is attached. As a result, the residual oil saturation decreases.

• Indirect mobilization of oil due to blocking of prolific flow paths. This leads to flow through less permeable zones enhancing the sweep efficiency.

• Clay particles acting as surfactant on oil-water interfaces. This results in stabilized oil-water interfaces enhancing the displacement.

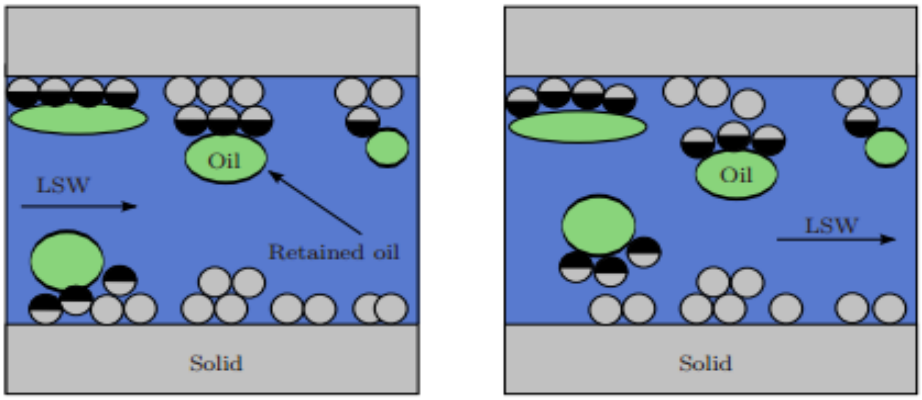

Figure 2.3 Illustration of Clay/fines migration during Smart water flooding in mixed wet rock (after Tang and Morrow 1999 [45] and De Bruin [13])

On the other hand, BP claimed not to see any fines migration in their works (Lager et al. [30]). Pu et al. [41] also noted even without significant clay content there was additional oil recovery. While Nasralla et al. [38] noted that samples with high incremental recovery did not show fines production.

2.1.3 Wettability Alteration

Another proposed mechanism during Smart water flooding is wettability alteration which commonly seen in experimental work. It will change wettability of the reservoir in which originally oil-wet to water-wet condition; thus improving oil recovery during water flooding. Some theories that trigger wettability alteration have been proposed to reveal mechanisms behind this wettability change. There are double layer expansion, multi ionic exchange, pH induced oil desorption and dissolution/precipitation.

2.1.3.1 Double Layer Expansion

At the interface between a charged surface and a solution, a potential will develop. This potential difference builds up out of two distinct layers, with their respective properties. Because of these two layers, it is called the electrical double layer (EDL). A schematic overview of the EDL is shown in Figure 2.4. The two layers within the EDL are:

(a) Stern layer: a compact layer close to the charged surface with a thickness of about 1 nm. Ions in this layer are fixed. The major part of the potential drop will occur over this layer [20].

(b) Diffuse layer: a layer with varying thickness between 1-500 nm, depending on the extent of double layer expansion. Ions of opposite sign with respect to the charged surface are attracted as a result of electrostatic forces [48].

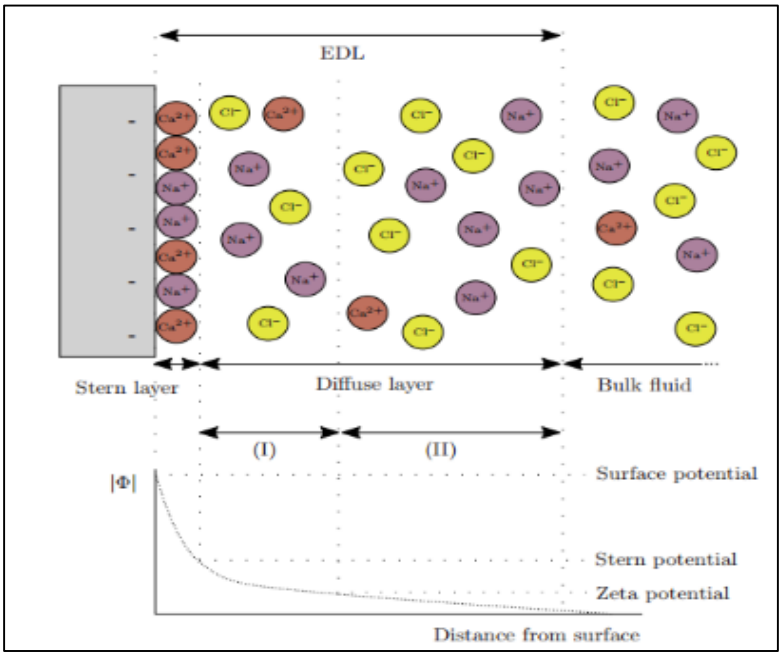

Figure 2.4 Potential layers in Rock-fluid interaction (After De Bruin [13])

The diffuse layer is split into two separate regions by the Zeta potential. The equipotential plane formed by the Zeta potential is also called the slipping plane as it defines the region of ions that can move (slip) along the region with more tightly fixed ions:

(I) Region Stern Potential-Zeta Potential: In this region the ions will not be affected by tangential stress, such as water flowing past the solid's surface (e.g., clay). The ions are tightly bound to the solid's surface in the double layer.

(II) Region Zeta Potential-Bulk Fluid: In this region of the diffuse layer the ions can move under influence of tangential stress. That is, the force that keeps the ions in place can be overcome by water flowing past the solid's surface.

In general, it holds that ions further away from the charged surface easier to displace than ions close to the charged surface. The potential drop over the diffuse layer is more gradual compared to the potential drop in the Stern layer. The thickness of the EDL is dependent of the ionic strength of the solution.

When low salinity water flooding is taking place, the electrolyte concentration of the bulk water solution diminishes, which effectively leads to an expansion of the EDL. Especially the diffuse layer will behave in this fashion. However, for an increase in electrolyte concentration the EDL thickness will be significantly compressed. Nasralla et al. [38] and Ligthelm et al. [32] agree to this concept that expansion of the double layer is most likely the main mechanism of low salinity water flooding, which is followed by oil desorption from the clay surfaces.

On the other hand, Austad et al. [6,7] from University of Stavanger, suggested that double layer expansion was not the main mechanism, but the mechanism was triggered by pH

Induced Desorption of Organic Material. Nasralla et al. [37] also stated that double layer expansion considered as contributor rather than low salinity waterflooding's mechanism.

2.1.3.2 Multi Ion Exchange (MIE)

Lager et al. [30] stated that during low salinity waterflooding some conditions were required to be present such as the presence of clays, preferably kaolinite, connate water contained some concentration of Ca^{2+} ions, as well as crude oil that contained polar compounds. These conditions will trigger multi ionic exchange such that free multi-charged cations replace the double layer cations that form complexes with organic functional groups at the clay surfaces. The rock condition became more water-wet and also result in oil components mobilization. In addition, the effect of pH has to be included as ion exchange by H^+ ions besides the effect of other cations, principally Na^+, K^+, Ca^{2+} and Mg^{2+}.

Figure 2.5 illustrates the basic idea behind the ion exchange mechanism. During high salinity flooding, with formation brine or seawater, charged oil particles will mostly remain attached to the cation exchanger sites. During injection of low salinity water in a reservoir containing calcite, the amount of Ca^{2+} attached to the cation exchanger sites will increase. As a result of this process, positively charged oil particles and organometallic complexes from the exchanger will detach.

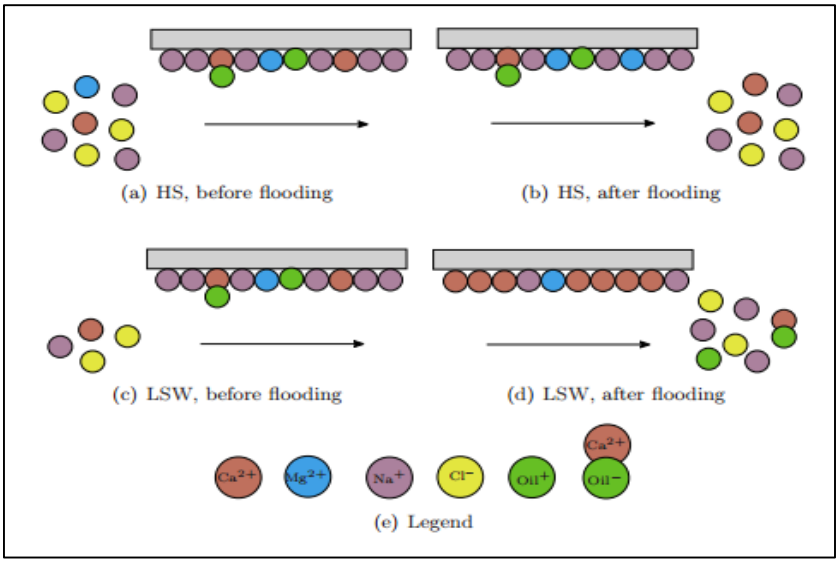

Figure 2.5 Scheme of Multiple ion Exchange during Low salinity flooding (after De Bruin [13])

Ligthelm et al. [32], Lee et al. [31], and Nasralla et al. [38] also support the idea that wettability condition toward water wet was due to Ca^{2+} ions were substituting bound charged organic components of the oil in which triggered by Cation exchange capacity (CEC) of the clay complex and double layer expansion.

On the other hand, Tang [45] and Austad [7] reported that low salinity brines without Ca^{2+} and Mg^{2+} ions have been seen to increase recovery. In addition, many experiments showed that the presence of clay minerals especially kaolinite might improve oil recovery by improving the effectiveness of wettability alteration. But contradictive issue regarding to clay presence are also presented by Cissokho et al. [11] and Pu et al. [41], namely, even without the significant clay content or kaolinite, Smart water flooding still gives incremental oil recovery.

2.1.3.3 Mineral Dissolution

During Low salinity flooding, Pu et al. [41] showed that wettability shifting towards more water wet was due to dissolution of anhydrite which in turn causes more acidic water condition by an additional sulphate ion content. This process also suspected in conjunction with Multicomponent Ion Exchange (MIE).

Yousef et al. [52] showed that during stepwise dilution in carbonate core flooding, there was a shift in the NMR result before and after core flooding test. Some tests are taken and there is a diffusion coupling in the pore network which initially didn't exist in NMR result, which is an indication of rock dissolution. Furthermore, contact angle measurement was conducted to assure the wetting condition in which the result showed that wettability alteration happened after the core flooding.

Figure 2.6 shows the result of NMR before and after the core flooding tests. As can be seen, there are connections within pore networks in all experiment tests.

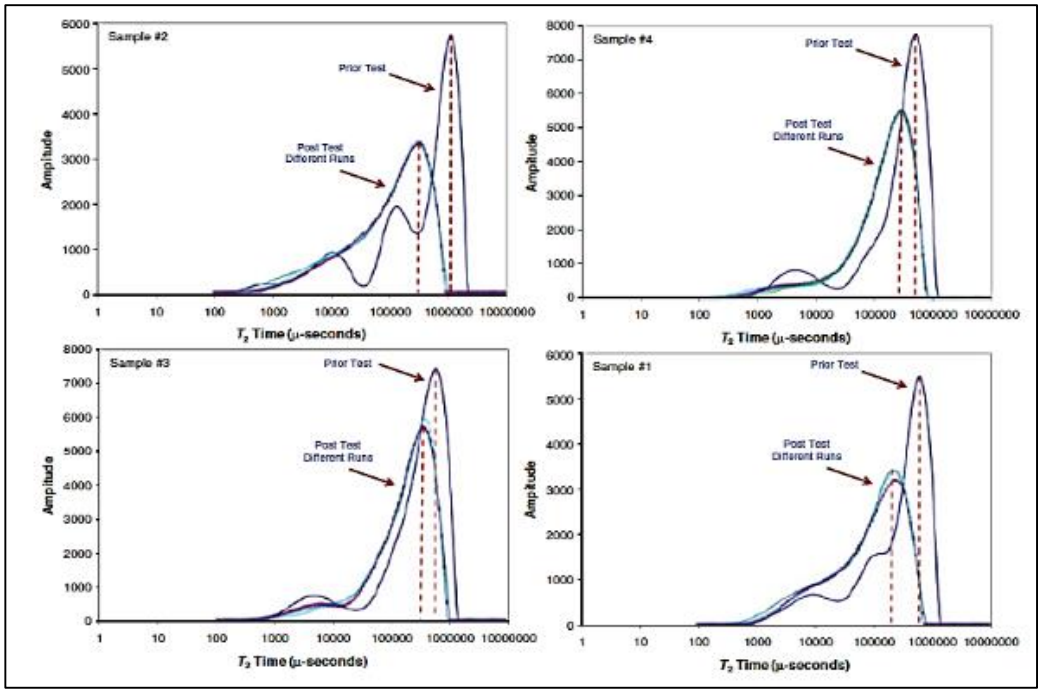

Figure 2.6 NMR results of Smart water flooding in carbonate cores (after Yousef et al. [52])

2.1.3.4 pH induced Desorption of Organic Material

Austad et al. [7] suggested the mechanism behind wettability alteration that have similar condition such in MIE. These required condition such as polar compounds in the crude oil, presence of clays with high CEC and certain Ca^{2+} ion concentration in the Formation brine. In this mechanism, there is a local increase in pH of the clay surfaces, because the Ca^{2+} ions adsorbed on to the clay are substituted by H^{+}. Local increase in pH was followed by desorption of oil/organic components since adsorption of these components were very pH sensitive. Finally it enhanced rock wettability towards more water-wet.

Since pH plays an important role in this mechanism, it required to benchmark reservoir condition pH environment in every laboratory experiments.

On the other hand, Cissokho et al. [11] considered pH to be an effect of low salinity incremental recovery rather than the cause. They also showed that increase in pH and pressure drop is not always in conjunction with incremental oil production. Similar to the explanation of IFT reduction in section 2.1.1.

2.2 Simulation Models

Modelling Smart water flooding have attracted many researchers these recent years. Figure 2.7 shows the milestone of modelling Smart water flooding from many institutions in the world. At the early stage, some researchers such as Aladasani et al. [1], Yousef et al. [52], and Al Shalabi et al. [4], attempted to model smart water flooding by modifying Corey's relative permeabilities to account for wettability alteration. Although the model was able to match some coreflooding experiments, it did not answer the mechanism behind wettability alteration. Then, Wu et al. [50], Omekeh et al. [39], and other researchers introduced more robust model that consider the importance of ions behavior such as MIE and mineral-aqueous equilibrium. Furthermore, these recent years numerous smart water models are incorporated with geochemical model as introduced by De Bruin [13] and Korrani et al. [29] This geochemical coupling model are also applied in other EOR model such as CO2 flooding and Alkaline Surfactant flooding (ASP) flooding. Group of researchers and their modelling work of smart water model are presented in the following section.

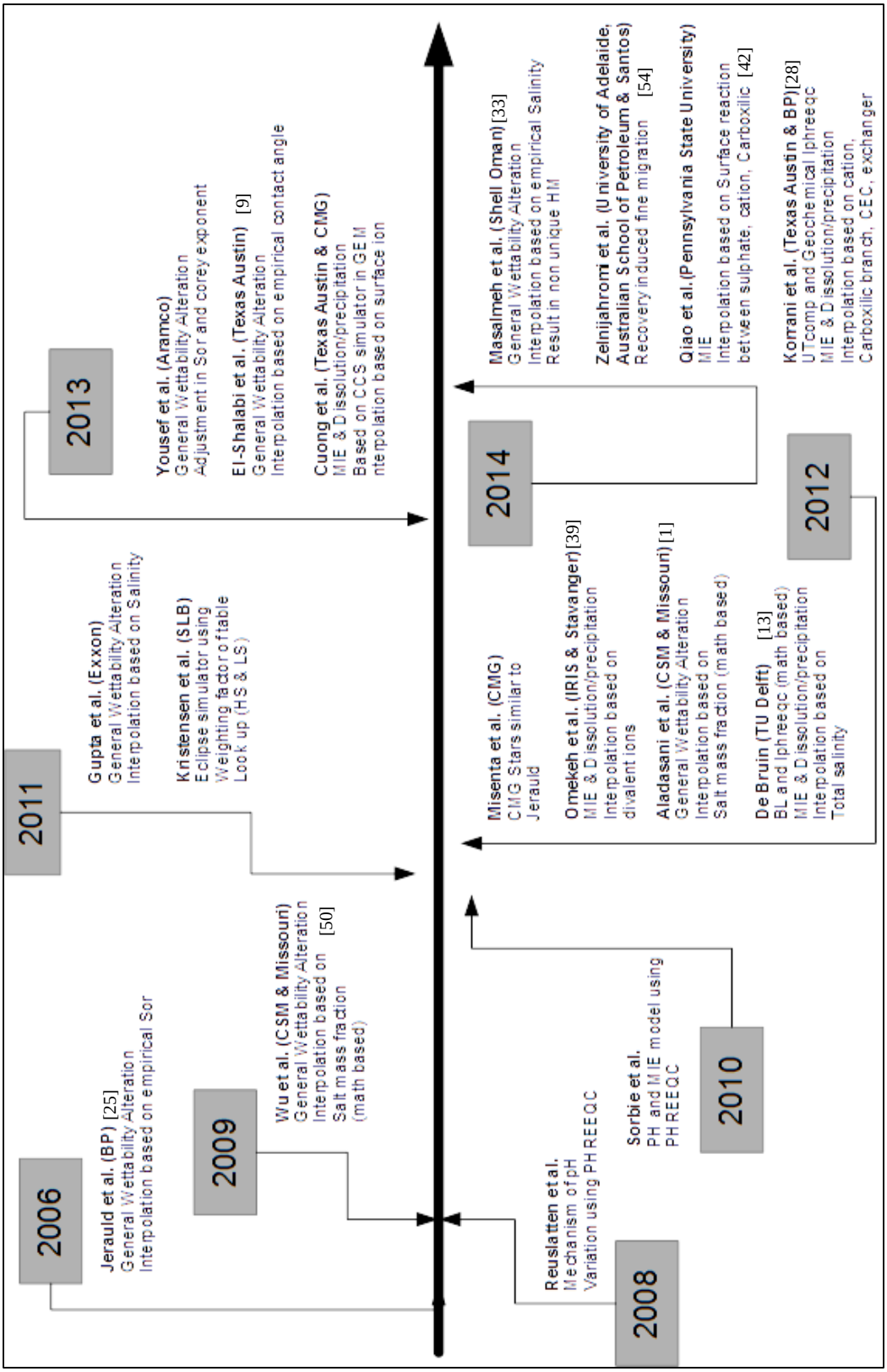

Figure 2.7 Milestone of modelling Smart water/ Low salinity flooding

2.2.1 Recovery Induced by Fines Migration Model

Zeinijahromi et al. [54] attempted to model Smart water flooding based on induced fines migration case. The main idea was displacing of oil by slug of low salinity water with high salinity drive from two layers cake reservoir with contrast permeability (Figure 2.8). The displacement occurred first from the high permeable layer with its plugging by released fines with the following displacement from low permeable layer by water drive. In this case, no formation damage is induced in low permeable homogenous layer, avoiding the oil production decrease due to induced permeability damage in the low permeable layer. They also showed the competitive effects of fines migration on sweep enhancement and on oil production deceleration.

Some assumptions behind the model are the detached fines are inert, i.e. they are intact and keep their integrity during detachment; the effects of clay swelling are assumed to be negligible; for simplicity, the volumetric concentrations of attached and retained particles are negligibly small comparing to the porous space, i.e., the retention of fine particles does not affect the porosity; it is assumed that the initial salt concentration is the critical salt concentration for the reservoir fines which is the reservoir lines start leaving the rock surface with the decrease of salt concentration; the dissipation effects of diffusion and capillary pressure are negligibly smaller than those of fines straining. Alteration of water salinity affects the attached concentration stronger than the velocity alteration: therefore, the velocity dependency of the maximum concentration of attached tines is neglected. The permeability damage by lines straining is significantly higher than that by attachment. Other assumptions include constant temperature, incompressibility of water and oil, constant water and oil viscosities.

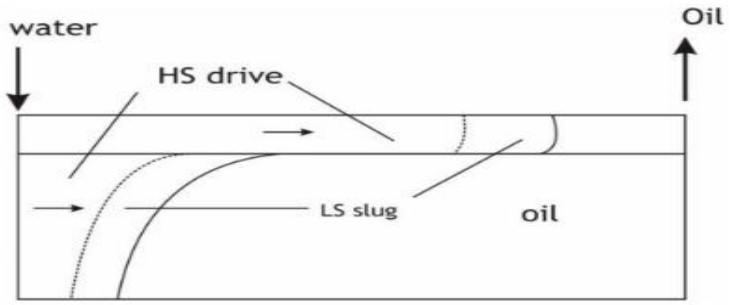

Figure 2.8 Illustration of two cake reservoir in Recovery Induced by Fines Migration Model (after Zelnijahromi [54])

Furthermore, this model will enhance the fractional flow curve similar to polymer flooding as depict in figure 2.9.

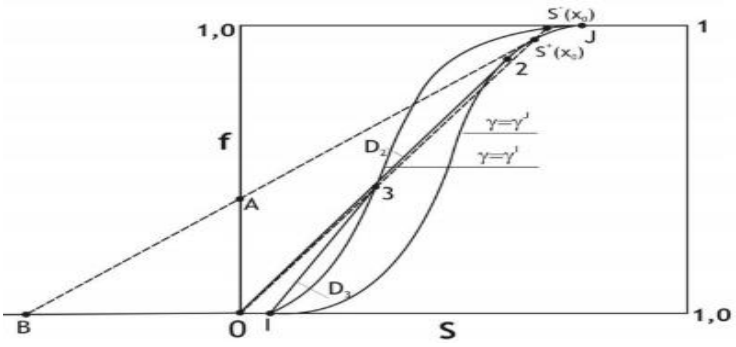

Figure 2.9 Fractional flow curve in Recovery Induced by Fines Migration Model (after Zelnijahromi [54])

2.2.2 General Wettability Alteration Models

In these models the researchers attempted to model smart water brine by adjusting certain parameters during history matching as a result of wettability alteration. Some of them including simulation model of Al- Shalabi et al. [4], Wu et al. [50], Masalmeh et al. [33], Jerauld et al. [25] and Al Sofi et al. [5].

In 2013 Al Sofi et al. [5] modeled their previous coreflooding work in composite carbonate core. They attempted to match oil production and pressure drop during the experiments using S_{or} and Corey exponent modification. For adjusting Corey exponent, they introduced oil exponent modifier which is basically parameter to shift the relative permeability. Some hypothesizes are made arguing the S_{or} value obtained in experiment was not absolute S_{or}. Thus the S_{or} obtained from experimental was stated as practical S_{or}. Moreover, some hypothetic 3D simulations was conducted using Eclipse and UTChem that resulting similar recovery although S_{or} was different. In other words, the work showed non uniqueness in history matching. Finally, they attributed the wettability alteration showed in experimental result as an increase in oil flow capacity (k_{ro}/k_{rw}).

Similarly, Al Shalabi et al. [4] investigated the core flooding experiment of Yousef et al. [52] in composite carbonate rock. They assessed the contribution of S_{or} and relative permeability which comprised of relative permeability end point and Corey exponents parameter using UTChem simulator. They assumed in ignoring dependence of S_{or} on capillary number option for simplicity. The results showed that S_{or} was not main contributor through history matching, and tuning Corey exponent and end point relative permeability showed good matched in oil production but poor matched in pressure drop profiles. Later work by Al Shalabi was modifying mathematical model of flow equation with molecular diffusion. Then relative permeability model that represent low salinity flooding was calculated using linear interpolation between set of parameters in high salinity and low salinity. These set of parameters were based on empirical contact angle in which salinity dependent. Figure 2.10 below shows the pressure drop matching of the third test of composite carbonate core flooding in Yousef et al. [52] experiment.

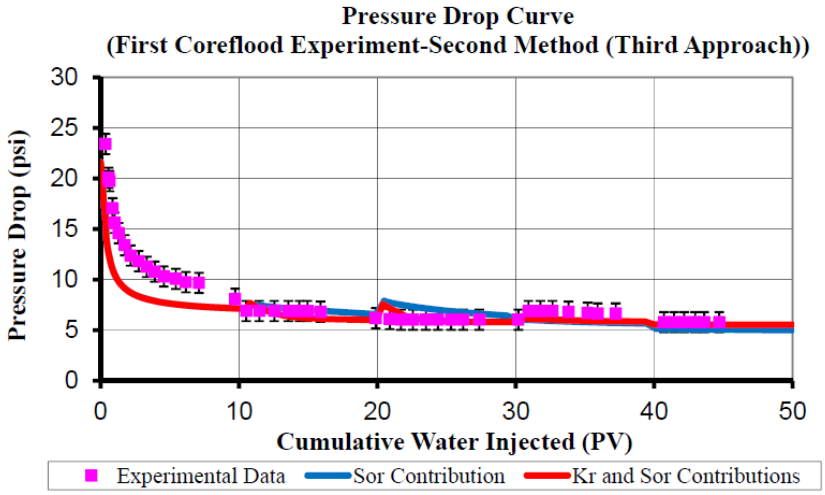

Figure 2.10 History matching of core flooding data using adjustable parameters, (after Al Shalabi et al. [4])

Jerauld [25] described the adaptations made to BP's in-house version of the VIP simulator to model low salinity water flooding. Salt or total dissolved solid was modelled as a single component in the aqueous phase which can be injected, initialized and tracked. Aqueous phase properties such as density and viscosity were salinity dependent. Also residual oil saturation, capillary pressure and relative permeability were between upper and lower salinity thresholds as salinity function. This threshold was approximated from common experimental results as depict in figure 2.11. High and low salinity relative permeability and capillary pressure curves were the inputs, above which high salinity curves were used, below which the low salinity curves were used and interpolation took place in between. Others features of Jerauld et al. [25] work were hysteresis between imbibition and secondary drainage, dispersion model using numerical dispersion.

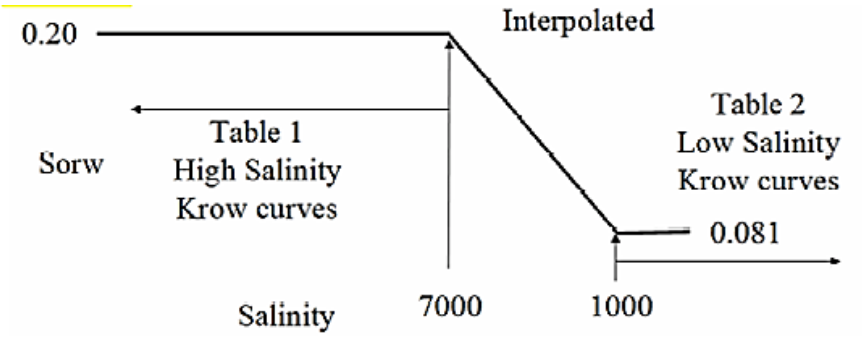

Figure 2.11 Schematic of linear interpolation used in Low salinity model (after Jerauld et al. [25])

Furthermore Masalmeh et al. [33], Wu et al. [50] and Aladasani et al. [1] also performed the similar approach like Jerauld et al.[25] by utilizing direct linear interpolation of relative permeability between high and low salinity sets, either based on empirical salinity value, salt mass fraction or other direct parameter).

2.2.3 Detail Wettability Alteration Models

These models attempt to mimic the detail mechanism behind wettability alteration including MIE and dissolution/precipitation. Many approaches have been conducted extensively by modifying certain simulator, coupling with geochemical simulator, build mathematical based model etc. Some of the researchers are Omekeh et al. [39], Qiao et al. [42], Dang et al. [12], Korrani et al. [28,29] and De Bruin [13].

Omekeh et al. [39] built mathematical model of low salinity flooding based on multi component ion exchange in sandstone Formation. They modeled transport flow equation considering oil phase, water phase and some ions equilibrium. The model was formulated such that the total release of divalent cations from the rock surface give rise to a change of the relative permeability such that more oil is mobilized. The combined effect of MIE and

dissolution/precipitation was modelled to determine how this will affect pH and the total release of divalent cations. Low salinity flooding was represented by relative permeability changes as a function of desorption of divalent ions (Ca^{2+} and Mg^{2+}). Furthermore, during the work they used synthetic high and low salinity relative permeability curve as the range limit of relative permeability model. The results were able to show ion profiles and oil production for history matching. Figure 2.12 shows the results of pH and ion concentrations in the model.

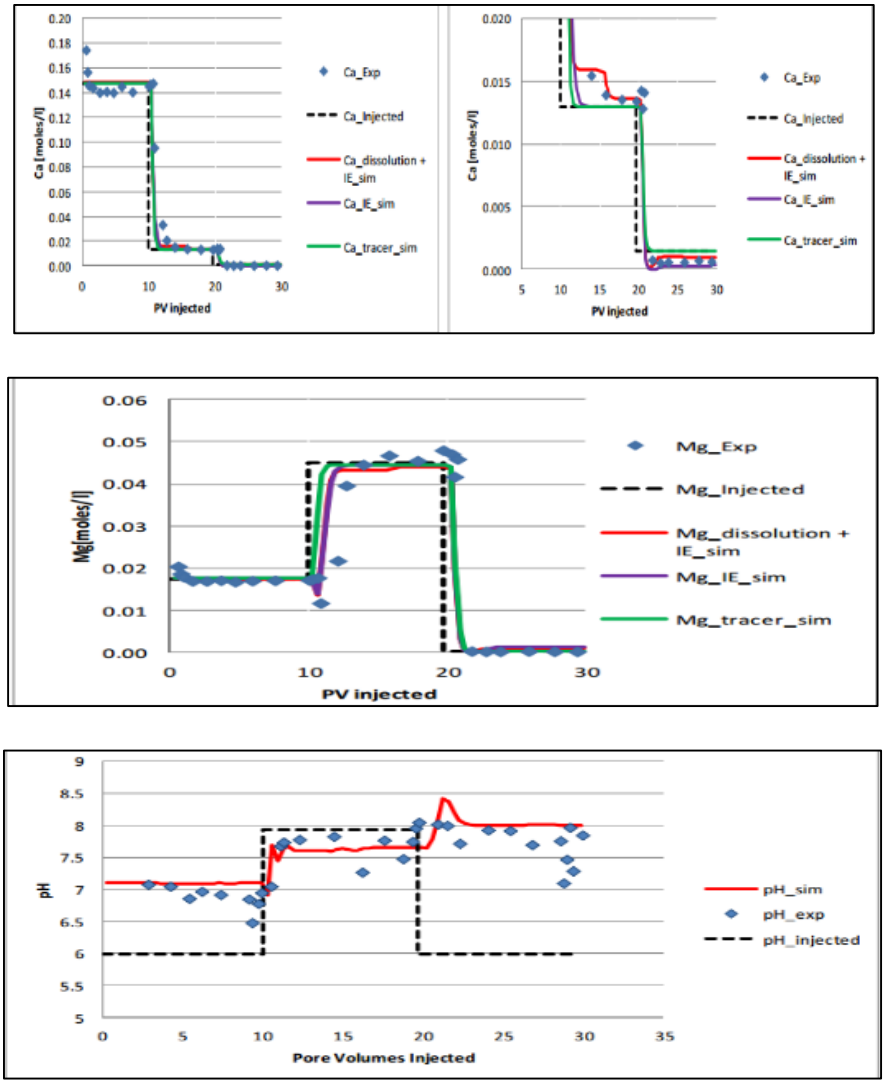

Figure 2.12 Concentration of Divalent ions and pH profiles (after Omekeh et al. [39])

Korrani et al. [28, 29] introduced the advancement in modelling low salinity through coupling of UTChem with IPhreeqc, geochemical simulator module. Simulation model started with initialization of total hydrocarbon and pressure, then, speciation of geochemical components was run in IPhreeqc. The results of geochemical reaction were transferred to UTChem to find saturation and relative permeability. In addition, transport flow equation assumed to be one aqueous/ geochemical entity. They believed that in multi-phase reactive transport modelling, hydrocarbon does not have to exist as additional phase but as a geochemical entity. The character of hydrocarbon was represented as acid/ basic component in aqueous phase. Simulation model covered geochemical reactions such as cation exchange, reaction term for aqueous and minerals etc. Relative permeability was modeled with weighting function of ionic strength that considers saturation index of clay mineral and CEC. The results were able to show ionic, pH and production profiles of the model. Keeping the same concept, the interpolating parameter is defined as follows:

$$\theta = \frac{\zeta_{\max} - \zeta(x,t)}{\zeta_{\max} - \zeta_{\min}} \qquad (2.1)$$

Where, $\zeta_{\max}$ is the fraction of organometallic complexes on the exchanger above which no wettability alteration would occur and $\zeta_{\min}$ is the value at which maximum wettability alteration would occur is given in

$$\zeta = \frac{(Fe\,A_w\,X + Mg\,A_w\,X + Ca\,A_w\,X + ...)}{CEC} = \frac{\sum_i I_i\,A_w\,X}{CEC} \qquad (2.2)$$

Where, Aw, X, and I, are representative of the carboxylic branch, exchanger, and divalent cations, respectively and CEC is the cation exchange capacitance of the exchanger. Figures 2.13 to 2.14 show the validation results and the coupling workflow.

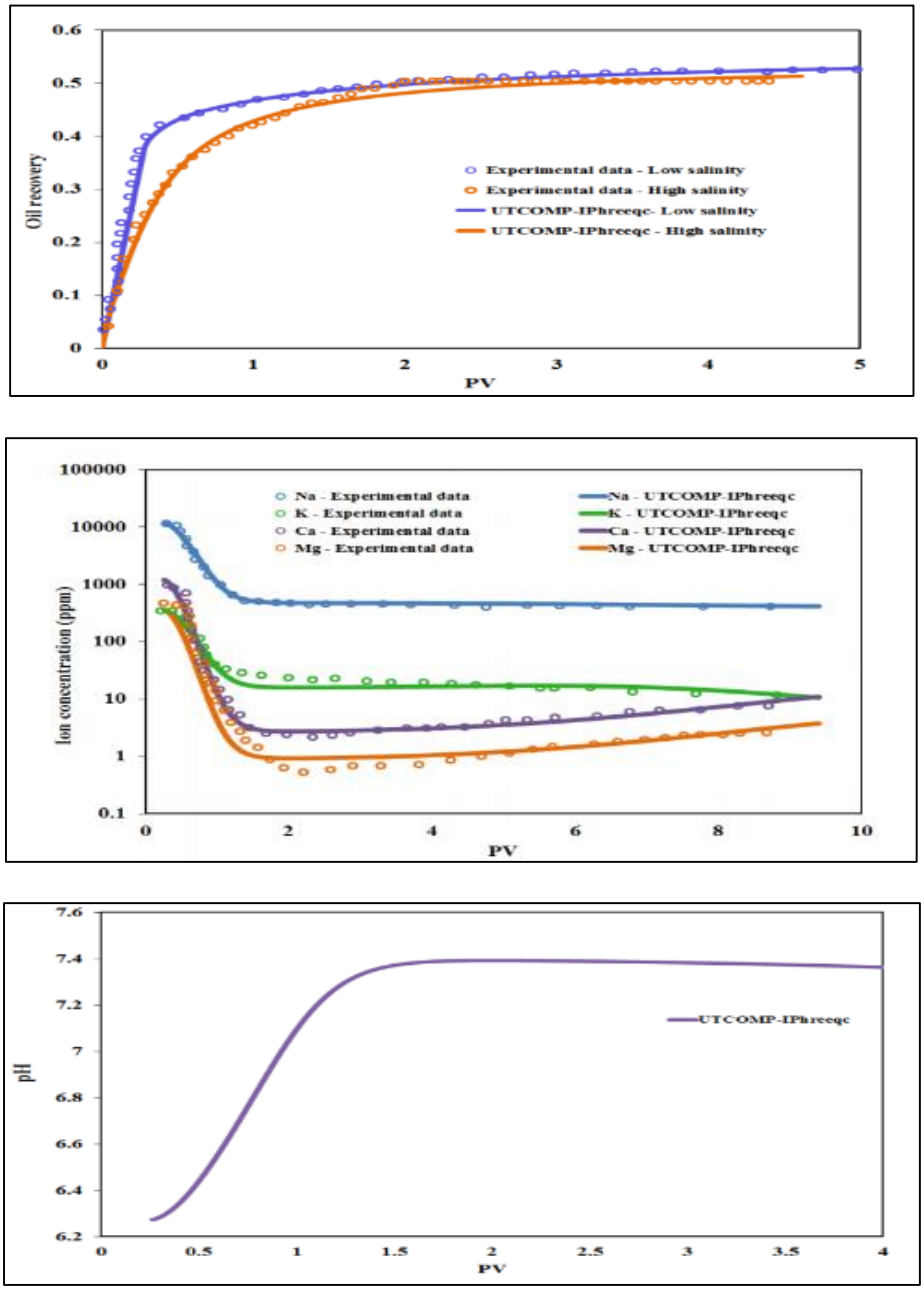

Figure 2.13 Results in Validation of Coupling Model (after Korrani et al. [28,29])

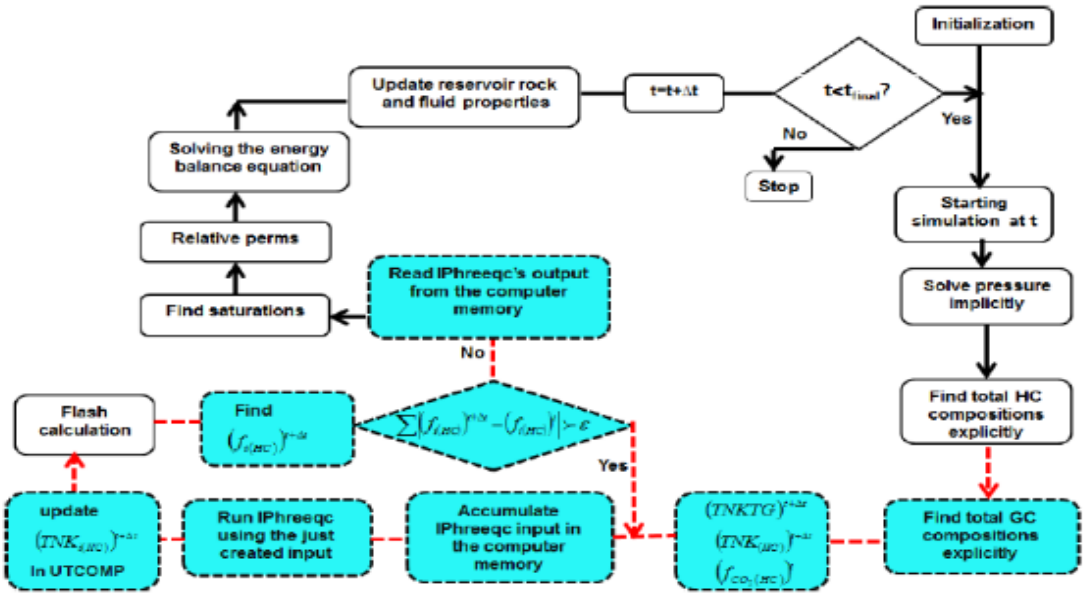

Figure 2.14 Flow chart of reservoir and geochemical coupled simulation (after Korani et al. [28,29])

De Bruin [13] emphasized the critical issue where simulations model for low salinity water flooding often do not include geochemical processes. Salt was modelled as aqueous tracer that does not react with the formation. The objective of his work was to improve the importance of geochemical processes on the mixing of formation brine and injection water, during low salinity water flooding. The geochemical processes taken into consideration were CO2-buffering, mineral dissolution and ionic exchange. The change in relative permeability can be implemented in the Buckley Leverett transport equation. By modelling the relative permeability as both a function of the water saturation and the salinity, the solution of the Buckley Leverett equation becomes more complex. The standard way of switching between relative permeability curves of high and low salinity is to define a salinity threshold. This approach was also adopted in his work. The salinity of a grid cell is calculated every time step by

$$\text{Salinity (ppm)} = 1000 \cdot X\gamma\, C\gamma\, M(\gamma) \qquad (2.3)$$

Where $\gamma \in \{Na+,Ca2+,Mg2+,...\}$, $C\gamma$ is the concentration in mol/L and $M(\gamma)$ is the molar mass in g/mol of ion type γ. Upon injecting LSW into the Formation the ion concentration will decrease, and consequently the salinity will decrease. The threshold model used in the simulator can be fully described by:

Relperm model = Low salinity if salinity < salinity threshold, and otherwise Relperm model = High salinity.

De Bruin [13] calculated the divalent concentration based on three mode option. First is Ion transport only where PHREEQC will not be part of the simulation. This means that no cation exchange or calcite dissolution is included in the simulation. Second mode of operation includes equilibrium chemistry. This will include cation exchange and calcite. Last mode is reaction kinetics where in each grid cell the amount of calcite can fully dissolve based on dissolution rate data. The advantage of this mode is that it incorporates the most detailed model.

If the first mode of operation is used, no communication with PHREEQC is performed and the results of the ion transport simulation will be saved directly after the Buckley-Leverett transport. For the other two modes, PHREEQC data files will be generated based on the Buckley-Leverett transport results, and send to the PHREEQC simulator via a COM module. The results of the geochemical simulation performed will be saved. The level of detail in the information that will be saved depends on the mode of operation. When all data for the specific mode of operation are saved, the process is repeated for the next grid cell / time step.

2.3 Critical Review of Smart Water Flooding

Previous laboratory works show different conclusions regarding the mechanism of Smart water flooding. Most of the concluded mechanisms encounter contradiction. These discrepancies might be addressed to the objectives and technical issue in performing core flooding experiment such as the type of cores, length of cores, homogeneity of cores, usage of injection rate, operating pressure and temperature, etc. Thus, careful look at the measurement and isolation of unnecessary parameters that affect the benefit of Smart water brine are a big concern.

Summaries of proposed mechanisms from previous sections are as follows:

- Noticable decrease in interfacial tension (IFT) occurs at the breakthrough recovery proposed by Aladasani et al. [1] also has contradiction to Yousef et al. [52] which shows that IFT reduction was not significant (40 – 32 dyne/cm).
- Austad et al. [7] and Nasralla et al. [38] showed that pH as a control on rock wettability during injecting low salinity brine. Condition where pH of the water effluent was lower will recover less oil than the original pH because reduction of the low salinity benefit. On the other hand, Chissoko et al. [11] showed that increased oil production also were not a direct relationship with pH and pressure drop. Unfortunately the experimental condition by Chissoko et al. [11] was conducted not at high temperature condition.
- Another point of view is ionic profiles during Smart water flooding. The results of Chissoko et al. [11] showed that once low salinity injected into the core, the concentration of ions were changing which indicate the importance of ionic

exchange mechanism. Contradiction are claimed when Lee et al. [31], and Nasralla et al. [38] showed that smart water brine will trigger multi ionic exchange such that free multi-charged cations replace the double layer cations that form complexes with organic functional groups at the clay surfaces leading to an increase in the water wetness of the formation. This is not necessarily true since low salinity brines without Ca^{2+} and or Mg^{2+} ions showing additional recovery (Tang et al. [45], Austad et al. [6,7], Chissoko et al. [11]).

- Presence of clay minerals, mostly in sandstone, especially kaolinite might improve oil recovery by improving the effectiveness of wettability alteration. But contradiction regarding clay presence are also presented by Cissokho et al. [11], Pu et al.[41], namely, even without significant clay content or kaolinite, Smart water flooding still gives incremental recovery.
- Wettability alteration seems to widely occurred mechanism seen by researchers either it can increase oil flow capacity and or reducing residual oil saturation. The triggers of wettability alteration might be mineral dissolution and or MIE. Yousef et al. [52] showed that there was diffusion coupling in the pore network which initially didn't exist in NMR experiment, which is an indication of rock dissolution. Pu et al. [41] also showed that wettability shifting towards more water wet was due to dissolution of anhydrite which in turn causes more acidic water condition by an additional sulphate ion content.
- Straight dilution of Seawater might not represent best oil recovery since distilled water results in less recovery. Furthermore in carbonate Formation (chalk and limestone) the role of certain ions in injection water such as SO_4^{2-} and Ca^{2+} are

suggested as determining ions that affect ultimate oil recovery during wettability alteration, Fathi et al. [14] and Al Attar [2].

From modelling point of view, the approach of building smart water flooding model have attracted many researchers, recently. At early modelling development, researchers utilized uncertainty parameter in history matching Smart water flooding experiment, such as, relative permeability end point, Corey oil exponent and residual oil saturation. These final adjustable parameters will represent the benefit of Smart water flooding. Later on, most of researchers took the modelling approach or mathematical model proposed by Jerauld et al. [25] which is salinity dependence of relative permeability, capillary pressure, and residual oil saturation. The common inputs are typical/synthetic high and low salinity relative permeability curve as the range limit of relative permeability model. Some researchers also put the dependence of contact angle which needs assumptions of dependent brine parameter or empirical trends between brine and contact angle for example. Unfortunately, the works ended up with non-uniqueness results to obtain profile matching in cumulative oil recovery and pressure drop. In other words still cannot answer the mechanism.

Recent publications of De Bruin [13] and Korrani et al. [28, 29] utilized reservoir simulation (mathematical based Buckley Leverett or established simulator) coupled with geochemical simulation. In Korrani et al. transport flow equation assumed to be one aqueous/ geochemical entity. They believed that in multi-phase reactive transport modelling, hydrocarbon does not have to exist as additional phase but as a geochemical entity. The character of hydrocarbon was represented as acid/ basic component in aqueous phase. This basic/acid oil representation concept is strengthened by Fjelde et al. [15]. They showed that the effect of crude oil composition in low salinity water flooding is represented

by base/acid ratio. It showed that the retention was sensitive to the concentration of acids in crude oil and was increasing with increasing base/acid ratio. Cissokho et al. [11] showed that the presence of oil (two phase) gave different salt concentration profile against only brine to brine injection (one phase), which indicate the importance of oil parameter. In other words the hydrocarbon interaction in geochemical reaction plays a role.

In addition, regarding simulation works, core flooding experiments usually become validation of simulation models. Unfortunately some of them used other result of core flooding experiments that were not clear enough to emphasize the magnitude of oil recovery. Also the relative permeability result of these experiments are not fully hold in the history matching. Meaning that the measurement of the experiments parameter/result has a doubt. It suggests the need of comprehensive work from core flooding design until simulation model that really emphasize the benefit of Smart water flooding. For example close look at the ionic concentration and pH profiles of effluent, homogeneity of core system, careful operating condition etc.

CHAPTER 3

METHODOLOGY

Core flooding experiments were conducted to obtain the relative permeability data that represent low salinity/Smart water flooding benefits. Literature review shows that the contributing factors in most Smart water flooding mechanism are the type of rock formation (mineralogy, homogeneity), richness of clay, ionic compositions in injection brine (Ca^{2+}, Mg^{2+}, SO_4^{2-}, Cl^-), oil compositions (chain of fatty/carboxylic acid and acid number) and environmental condition (pH, temperature, pressure). Some of these factors might be unnecessary present in carbonate rock, such as, the portion of clay that might be insignificant. Furthermore, factors influencing Smart water flooding in carbonate limestone will carefully be considered in the experimental criteria, procedures and analysis of post core flooding.

In the last section of this chapter, some basic assumptions of simulation methodology are presented. Together with structure of geochemical model using PHREEQC.

3.1 Experimental Materials

3.1.1 Brine Compositions

This study will focus on using brines representing Middle-East oil field condition. The initial water saturation of formation brine will use Arab-D formation brine with

approximate TDS of 206,911 ppm and seawater with approximate TDS of 57,670 ppm. Meanwhile, for injection brines compositions, 10 times (10x) diluted seawater with approximate TDS of 5,670 ppm was selected. All brines are synthetically prepared from analytical grade salts and de-ionized (DI) water. The composition of brine solutions used in this study are summarized in Table 3.1.

Table 3.1 Brines Compositions

Ions	**Formation brine (FW)**	**Seawater (SW)**	**10x Diluted SW (DSW)**
Na^+	62000	18300	1830
Ca^{2+}	23314	650	65
Mg^{2+}	1268	2110	211
Cl^-	120000	32200	3220
SO_4^{2-}	250	4290	429
HCO_3^-	79	120	12
TDS (ppm)	**206911**	**57670**	**5767**

The 10x diluted seawater (DSW) is a brine with 10 times dilution of seawater which can be considered as smart water/ low salinity brine. This 10x diluted seawater was found to be more effective when used after seawater flooding stage and gave approximate additional gain up to 10% of oil recovery as reported in experimental result of Al-Hashim et al [3] and Yousef et al. [52]. Thus, clear additional gain is expected from this smart water.

Pre-laboratory measurements showed that formation brine has room temperature density of 1.149 g/cc and viscosity of 1.312 cp, whereas, seawater brine has room temperature density of 1.036 g/cc and viscosity of 1.002 cp.

3.1.2 Crude Oil Properties

Crude oil is part of the factors affecting smart water flooding benefit. This study will use UTMN crude oil (dead oil) that has low acid number to minimize the retention of polar oil compounds in order to highlight benefit of smart water flooding. The oil was filtered to remove any suspended particles and water. Approximately, the crude oil has an API gravity of 30 and its composition is shown in table 3.2.

Table 3.2 Crude Oil Composition

Component	Moles	Moles (%)
C5	0.00216	1.23
C6	0.007434	4.23
C7	0.018767	10.67
C8	0.027806	15.81
C9	0.025519	14.51
C10	0.025371	14.43
C11	0.019607	11.15
C12+	0.049211	27.98

Pre-laboratory measurement show this dead oil has room temperature density of 0.869 g/cc and viscosity of 10.2 cp, whereas, at 100^{o}C the dead oil viscosity is about 1.649 cp.

3.1.3 Core Plugs Properties

Limestone core plugs obtained from outcrops of Indiana Limestone carbonate rock are used in this study. To minimize capillary end effect and heterogeneity of the typical carbonate rock, the selection of the core samples is crucial. The core sample has dimensions of 1.5" diameter and 12" of total length of composite cores; which is long enough to minimize

capillary end effect [43]. The homogeneity of these cores will be examined by CT scan, Thin-section Analysis and its rock properties (porosity and permeability) will be measured. Figure 3.1 shows the trimmed core samples sets used in this study namely core set B that comprises of B1, B2, B3 and B4 and core set C that comprises of C1, C2, C3 and C4. While the dimensions and dry weight of these set of cores are presented in table 3.3.

Figure 3.1 Indiana Limestone Core Sample (B1-B2-B3-B4-C1-C2-C3-C4)

Table 3.3 Dimensions and Dry Weight of Core Samples

Core	L (in)	D (in)	Dry Weight (gr)
B1	2.98	1.48	185.9
B2	2.92	1.48	184
B3	2.75	1.48	172.3
B4	2.98	1.48	183.7
C1	2.984	1.48	184.6
C2	2.874	1.48	178.2
C3	2.902	1.48	178.2
C4	2.945	1.48	182

3.2 Experimental Criteria

This study proposes some important points during unsteady state core flooding in order to obtain representative and reliable relative permeability curves.

First, during core flooding preparation; selection of injection rate and core sample characteristic should be well defined. These parameters are crucial to minimize capillary end effect. Some researchers question whether typical high laboratory injection rate will result in similar relative permeability with practical low field injection rate. Chen et al. [10] based on their investigation of imbibition steady state core flooding, stated that both measurements of relative permeability of those flow rates produce the same results in water wet and intermediate rock system. Another investigation by Fulcher et al. [17] stated that magnitude of the minimum rates in typical laboratory core flooding to overcome saturation gradient at outer face of the core is in the range of 80 ml/hour (equals to 1.33 ml/min or 16 ft/day) to 400 ml/hour (equals to 6.67 ml/min or 80 ft/day).

To emphasize the objective of this study, the selected injection rate should be large enough to avoid the dominant force of capillary end effect and small enough than the upper limit of the critical capillary number in order to isolate the effect of residual oil saturation (S_{or}) reduction due to rate above the critical capillary number.

Some scaling numbers assessment are conducted, some of the common scaling criteria are Rapoport and Leas scaling [43] and Lake [44] which is modification of Rapoport scaling criteria. These scaling criteria have the objective to avoid capillary end effect by considering length of core, injection rate, and rock and fluid property**.**

$$Rapoport\ Scale = L(cm)\,x\,\mu_w(mPa.s)\,x\,v(cm/\min) \qquad (3.1)$$

$$N_{RL} = (\phi/k)^{1/2}\,[(\mu_w\,v\,L)/(k_{rw}{}^{*}\,\sigma\cos\theta)] \qquad (3.2)$$

Where L is length of core is cm, μ_w is water viscosity in cp or mPa.s, σ is interfacial tension in mN/m, θ is contact angle, k is permeability in μm^2 and krw* is end point water relative permeability at S_{or}. In order to get minimum rate of injection, Lake N_{RL} criteria should be at least 3 which corresponds to a scaling of 1 in Rapoport and Leas data. Taking some assumptions and applying these formuli, core set B shows the minimum rate of 0.27 – 0.44 cc/min and core set C shows minimum rate of 0.24 – 0.405 cc/min in Lake scaling. Meanwhile, Rapoport and Leas shows a minimum rate of around 0.1 cc/min for both cores. The assumptions are based on Amjed Hassan [21] on seawater fluid, with σ of approximately 15 mN/m. Whereas viscosity of about 0.45 cp at 100°C, cos θ of 0.25, core length of 28 cm, porosity of 0.2, krw* = 0.3-0.5 and core sets B and C absolute permeability of 192 and 356 mD.

Another aspect to be considered is the critical capillary number of carbonate samples. The upper limit of a typical critical capillary number in carbonate based on Kamath et al. [26] with 4 carbonate samples is about Nc of $4x10^{-7}$ (based on high carbonate core properties in reported experiment, see figure 3.2). With another assumption of seawater fluid viscosity of about 0.45 cp at 100°C and σ of 15 mN/m, the calculated rate from this formula $N_c = \frac{\mu_w v}{\sigma_{ow}}$ shows that the calculated maximum flow rate is 0.9 cc/min. Based on the pros and cons of rate criteria, this study uses a value of 0.5 cc/min injection rate, since it covers Rapoport and Leas scaling and also Lake scaling in all core sets and it is less than maximum

rate from Nc of $4x10^{-7}$ reported by Kamath et al. [26]. This value is also a common practice in core flooding research.

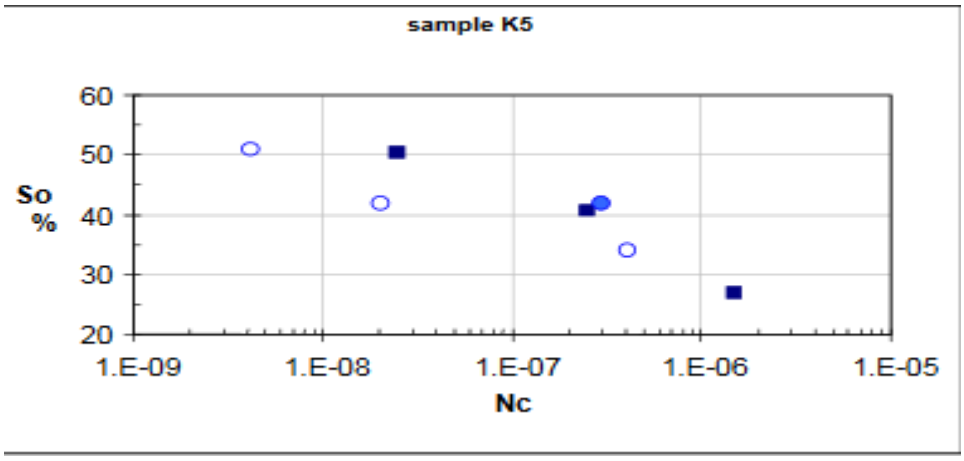

Figure 3.2 Capillary Number of Mixed Wet Rock of Carbonate Samples reported by Kamath [26]. Remaining oil saturation as function of Nc

Second issue is the core samples configuration. As investigated by Rapoport and Leas [43], at least 20 cm cores should be used to minimize capillary end effect. This study will select composite set of cores of 1 ft long. In this study, Huppler [24] ordering method is used to arrange the composite cores. Basically, Huppler ordering stated that harmonic average between core sections should be as close as possible to the overall average of the composite core. Also, the piece of core with permeability closest to the average is placed at the outlet position.

$$k_j = \sum_{i=1}^{j} L_i \Big/ \sum_{i=1}^{j} \frac{L_i}{k_i} \qquad (3.3)$$

$$F = \min[\frac{k_n}{n}(\sum_{j=1}^{n}\frac{1}{k_j} - \frac{1}{k_n})] \qquad (3.4)$$

F here is Huppler indicator of ordering, the limit is less than 1, with a smaller combination value is more favorable. After assessing all combination possibilities of core sets B and C, a very similar F values of both sets which is 0.025-0.026 were found. For set B, from inlet to outlet, the order is B3-B1-B4-B2, whereas set C from inlet to outlet, the order is C2-C3-C4-C1. This close value of Huppler ordering criteria between these two core sets, confirm the similarity of both core sets.

Third, crucial stage during successive/sequential unsteady state coreflooding is the period to switch to different brine. Cores saturated with oil and formation water at S_{wi} will be flushed with seawater then smart water brine. Switching period should consider the equilibrium state of the effluent. This condition is identified from the oil production profiles until the state of no more oil production in the collector tubes and supported by conductivity profile of the effluent. Other indication is stabilized pressure drop since only seawater is produced. Detail chemical state is also investigated by pH and ionic profiles intentionally for the predetermined ions such as Ca^{2+}, Mg^{2+}, Na^{+}, SO_4^{2-}, Cl^{-}, and HCO_3^{-} Some literatures show that during seawater injection, the formation water will be removed reflected by ionic concentration profile of the effluent. Therefore, sufficient time is needed.

In addition, for experimental conditions; temperature and pressure, and oil composition are isolated or set to be fixed. Next chapter will detail experimental criteria and its results.

3.3 Experimental Procedure

In this study, unsteady-state coreflooding experiments were designed to obtain reliable relative permeability data that can be used in modelling smart water flooding. Unlike the conventional smart water/ low salinity flooding experiments, two experiments were designed as follows:

– **Experiment 1,** formation brine was used to establish S_{wi} and also used to displace the oil till no more oil is produced. Then seawater was injected and continued till no more oil is produced again. Finally 10x diluted seawater was injected and continued until no more oil is recovered.

– **Experiment 2,** seawater was used to establish S_{wi} and also to displace the oil till no more oil is produced. Seawater was then followed by 10x diluted seawater was injected till no more oil is recovered.

While **Experiment 3,** was conducted following the conventional approach. It is expected to have an idea of mixing fluid reaction in conventional core flooding once the relative permeability results are compared.

This section will show procedures during preparation until post core flooding experiment. Details are presented below.

3.3.1 Core Characteristic and Preparation

Core characterization is important part of this study, since it describes not only the rock properties such as porosity and permeability but also some information that are needed to bridge the limitation of laboratory work and common linear displacement model namely

Buckley Leverett [9]. Such information refer to the heterogeneity of core samples and also ideas on its pore structures.

At first preparation, each piece of core samples are cleaned from the salt and or oil constituents with solvent within a day. Then put the cores in an oven to remove the solvent for some hours to obtain the dry core. Measure the dimension and weight of the dry core. From this state forward, these cores are treated both for core flooding preparation and some characterization tests. These tests are as follow: CT-Scan test, core thin section and absolute permeability measurements followed by other measurements of some basic properties of core samples.

Core CT-Scan

CT scan test could see similarity of core slices which implies degree of homogeneity of each individual piece of the cores resemble each other. There are about 70 slices of images (1mm thickness) and rear-top-front images of each piece of core set that have been conducted. Figures 3.3 to 3.4 show the CT scan image of each piece of core samples during saturated condition.

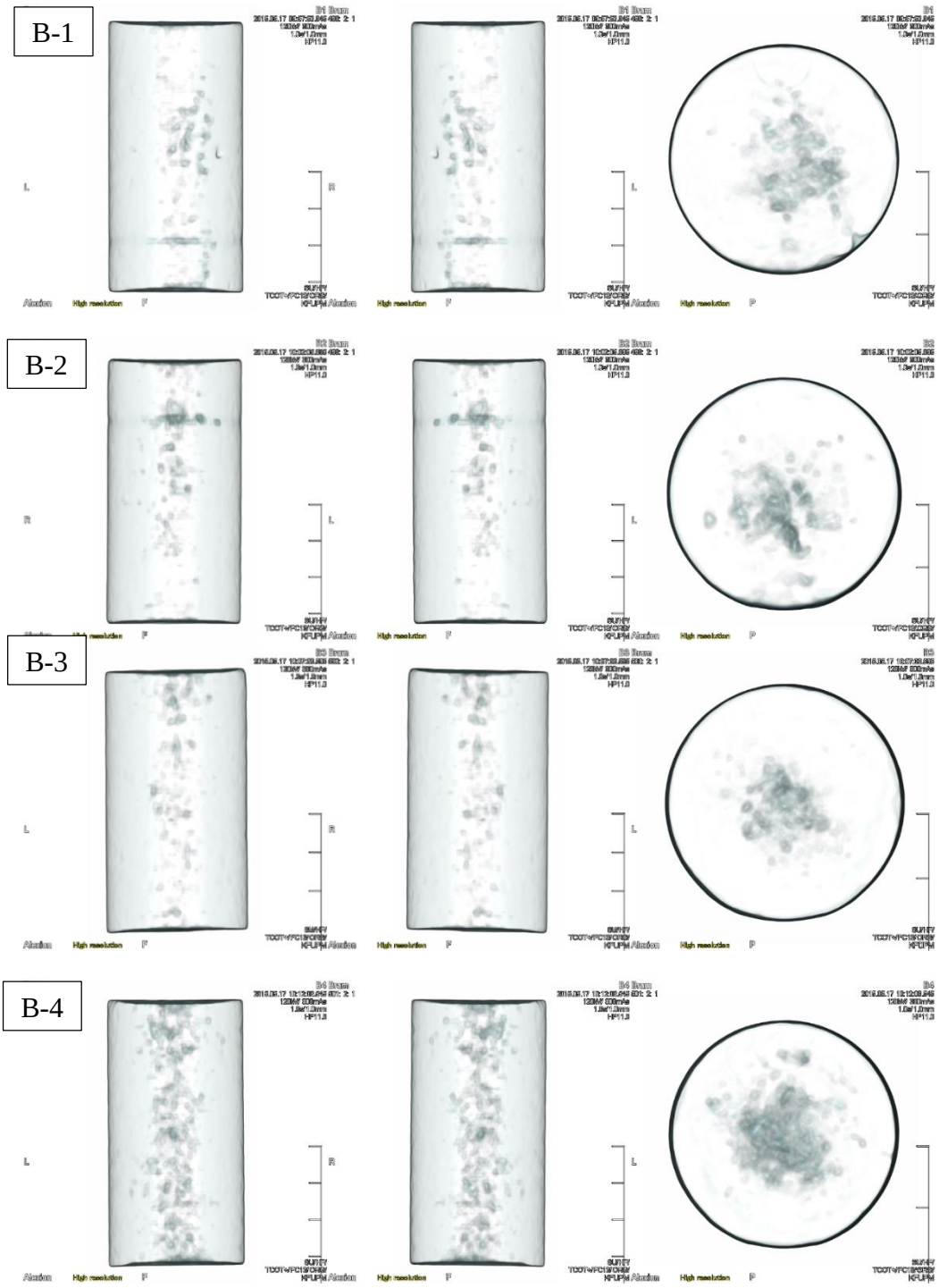

Figure 3.3 CT Scan of core Pieces in Set B (Right – Left – Top)

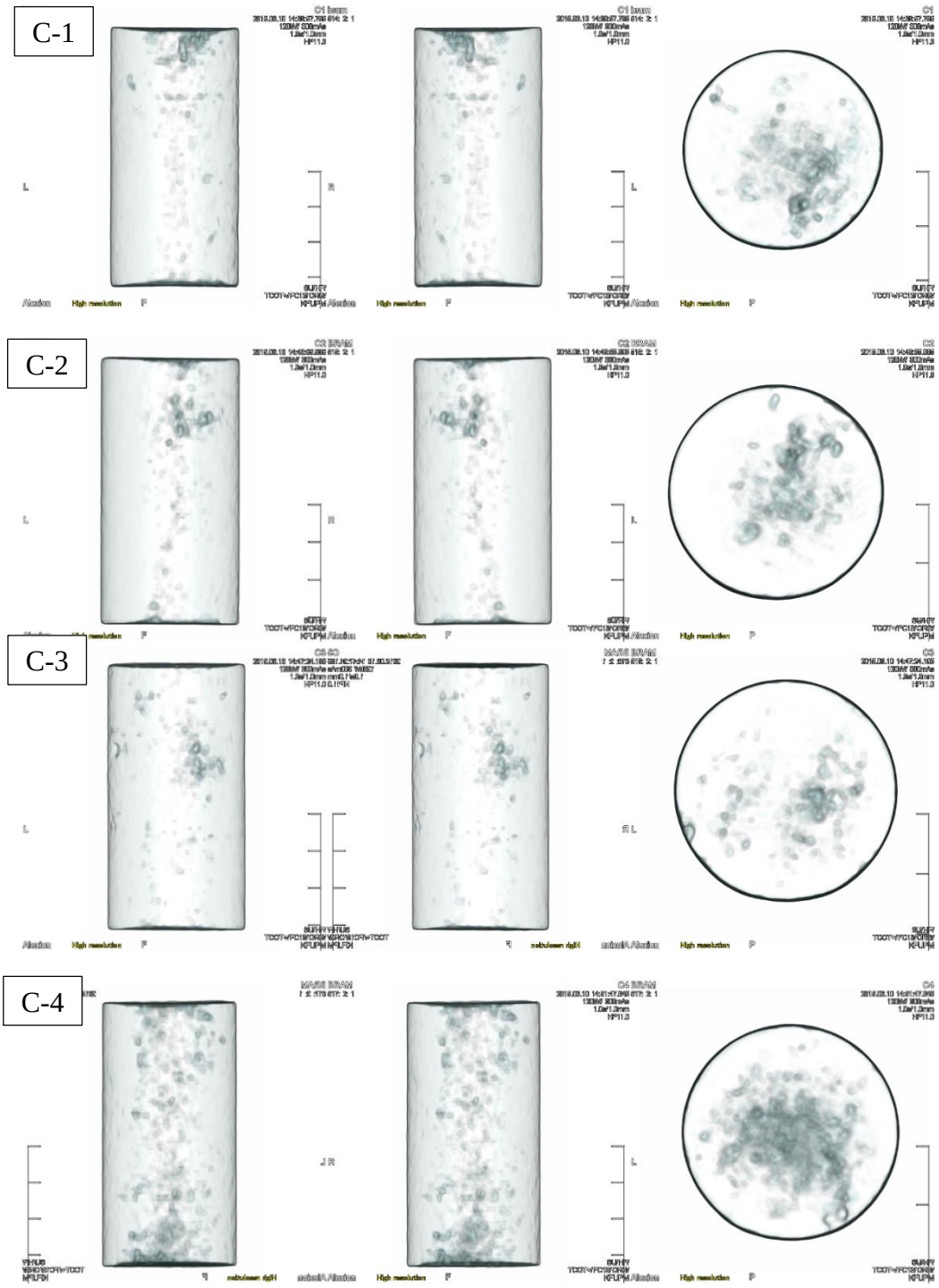

Figure 3.4 CT Scan of Core pieces in Set C (Right – Left – Top)

From the images above, set C has more porous state than core set B that is shown from the intensity of the color (darker areas) in slices images. This characteristic is represented by

CT-number which measures degree of x-ray attenuation in specific volume elements of material perpendicular to the motion of the scan. Average CT-number of set B is 2470 whereas average CT-number of set C is 2450 as seen in figure 3.5. Some of the slices show lower CT-number that represent low density or atomic number as shown by darker areas. Nonetheless both average CT-numbers indicate that these limestone cores show similarity of its porous state.

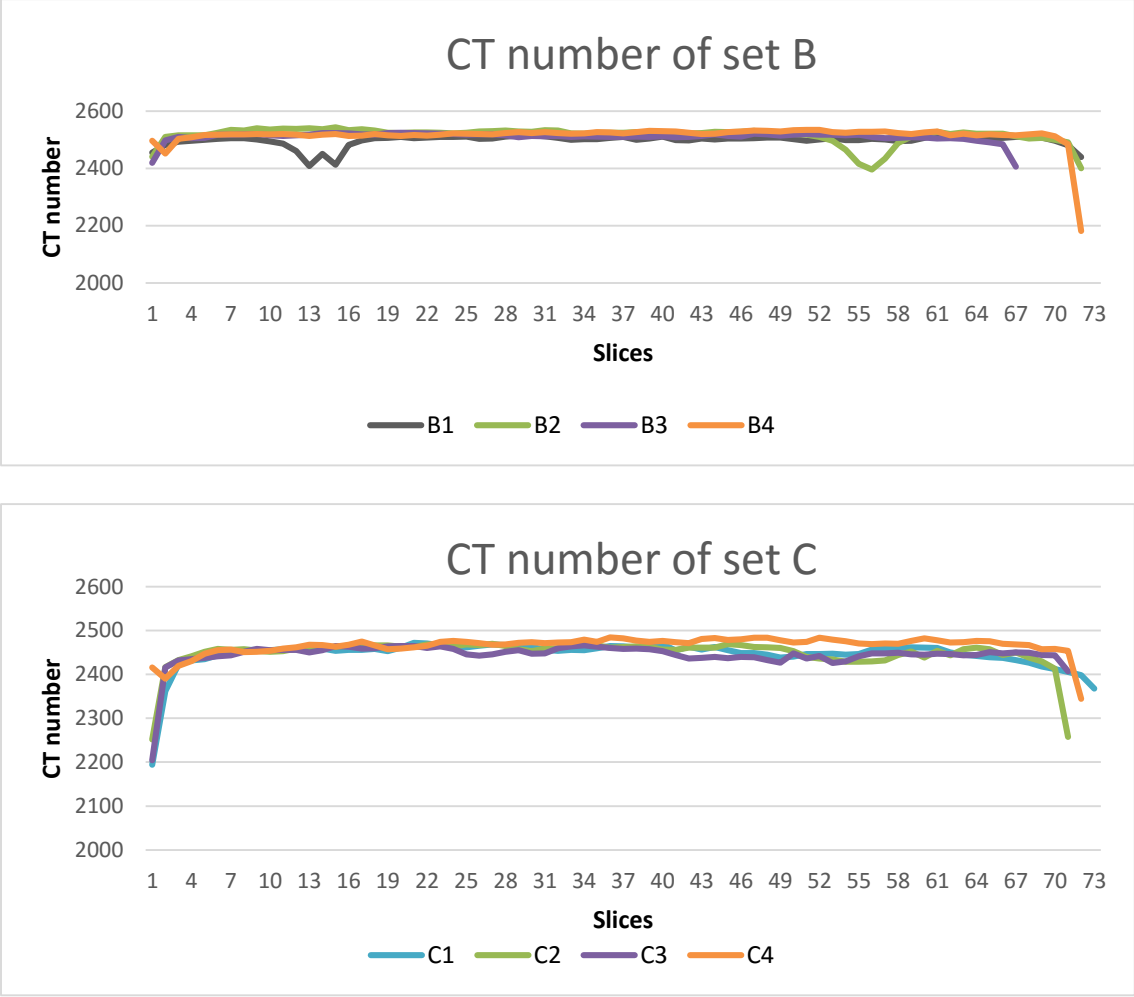

Figure 3.5 CT-number of Limestone Core Samples

Core Thin Section

Small part of core B-3 is trimmed about 1.27 mm of thickness for preparation of thin section analysis. Hereon, thin section of a core in sample B-3 is observed in ultra-microscope to characterize its carbonate limestone structures.

Thin section images show that even though limestone cores commonly have low network connectivity/ permeability state, but this sample shows the opposite. Figure 3.6 shows the snapshots of trimmed sample and its thin section.

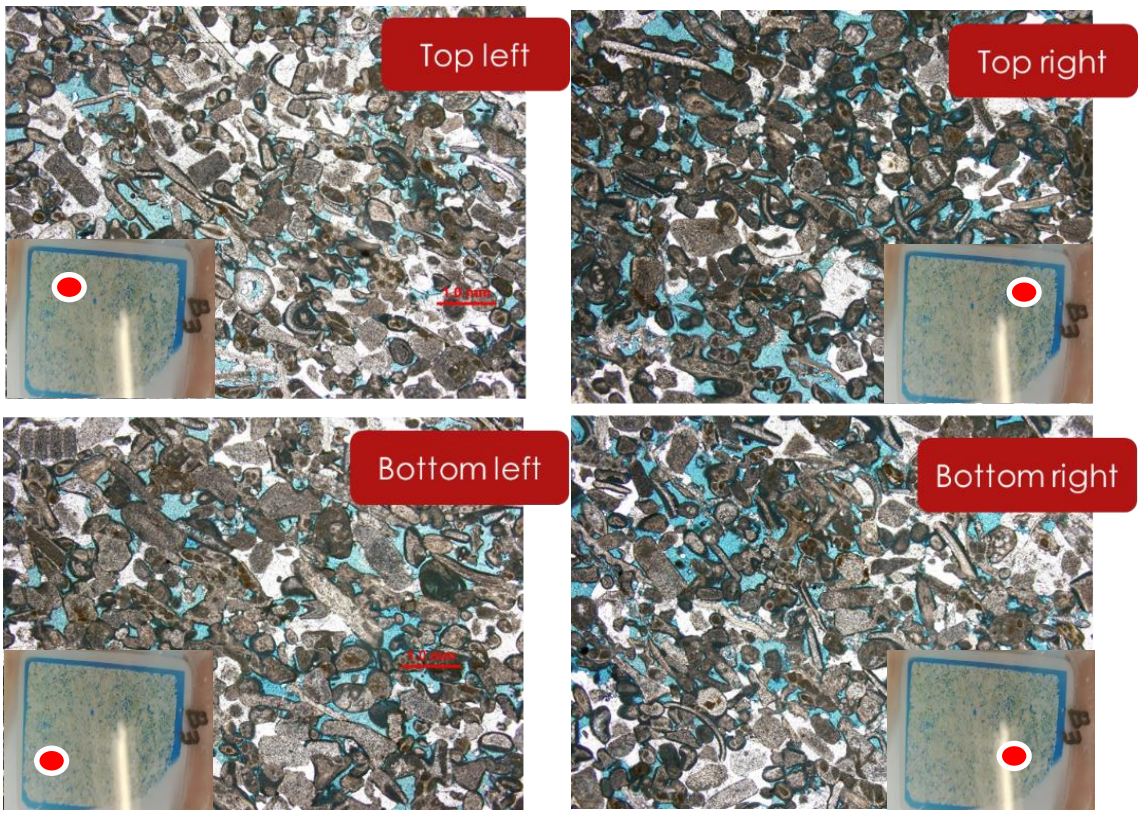

Figure 3.6 Thin Section Image of Sample B-3

Based on Dunham carbonate classification, this sample belongs to grain-stone dominated group. It consists of echinoids, foraminifera, bivalve, peloid, also ooids. The grains size is

medium and has a medium to well sorted sorting. There is partial cementation also, estimated about 15% distribution on network.

Estimation of this thin section image shows 20-25% of pore distribution with good connections. Thus, it implies that these core samples might have good property such as permeability which might differ from common carbonate rock.

Absolute Permeability Measurement

Absolute permeability measurement is carried out after brine saturation in core flooding preparation step (in the next subsection). Basically the core samples were saturated with certain single fluid and then put individual piece of cores in core holder in core flooding set up. Apply some different injection rates and measure the stabilize pressure drop from data acquisition system.

Since the cores were saturated with single fluid, the porosity of core was calculated by measuring dry and wet weight of each sample then the difference in mass is converted into volume by using saturating brine's density. Ratio of its volume and the bulk volume of each piece of core will give porosity value.

To be noticed, in these particular absolute permeability measurements, core samples B are saturated with formation brine, whereas core samples C are saturated with seawater. It does not matter since each core set is saturated with single fluid only. The data points of injection rates versus pressure drop in set B and set C are presented in figures 3.7 to 3.8.

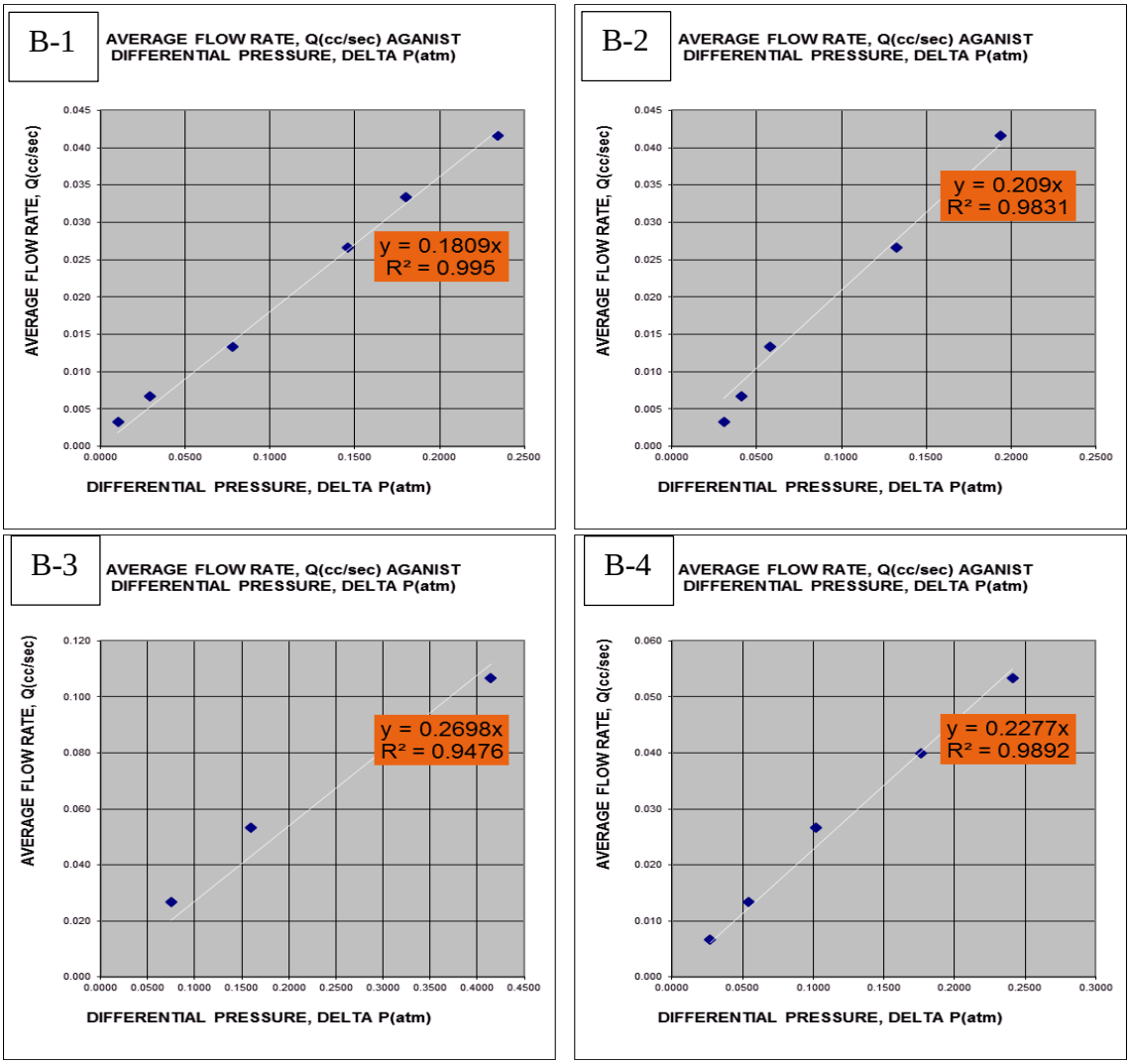

Figure 3.7 Flow rate versus pressure drop of Set B (B1-B2-B3-B4)

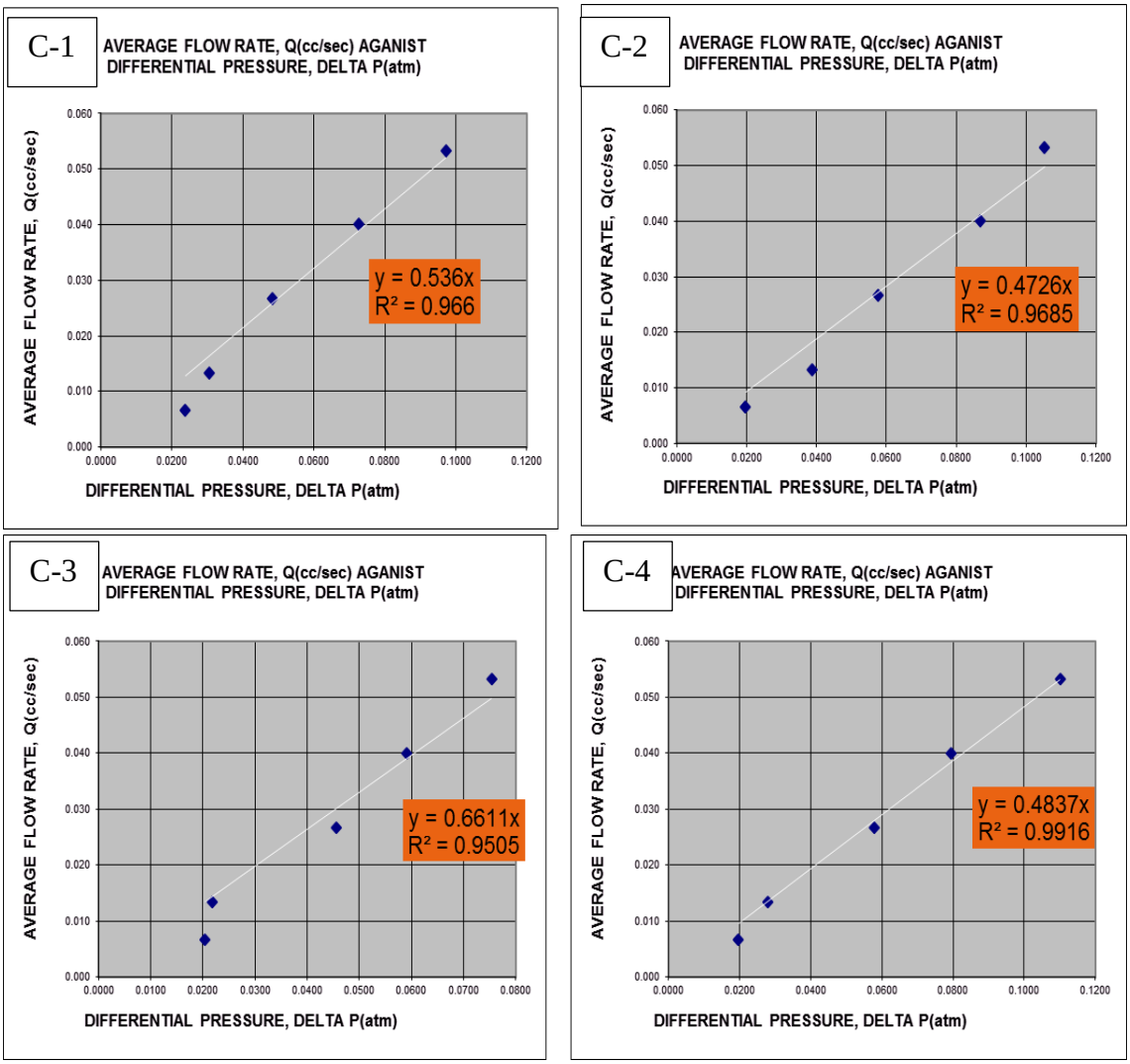

Figure 3.8 Flow rate versus pressure drop of Set C (C1-C2-C3-C4)

The slopes of these data will be used in Darcy equation to calculate absolute permeability of each core. Below is an example of the calculation and summary of calculated permeability and porosity of both sets.

Core Sample B-1 has geometry of 7.557 cm length, diameter of 3.759 cm, and 11.0989 cm^2 cross sectional area. Viscosity of saturating fluid is 1.313 g/cc which is Formation brine. And from core flooding in this B1, the ratio $\Delta Q/\Delta P$ or slope in the previous figure is

0.1809 cc/s/atm. Using Darcy law the absolute permeability of B1 core sample is simply

$$k_{abs} = \frac{slope\, x\, (\mu\, x\, L)}{A} x1000 = \frac{0.1809\, x\, (1.313\, x\, 7.557)}{11.0989} x1000 = 161.71 mD.$$

Then, properties of each piece of cores in Set B and C are presented in table 3.4.

Table 3.4 Summary of Core Samples Porosity and Absolute Permeability

Core	Dry Weight (gr)	Wet Weight (gr)	PV (cc)	BV (cc)	Por (%)	Perm abs (mD)
B1	185.90	202.20	14.19	84.01	16.90	161.71
B2	184.00	200.70	14.53	82.32	17.70	183.38
B3	172.30	186.80	12.62	77.53	16.30	222.94
B4	183.70	199.80	14.01	84.01	16.70	203.89
C1	184.60	200.75	15.57	84.12	18.30	361.81
C2	178.20	192.96	14.23	81.02	17.40	307.16
C3	178.20	193.65	14.90	81.81	18.00	433.89
C4	182.00	198.71	16.11	83.02	19.20	322.20

Table 3.4 above shows that Indiana limestone cores used in this study have very good properties in porosity and permeability. It aligns with previous core characterization results in CT scan and Thin-section.

3.3.2 Establishment of Initial Water Saturation

Using saturation cell set up, cores are put inside the cylinder and vacuum was applied with vacuum pump for at least 2-3 hours. Then the cylinder was filled with saturating brine whether by pump or automated brine filling from brine's tank due to less pressure in the cylinder. After the cylinder is fully filled with selected brine, then start build up the cylinder pressure that refer to confining pressure of core flooding experiment in this study which is 2500 psi. The main objective of this experiment is to get the cores with 100% saturated

brine or in other words 100% water saturation. After this step, all core samples should be immersed in the same saturation brine before used in the next step/ brine desaturation. Figure 3.9 shows the schematic of core brine saturation cell.

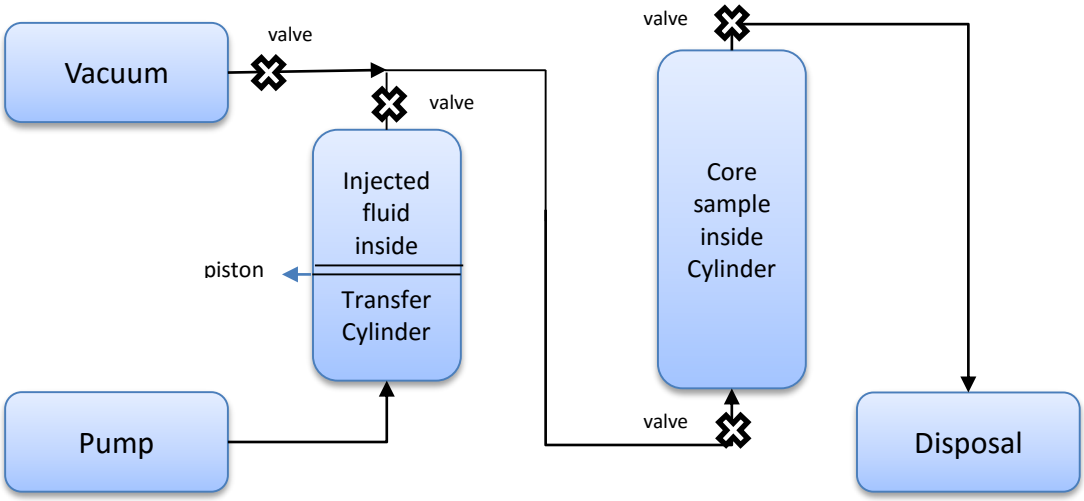

Figure 3.9 Core-Brine Saturation Cell Schematic

The saturated cores should be drained until it reached expected/ common initial water saturation which is around 20-25% PV (0.2-0.25 Swi) which is called brine desaturation process.

In this study, both Ultra-Centrifuge and Porous-Plate methods were used to conduct brine desaturation. During centrifuging, the cores are rotated in a specific rock rotor with 5000 RPM speed and the brine will come out due to centrifugal force towards outside of the rotor. While in Porous plate set up, the cores are displaced with non-wetting fluid which is air up to 200 psi at the inlet of each core and there is porous plate filter attached at the outlet of the set up that allows the brine to come out but not the injected air. Once the water saturation is close to our target initial water saturation, the displacement/ centrifuging

process are stopped. Then the cores are removed from the set up and covered with plastic and aluminum foil to avoid any evaporation.

Figure 3.10 Core Samples Conditions after Centrifuge

To be noted, that during centrifuging, two core samples were damaged little bit in one of each set which are B4 and C4 (figure 3.10). Both pieces of cores are trimmed a little bit to remove the broken edges. Then after experiment-2, set cores C is being used again and there is a little refinement in piece of core C4. Table 3.5 present a summary of S_{wi} for three main experiments obtained from Ultra-Centrifuge and Porous-Plate tests and the new dimension of the cores.

Table 3.5 Summary of Core Samples Swi

Experiment/Core	L (cm)	Balance Por (%)	Perm abs (mD)	PV	S_{wi}
Exp_1/B1	7.57	16.9	161.71	14.19	0.202
Exp_1/B2	7.42	17.7	183.38	14.53	0.194
Exp_1/B3	6.99	16.3	222.94	12.62	0.216
Exp_1/B4	6.25	14.1	203.89	10.06	0.151
average/total		**16.25**	**192.98**	**51.4**	**0.191**
Exp_2/C1	7.58	18.3	361.81	15.57	0.215
Exp_2/C2	7.3	17.4	307.16	14.23	0.177

Exp_2/C3	7.37	18	433.89	14.89	0.245
Exp_2/C4	6.25	12.9	322.20	9.20	0.217
average/total		**16.65**	**356.27**	**53.91**	**0.214**
Exp_3/C1	7.58	19.5	361.81	16.66	0.219
Exp_3/C2	7.3	18.2	307.16	14.98	0.238
Exp_3/C3	7.37	18.2	433.89	15.12	0.409
Exp_3/C4	5.5	17.5	322.20	10.83	0.527
average/total		**18.40**	**356.27**	**57.58**	**0.348**

3.3.3 Core Aging with Dead Oil

Cores were loaded in aging cylinder with a tag to label the cores. Basically, the principle is the same as brine saturation cell, the difference is the injected fluid in this stage which is oil and the cylinder will be kept at high pressure and temperature for certain periods. In this study, the oil used is UTMN dead oil and the aging conditions are 100^{o}C and 2500 psig for two weeks. This aging period is commonly used in core flooding experiments to restore reservoir wettability. Furthermore, all three experiments in this study are aged for 2 weeks period.

3.3.4 Unsteady State Core flooding set up

Unsteady state core flooding set up is the main experimental equipment in this study. This set up is equipped with data acquisition system to monitor pressure drop and fraction collector to collect the effluent. Experimental conditions for unsteady-state core flooding are selected similar to common condition of Middle-East oil field where the temperature is about 100^{o}C, overburden pressure of 2500 psig and pore pressure of 1500 psig.

Schematic of unsteady state core flooding set up is shown in figure 3.11. The procedures start from loading the core saturated with oil at initial water saturation into the core holder. Apply overburden pressure and back pressure/pore pressure as stated before.

In all experiments, oil is injected at least 1-2 pore volumes just before effective oil permeability measurements. After measuring the oil effective permeability, first injection fluid is conducted until no more oil is recovered. Once the pressure drop, pH, conductivity and ions profile of the effluent are stabilized beside no more oil production, second fluid is injected until no more oil is recovered. Same procedure was applied for next injection stage. Lastly, calculation of relative permeability curves uses JBN method based on production and pressure data of previous unsteady-state core flooding.

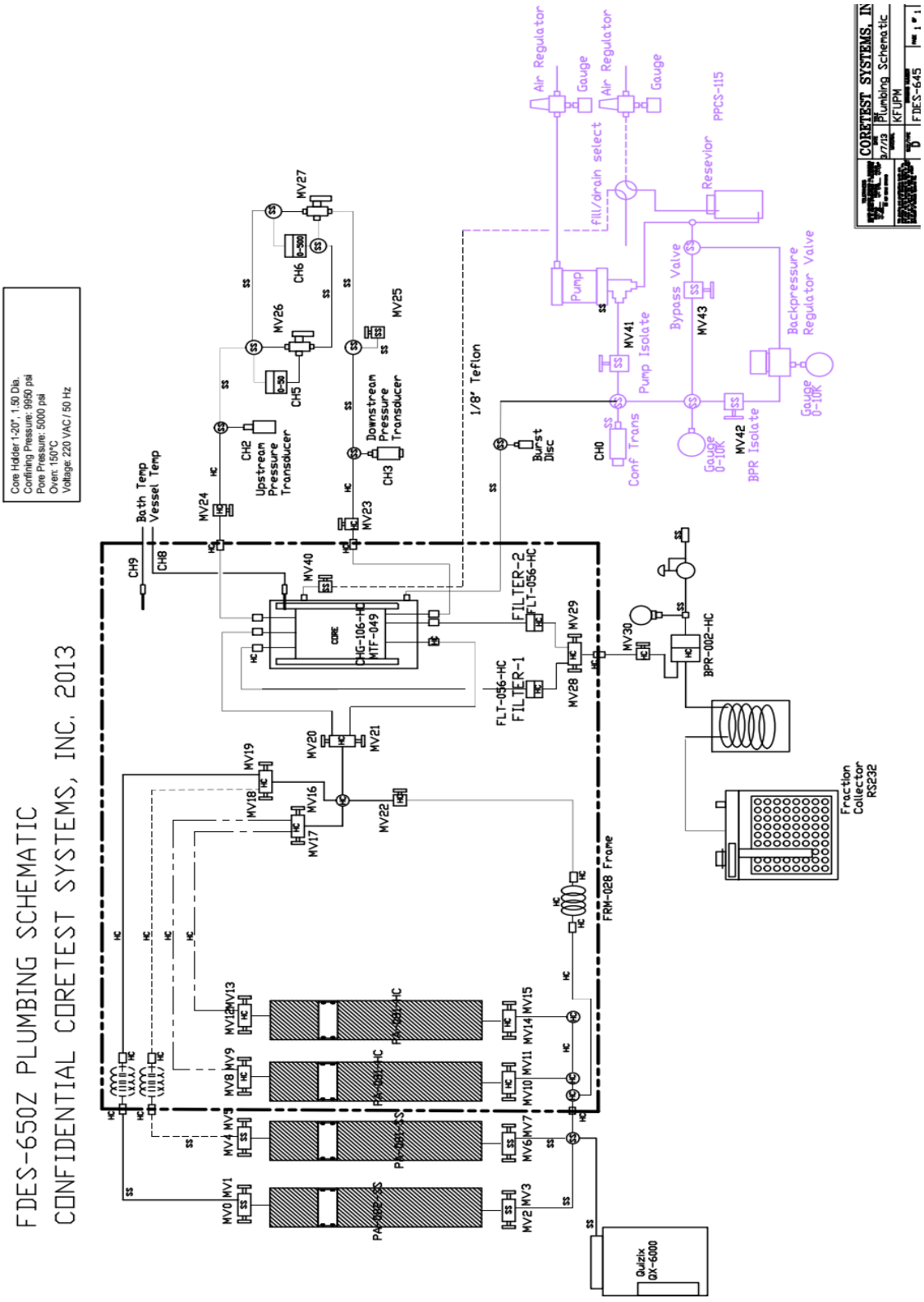

Figure 3.11 Schematic of Unsteady-state Core flooding Set up

3.3.5 Effluent Analysis

Some of representative production's tube from core flooding experiment are filtered with filter paper with size of 0.5 - 5 μm to remove any suspended particles and to separate the oil and the pure brine effluent. Then these brine effluents will be managed to do ion analysis using IC-Metrohm and ICP-MS and also alkalinity titration.

Both cations (Na^+, Mg^{2+} and Ca^{2+}) and anions (Cl^- and SO_4^{2-}) are analyzed using IC-Metrohm 850 Professional Ion Chromatograhy (Magic Net IC). There were conductivity detectors with column type of Metrosep C 4 -250/4.0 for cations and Metrosep A Supp 7 – 250/4.0 for anions. Eluent type were mainly nitric acid and sodium carbonate solutions for cations and anions respectively. Whereas, ICP-MS uses argon gas as the eluent and this test has a purpose to crosschecked the concistency of IC-Metrohm result for cations (Na^+, Mg^{2+} and Ca^{2+}).

For both IC-Metrohm and ICP-MS, Effluent samples were diluted from range of 50 to 1000 times with deionized (DI) water based on the level of electric conductance of each samples. Replicate analyses were determined to ensure quality control and maintain system stability once the significant salinity changes between samples are analyzed.

Last anion HCO_3^- will be tested with wet method or alkalinity titration. Effluent samples are diluted 25 times with DI water to cover minimum volume of the instruments.

Daily Calibrated pH meter with ±0.5 tolerance and Calibrated electric conductance with ± 0.01-0.02 milimho tolerance will measure pH and conductivity of effluent samples.

3.4 Modelling Smart Water Flooding

One dimensional reactive transport of Smart water flooding will integrate Buckley Leverett transport flow simulation with the aid of PHREEQC's module namely IPhreeqc. Buckley leverett has a simplicity to model two phase flow in 1D displacement, whereas, the IPhreeqc module offers the capability of PHREEQC geochemical simulator to model complex geochemical reactions. Some modifications are introduced here, for example defining the threshold/ extrapolated parameter during switching into Smart water. Also the use of relative permeability core flooding result by JBN method during history matching.

The effect of Smart water/ low salinity brine will depend on the observed mechanisms during core flooding. Then select its representative's mechanism parameter as extrapolant between brines which correspond to changing relative permeability set. Relative permeability by JBN method verified by analytical solution of Buckley Leverett will become constraints/ the objective of extrapolation.

In addition, the ionic profiles and pH profiles matching will determine geochemical reactions in this process. The geochemical reactions are selected based on the revealed or most likely mechanisms observed during the core flooding in carbonate rock. Here are basics overview of Buckley Leverett and PHREEQC geochemistry model and also its module, IPhreeqc.

3.4.1 Buckley Leverett Model

Buckley and Leverett presented their famous transport equation in the paper 'Mechanism of Fluid Displacement in Sands' in 1942 [9]. This equation is now recognized as a basic method for describing immiscible displacement. The displacement mechanism can be

illustrated as production of oil using water injection. For the simple scenario in which a 1-D flow is considered, the Buckley-Leverett equation can be used to model the oil-water two-phase flow. Some important assumptions behind the Buckley-Leverett equation are as follow:

- The horizontal reservoir of length L has a constant thickness h.
- The reservoir is bounded by impermeable boundaries above and below.
- Both the rocks and fluids are considered incompressible.
- The porosity and absolute permeability are constant.
- Water and oil flow are independent from each other and obey Darcy's law.
- Capillary forces and Gravity forces are negligible.
- The pressure is a function of the x-coordinate only, thus it is one-dimensional model.
- The total flow rate q_t is constant throughout the whole reservoir length, which implies that the injection rate is also constant and $q_t = q_w$ must hold at the inlet end.

Upon injection of water, assumed as being equal in salinity as the Formation water for this purpose, a single shock front will be establish in the reservoir. Until water breakthrough has occurred, only oil will be produced. The oil production rate will be constant and equal to the injection rate, as long as no water breakthrough has occurred. The mathematical model and details of numerical solution will be explained later in the simulation chapter 5.

3.4.2 Geochemical Reactions Model

PHREEQC program is based on equilibrium chemistry of aqueous solutions interacting with minerals, gases, solid solutions, exchangers, and sorption surfaces, but also includes

the capability to model kinetic reactions with rate equations that are completely user-specifies in the form of *Basic* statements [40].

There are different thermodynamic databases distributed with PHREEQC. Thermodynamic databases are the primary source of information of all geochemical modeling programs. A database contains definitions of chemical species, complexes, mineral solubility etc. which are needed to do the calculations. The need for different databases is that some elements, species or constants that are needed for a specific problem might be unavailable in one or more of the databases. Databases distributed with PHREEQC:

- phreeqc.dat --- the standard database;
- wateq4f.dat --- has more metals;
- minteq.v4.dat --- from EPA, has some organics;
- llnl.dat --- from LLN Lab, encompasses almost the complete periodical system;
- pitzer.dat --- uses Pitzer equations for activity coefficients, meant for saline solutions;
- iso.dat --- for (equilibrium) isotope fractionation.
- t_h.dat --- for sorption on organic matter.

Generally the database is structured by a number of keywords, each followed by chemical definitions and constants needed to do the calculations [40]. The database keywords overview are detailed below:

- The first keyword is SOLUTION_MASTER_SPECIES and defines the elements in solution. The first column gives the elements name. Elements with several redox levels may be repeated with the number of electrons lost. The second column lists

the aqueous species that are used primarily in the speciation calculation. The third column gives the contribution of that species to the alkalinity when titrating down to pH = 4.5. The next two columns give the chemical formula that is used to convert grams into moles, and the atomic weight of the element.

- The second keyword, SOLUTION_SPECIES, defines the various aqueous complexes. These are tabulated in the form of an association reaction, with log_k, the association constant. Changes of log_k with temperature are calculated from the reaction enthalpy delta_h or with an analytical expression. The different options to calculate the activity coefficient from the ionic strength are controlled by the parameter –gamma. For major ions the Truesdell-Jones equation is used, and the two parameters A and B follows –gamma. For minor ions the Debye-Hückel equation is used, and å is given as the first parameter following gamma. If the line –gamma is absent then the Davies Equation is used.
- Keyword PHASES lists minerals and gases for which saturation indices are calculated. The equations are written as dissociation reactions, therefore log_k for dissociation reaction. The variation of log_k with temperature is again calculated from the reaction enthalpy or from an analytical expression.
- Keyword "EXCHANGE-MASTER_SPECIES" followed by exchange half-reactions under keyword "EXCHANGE_SPECIES", which is necessary data to model MIE or ion exchange model. The exchanger composition can be calculated by combining the mass action expressions with the mass balance for the sum of exchangeable cations.

- Another keywords in the database is “SURFACE_MASTER_SPECIES” followed by keyword “SURFACE_SPECIES”. “SURFACE_MASTER_SPECIES” is the keyword used to define the correspondence between surface binding-site names and surface master species to model surface complexation model. “SURFACE_SPECIES” is the keyword data used to define a reaction and log K for each surface species, including surface master species.
- For kinetic calculations a reaction rate equation must be programmed in *Basic* using keyword RATES. This reaction rate is called with keyword KINETICS which can also pass parameters to the rate.

More detailed structure of PHREEQC database for any geochemical reaction can be seen by open .dat file of PHREEQC database in installation folder.

CHAPTER 4

EXPERIMENTAL RESULTS

This Chapter shows the results of laboratory work from unsteady state core flooding and effluent analysis after core flooding experiments. These results will be interpreted using JBN method to obtain relative permeability as reference for 1-D simulation model.

4.1 Unsteady State Core Flooding Results

As stated earlier, three unsteady state core flooding experiments were conducted. The section below shows results of all experiments including pressure drop, oil production and potential determining ions profiles.

4.1.1 Pressure drop and Production Data Acquisition

During the experiment, pressure drop and produced fluids are monitored as a function of time. Early period of core flooding were used to estimate effective oil permeability. Initial pressure drop data of all experiments, show some scattered points due to the frequency of data acquisition selection. After removing outliers and wavelet filtering the trends became clearer as it will be used in further interpretation.

Experiment-1, Figures 4.1 and 4.2 show initial pressure drop filtering and trend of injection rate versus pressure drop for effective oil permeability. While figure 4.3 presents the oil recovery in cc and percent of (original oil in cores) OOIC as a function of pore

volume injected respectively. The pressure drop during the injection of formation brine, seawater, and 10x diluted seawater is also presented in this figure.

Experiment-2, Figures 4.4 and 4.5 show initial pressure drop filtering and trend of injection rate versus pressure drop for Effective oil permeability. While figure 4.6 presents the oil recovery in cc and percent of OOIC as a function of pore volume injected respectively. The pressures drop during the injection of formation brine, seawater and 10x diluted seawater is also presented in this figure.

Experiment-3, Figures 4.7 and 4.8 shows initial pressure drop filtering and trend of injection rate versus pressure drop for Effective oil permeability. While figure 4.9 presents the oil recovery in cc and percent of OOIC as a function of pore volume injected respectively. The pressure drops during the injection of formation brine, seawater and 10x diluted seawater is also presented on this figure.

Tables 4.1 to 4.3 show basic condition of the core before and after core flooding. Slight changes were occurred in terms of dry weight of all cores after core flooding. Fortunately these still in a good tolerance which are less than 1 percent weight. Table 4.4 presents a summary of cumulative oil recovery due to all injection fluids. Cumulative oil production of first injection (formation brine in Exp-1 and seawater in Exp-2) can reach about 50% oil recovery after about 8 PV. Additional oil recovery due to Seawater is about 2%, while additional oil recovery due to smart water/ low salinity brine is about 1-4%. Additional gain of smart water is less than the expected outcome as reported in literature review. Nevertheless, these results are still showing positive benefit in oil production due to Smart water injection. In addition, the result of experiment-3 shows higher oil recovery but in fact close cumulative oil production volume.

Table 4.1 Core Properties of Exp-1

	Basic Core Properties	B1	B2	B3	B4	Total/average
1	Length, cm	7.569	7.417	6.985	6.248	28.219
2	Pore Volume, cc	14.186	14.534	12.620	10.061	51.401
3	Porosity, %	16.900	17.700	16.300	14.100	16.250
4	Effective oil permeability(composite), mD					66.19
5	Irreducible Water Saturation(Swir), %PV	0.202	0.194	0.216	0.151	0.191
6	Oil in Place/OOIC, cc	11.321	11.715	9.894	8.542	41.471
7	Dry weight before Core-Flooding, g	185.920	184.000	172.290	151.150	173.340
8	Dry Weight after Core-Flooding, g	184.950	182.580	170.140	152.870	172.635
9	Percent difference, %	**0.522**	**0.772**	**1.248**	**-1.138**	**0.351**

Table 4.2 Core Properties of Exp-2

	Basic Core Properties	C1	C2	C3	C4	Total/average
1	Length, cm	7.579	7.300	7.371	6.248	28.498
2	Pore Volume, cc	15.574	14.233	14.899	9.204	53.910
3	Porosity, % BV	18.300	17.400	18.000	12.920	16.655
4	Effective oil permeability(composite), mD					112.79
5	Irreducible Water Saturation(Swir), %PV	0.215	0.177	0.245	0.217	0.214
6	Oil in Place/OOIC, cc	12.225	11.714	11.249	7.207	42.395
7	Dry weight before Core-Flooding, g	184.600	178.200	178.200	150.560	172.890
8	Dry Weight after Core-Flooding, g	183.600	176.600	176.600	149.700	171.625
9	Percent difference, %	**0.542**	**0.898**	**0.898**	**0.571**	**0.727**

Table 4.3 Core Properties of Exp-3

	Basic Core Properties	C1	C2	C3	C4	Total/average
1	Length, cm	7.58	7.3	7.37	5.5	27.750
2	Pore Volume, cc	16.66	14.98	15.12	10.83	57.58
3	Porosity, % BV	19.5	18.2	18.2	17.5	18.4
4	Effective oil permeability(composite), mD					75.66
5	Irreducible Water Saturation(Swir), %PV	0.219	0.238	0.409	0.527	0.348
6	Oil in Place/OOIC, cc	13.003	11.410	8.938	5.126	38.477
7	Dry weight before Core-Flooding, g	183.600	176.600	176.600	135.300	168.025
8	Dry Weight after Core-Flooding, g	183.300	176.000	175.900	134.000	167.300
9	Percent difference, %	**0.163**	**0.340**	**0.396**	**0.961**	**0.465**

Table 4.4 Summary of Oil Produnction

Experiment	Cumulatives Oil Volume and Recovery (%OOIC)					
	Sequence of Injected Brines					
	FB		Swt		10x Dil Swt	
	%	cc	%	cc	%	cc
1	50.173%	20.87	52.240%	21.73	53.081%	22.08
2	-	-	54.292%	23.02	56.580%	23.99
3	-	-	64.404%	24.17	68.774%	25.81

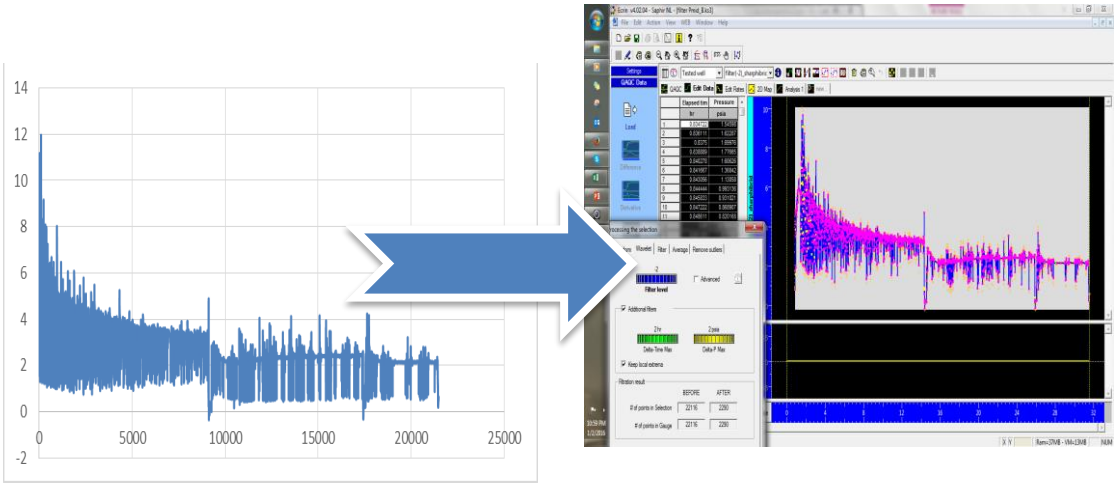

Figure 4.1 Pressure Drop Filtering Exp-1

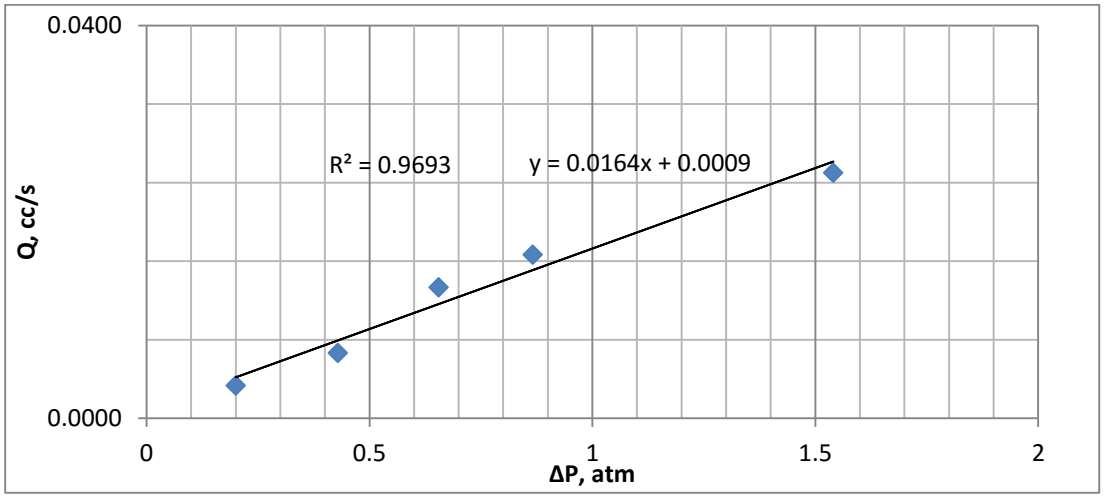

Figure 4.2 Rate versus Pressure drop during Ko Measurement Exp-1

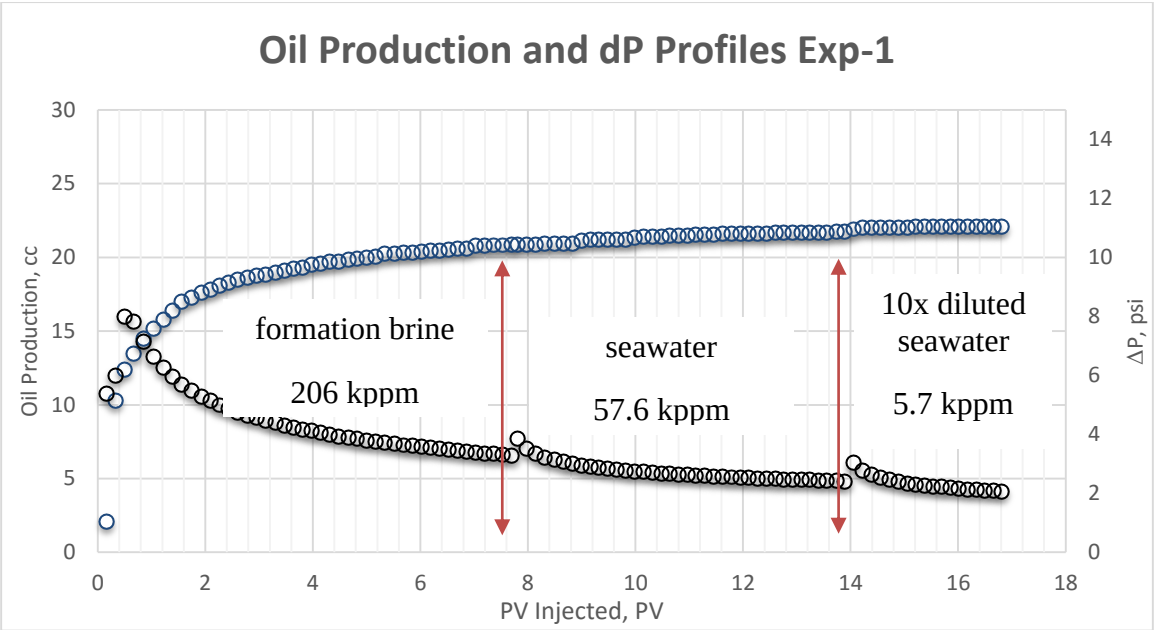

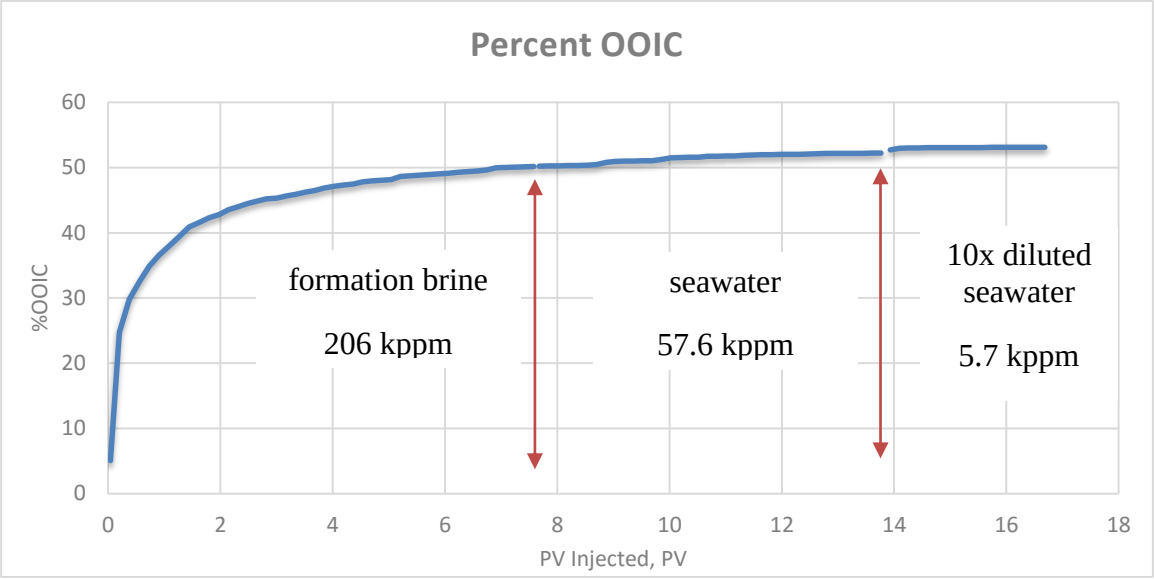

Figure 4.3 Oil Production, %OOIC and dP Profiles of Exp-1

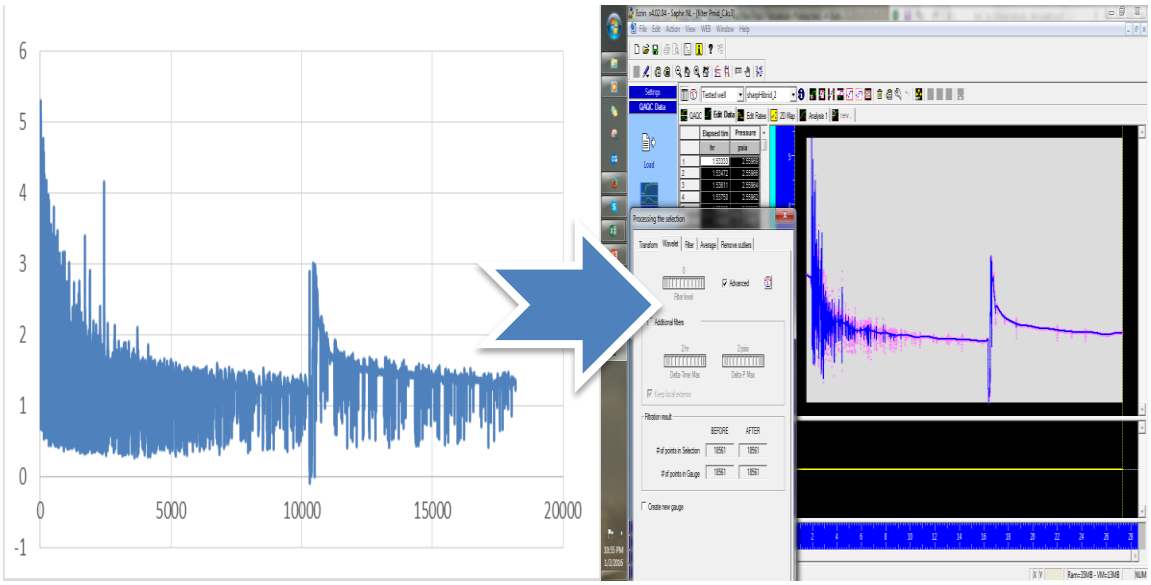

Figure 4.4 Pressure Drop Filtering Exp-2

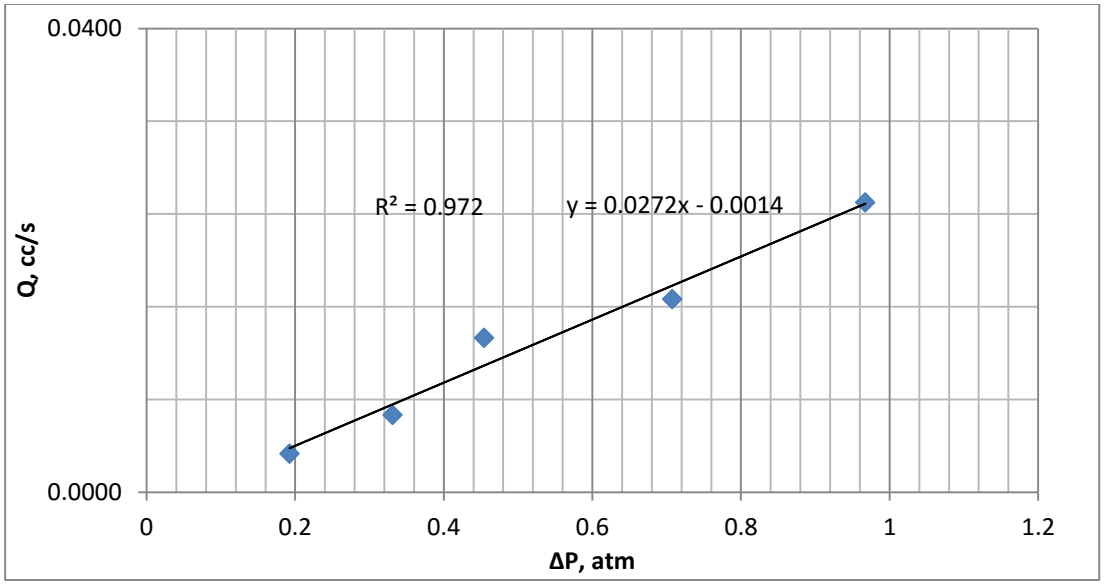

Figure 4.5 Rate versus Pressure drop during Ko Measurement Exp-2

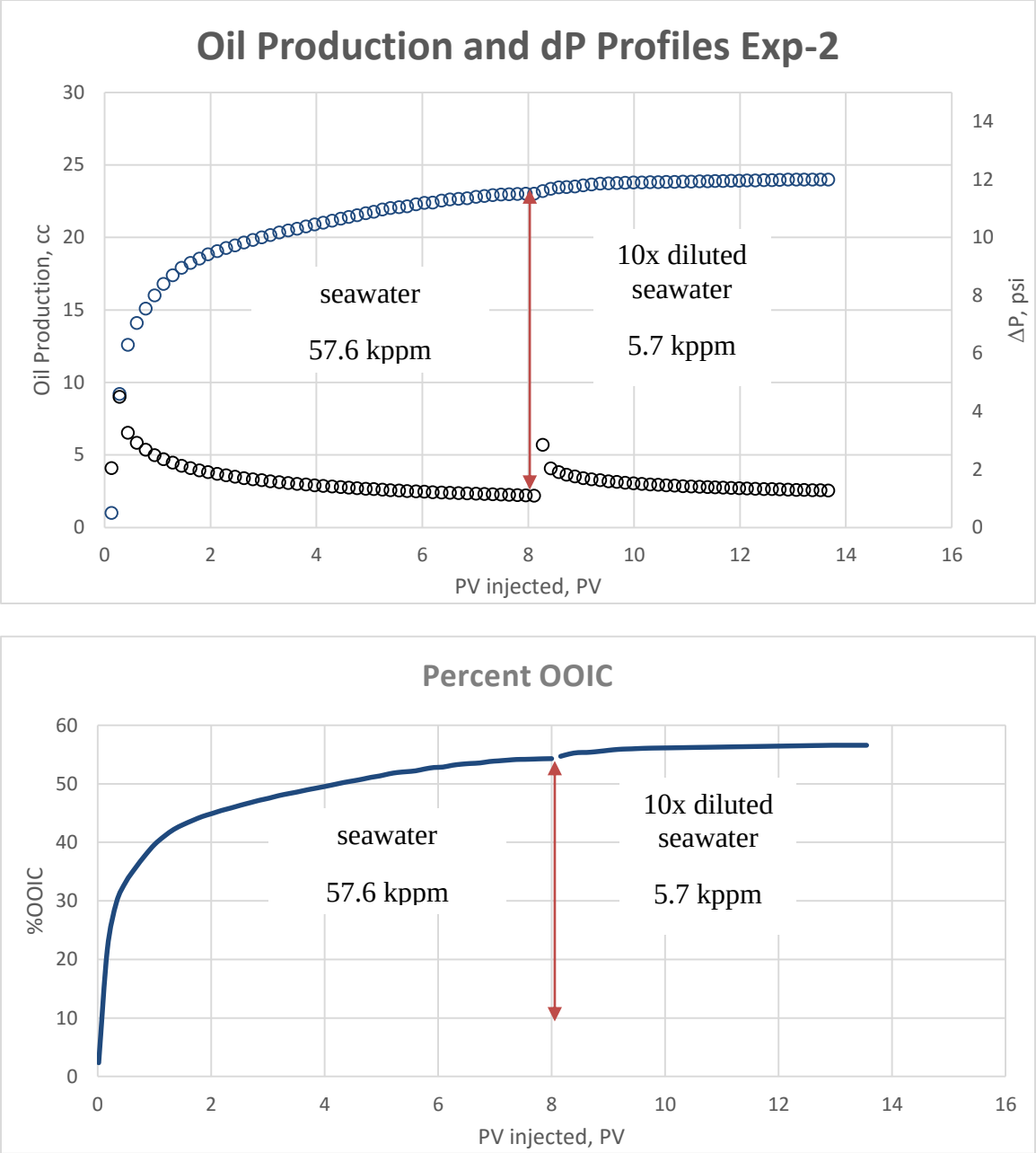

Figure 4.6 Oil Production, %OOIC and dP Profiles of Exp-2

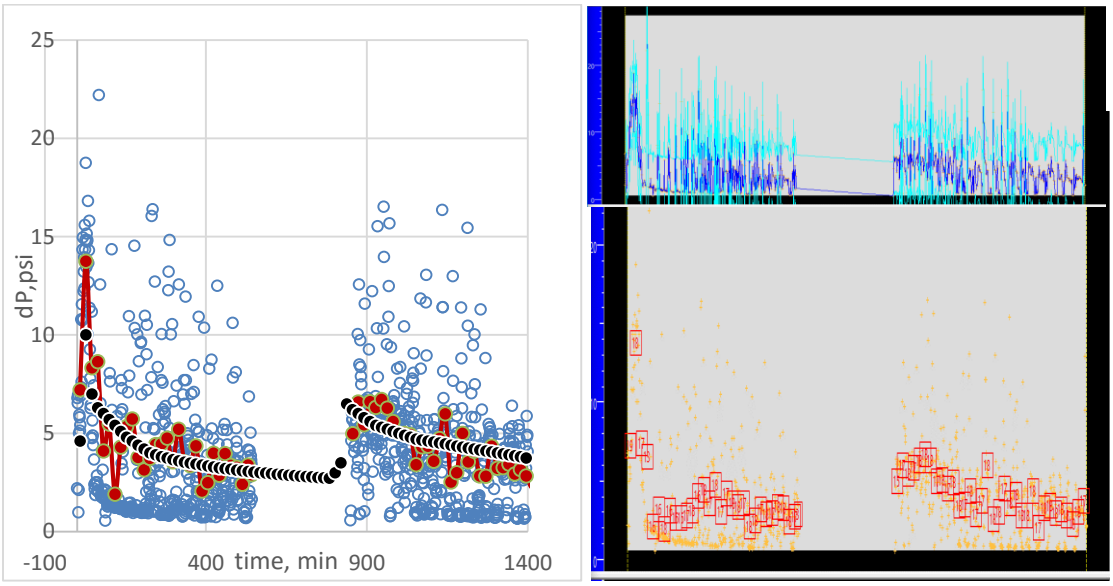

Figure 4.7 Pressure Drop Filtering Exp-3

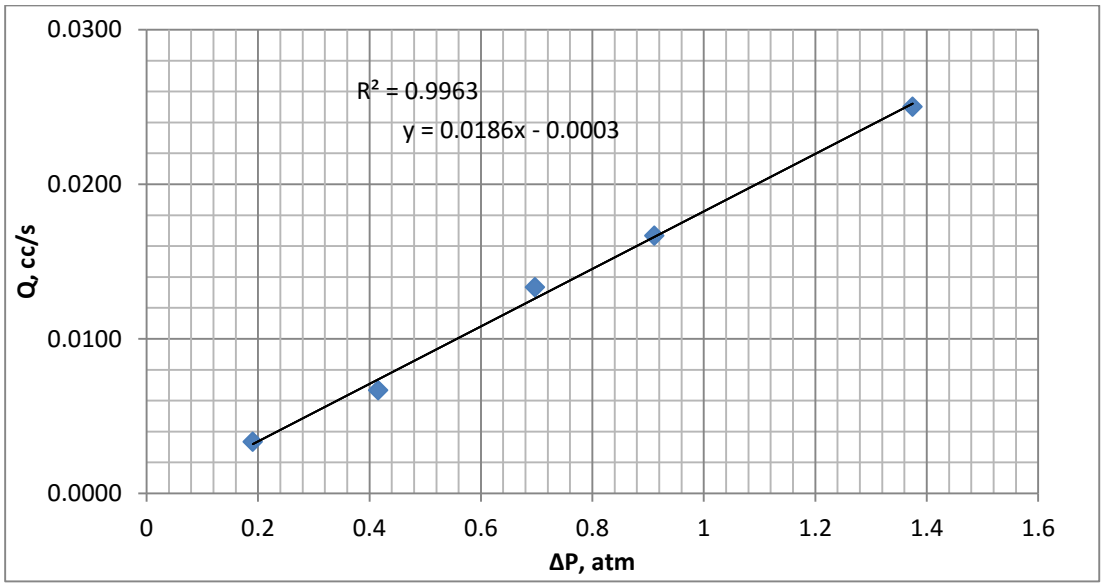

Figure 4.8 Rate versus Pressure drop during Ko Measurement Exp-3

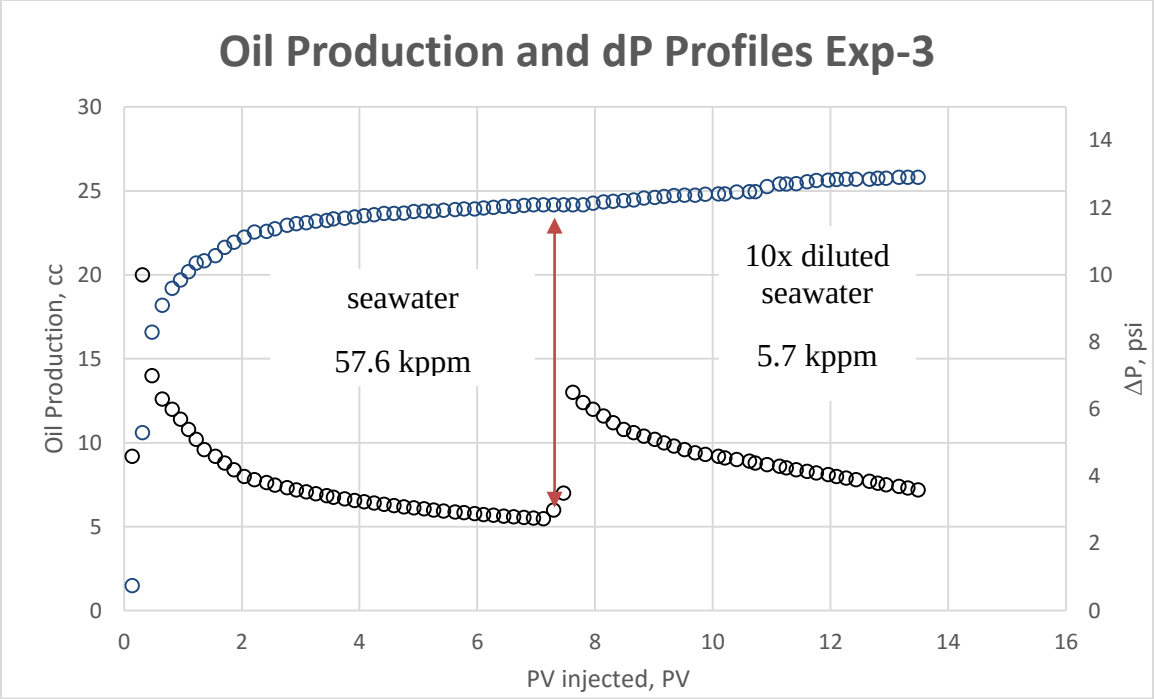

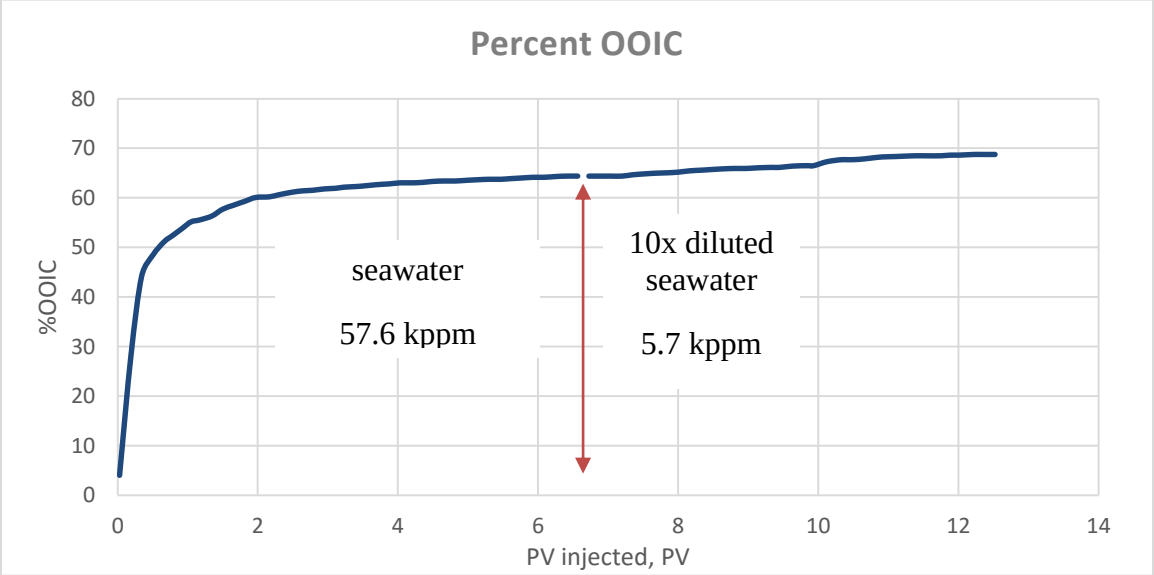

Figure 4.9 Oil Production, %OOIC and dP Profiles of Exp-3

4.1.2 Post Core flooding Measurements

Other important results to be noted are analyzing the effluent results and NMR test of the cores before and after coreflooding experiments at fully saturated stage. Some predetermined cations (Ca^{2+}, Mg^{2+}, Na^{+}) and anions (SO_4^{2-}, Cl^{-}) are analyzed using IC-Metrohm with a crosscheck from ICP-MS instruments. Another anion which is HCO_3^{-} is analyzed with manual titration method. While, pH and conductivity have been also measured with pH-meter and electric conductance meter.

Aqueous phase of these effluent tubes are separated from the oil using filter paper with size of 0.5 – 5 μm and syringe. The aqueous phase were kept in a screw sealed vials and submitted for effluent analysis. It should be noted that not all effluent tubes are analyzed. Thus, several tubes are taken to represent the effluent profiles of all experiments as presented in figure 4.10.

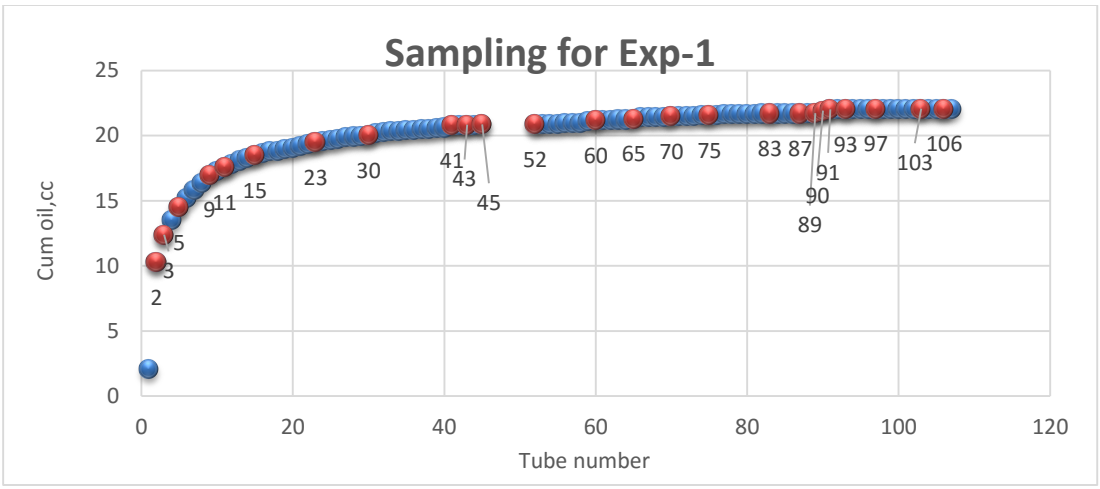

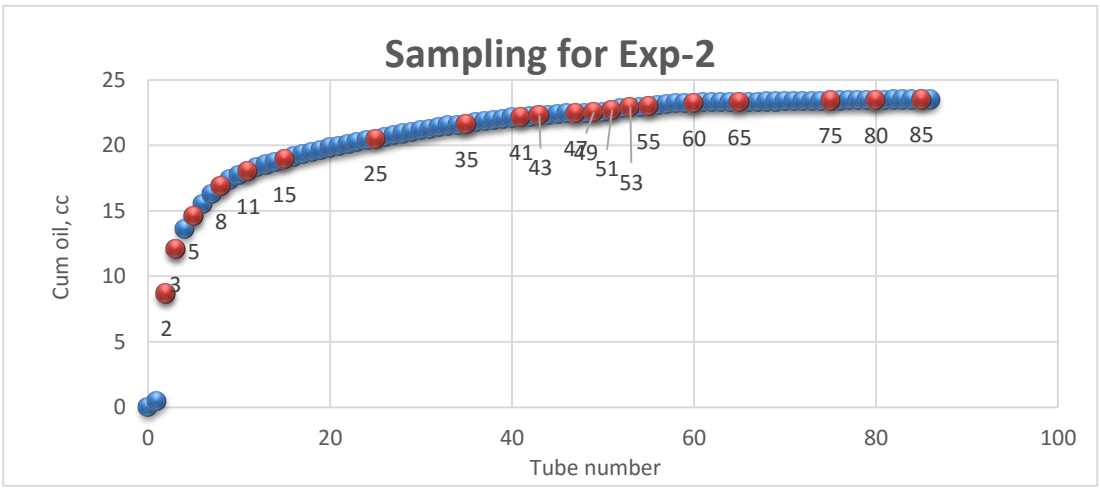

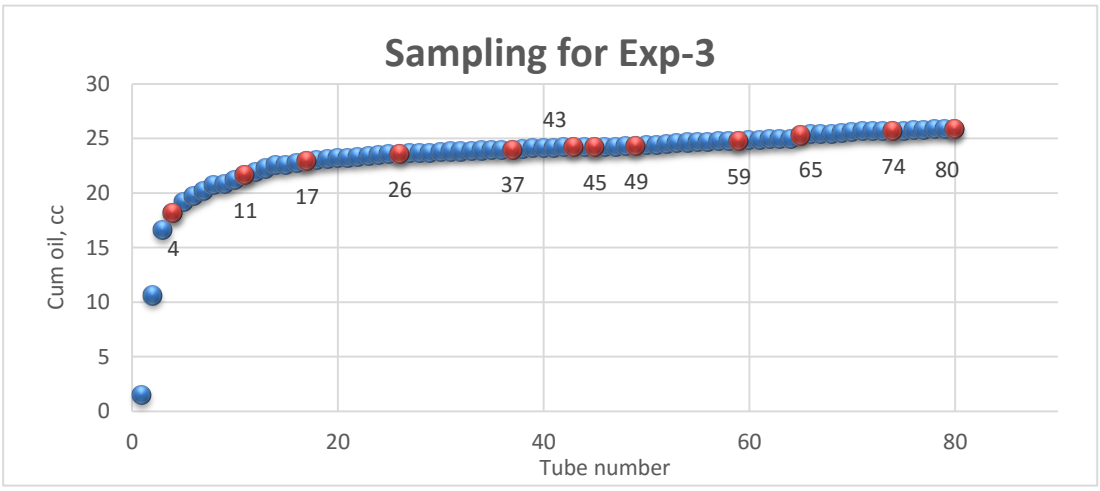

Figure 4.10 Sampling Tube from Fraction Collector

Ion profiles

Two instruments were first used to analyze the effluent, IC-Metrohm and ICP-MS. the results of both methods are relatively close to each other. Some quite difference between the two measurements is mainly shown in calcium ion. This could be due to interference in ICP-MS, as gas Argon (39,9) used as injection fluid has an atomic mass that is close to the atomic mass of Calcium (40). Nonetheles overall measurements of both methods show good concictency in their trends.

Figures 4.11 to 4.13 show the cation profiles while figures 4.14 to 4.16 show the anion profiles of all experiments as analyzed by IC-Metrohm. The black lines are reference lines of injected fluids. The cation profiles, clearly show that in experiment 1 and 2, there is no or relatively insignificant changes during the first injection sequence as same water was used for S_{wi} and for displacement of oil (figures 4.11 a and b – 4.16 a and b). A little changing is addressed as mineral equilibrium process with particular fluid. Later on, just before switching to another injection brine, the cations dropped to the reference lines of injected fluid except for calcium ion in Smart water injection during all experiments. The profiles are a little bit off from reference line which might indicate slow reaction againts calcium ions due to additional calcite dissolution, or might be surface adsorbtion. Moreover, anion profiles for first injection in Experiments 1 and 2 are also align with the reference injected fluid. Interesting trends of bicarbonate during smart water injection indicates similar behavior of calcium ion. An attempt to clarify these phenomena will be described and further discussed in geochemical simulation in Chapter 5.

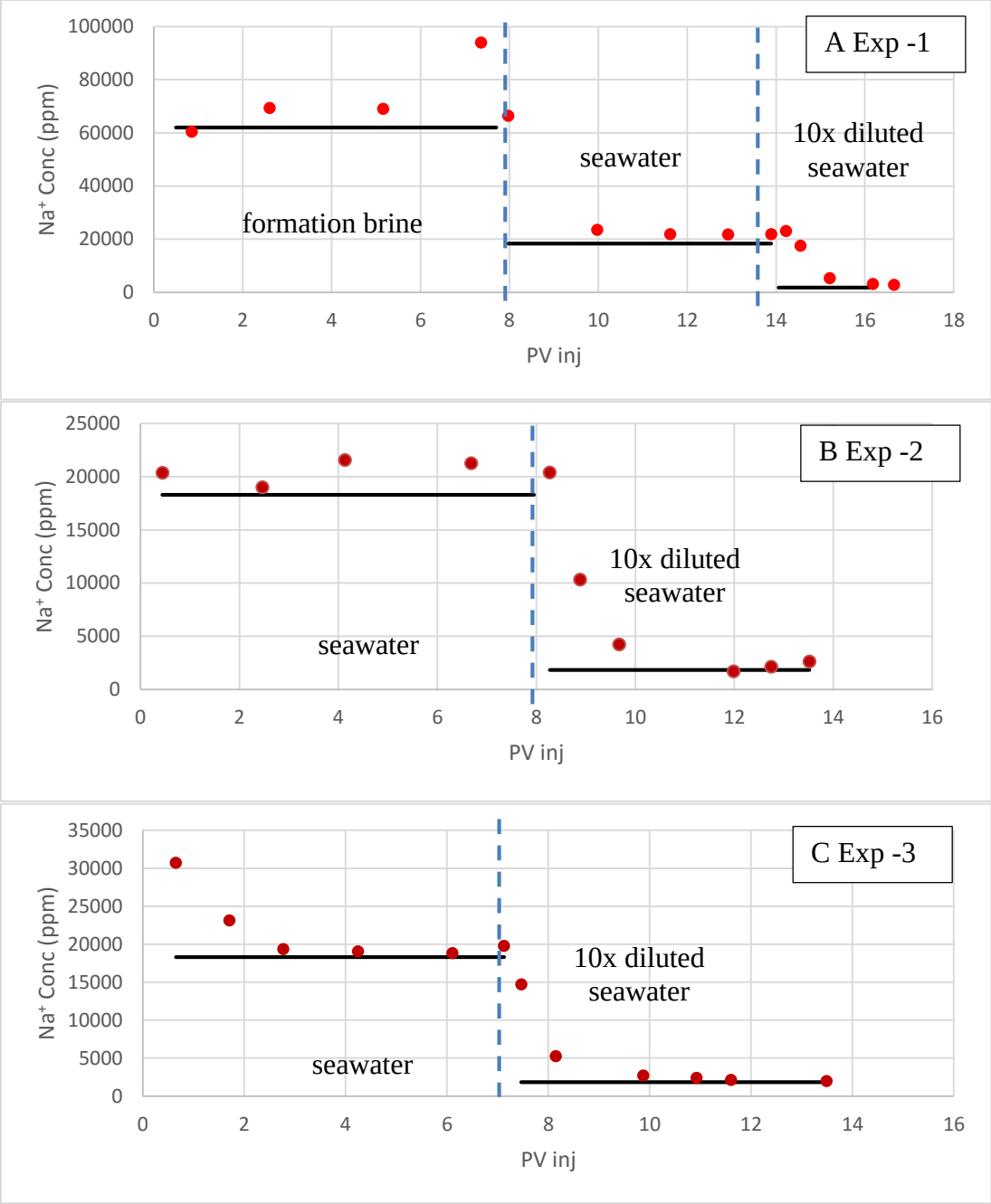

Figure 4.11 Na^+ Ion Profiles in All Experiments

Na^+ ion in all experiments shows that it follows injection fluid level even during smart water injection. As expected since Na^+ ion will behave like a passive tracer that will not react during injection.

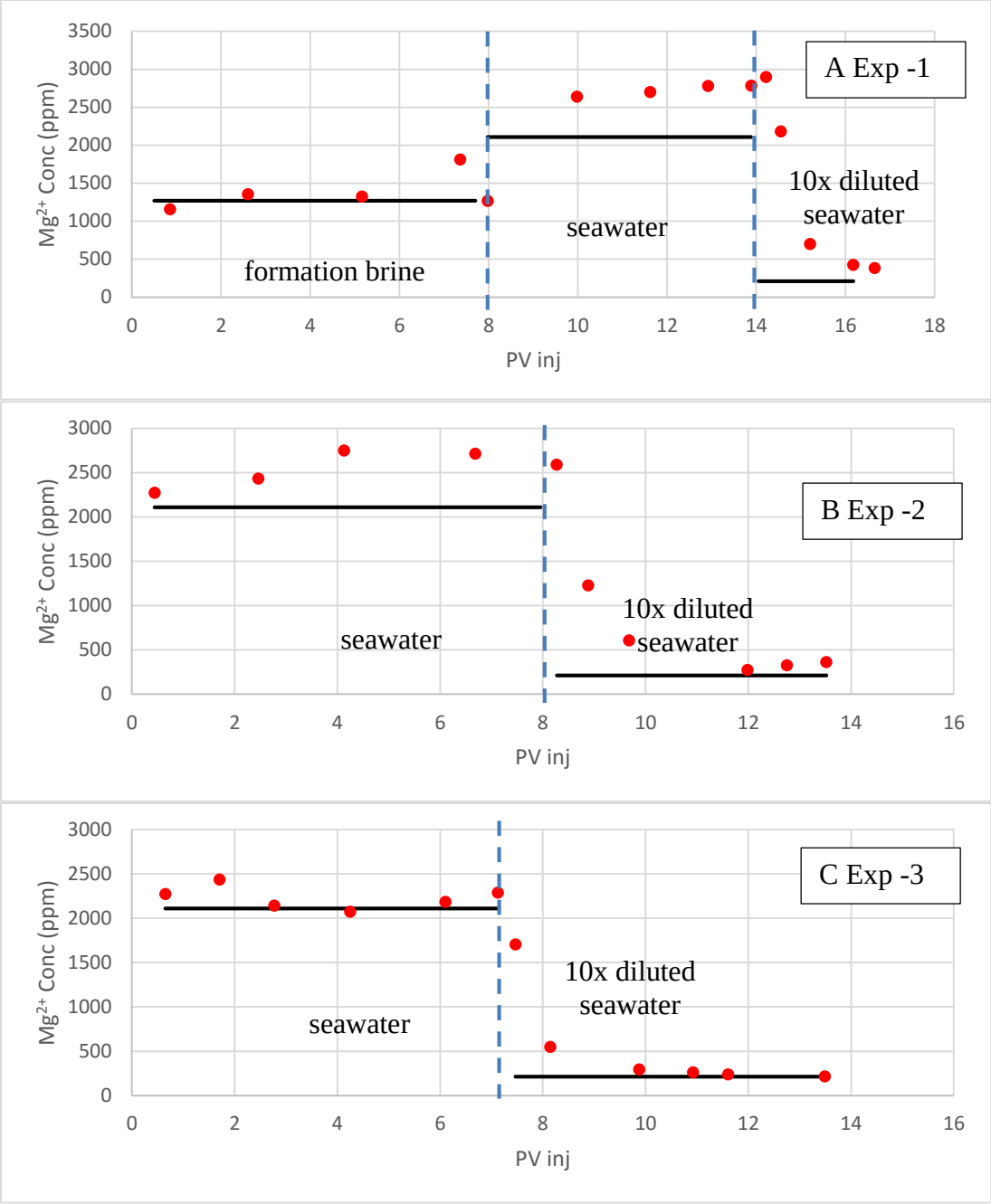

Figure 4.12 Mg^{2+} Ion Profiles in All Experiments

Mg^{2+} ion in all experiments will approach injection fluid level even during smart water injection. In experiment-1 and 2, Mg^{2+} ion show slightly higher profile in seawater injection than experiment-3. It can be addressed as some additional dolomite dissolution, but most likely less mixing time on that particular sample during dilution before IC test.

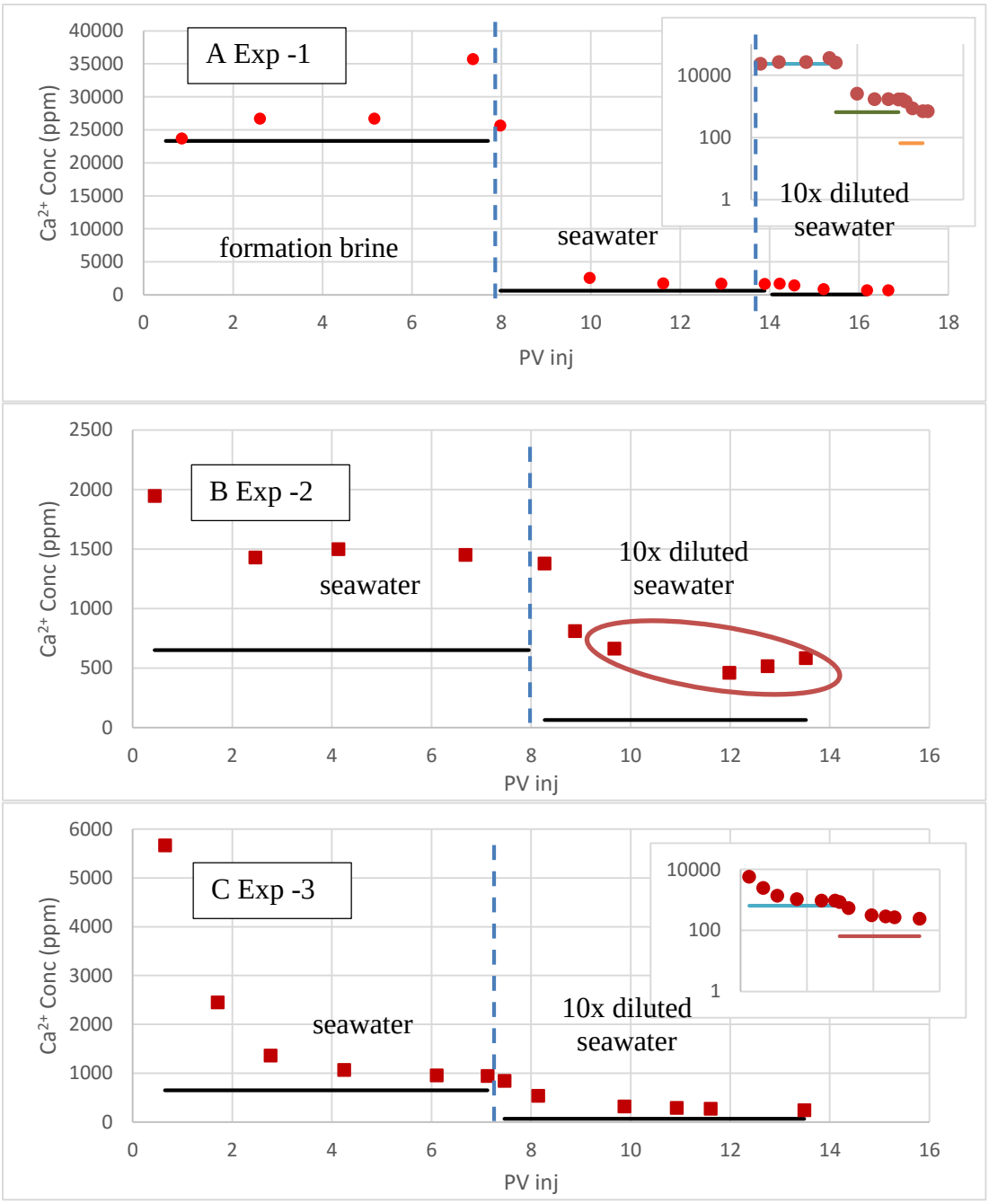

Figure 4.13 Ca^{2+} Ion Profiles in All Experiments (Small graphs show Semilog scale)

Ca^{2+} ion will approach formation brine level during experiment-1, while during seawater injections they show a little big gap to seawater level then relatively even bigger gap during smart water injection as shown in semilog scale in experiment-1 and 3.

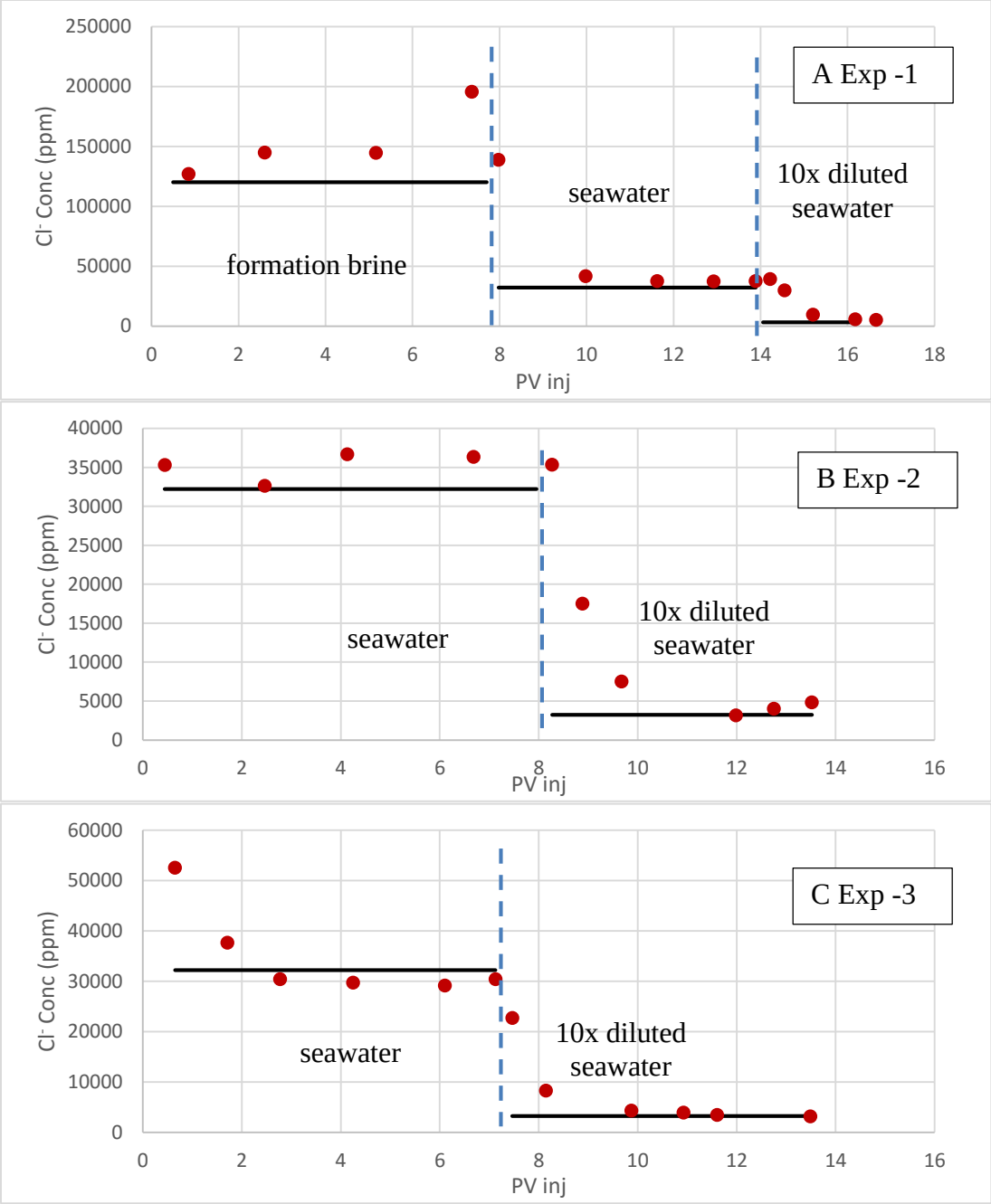

Figure 4.14 Cl^- Ion Profiles in All Experiments

Similar to Na^+ ion, Cl^- ion will approach injection fluid level during all experiment since it behaves like passive tracer.

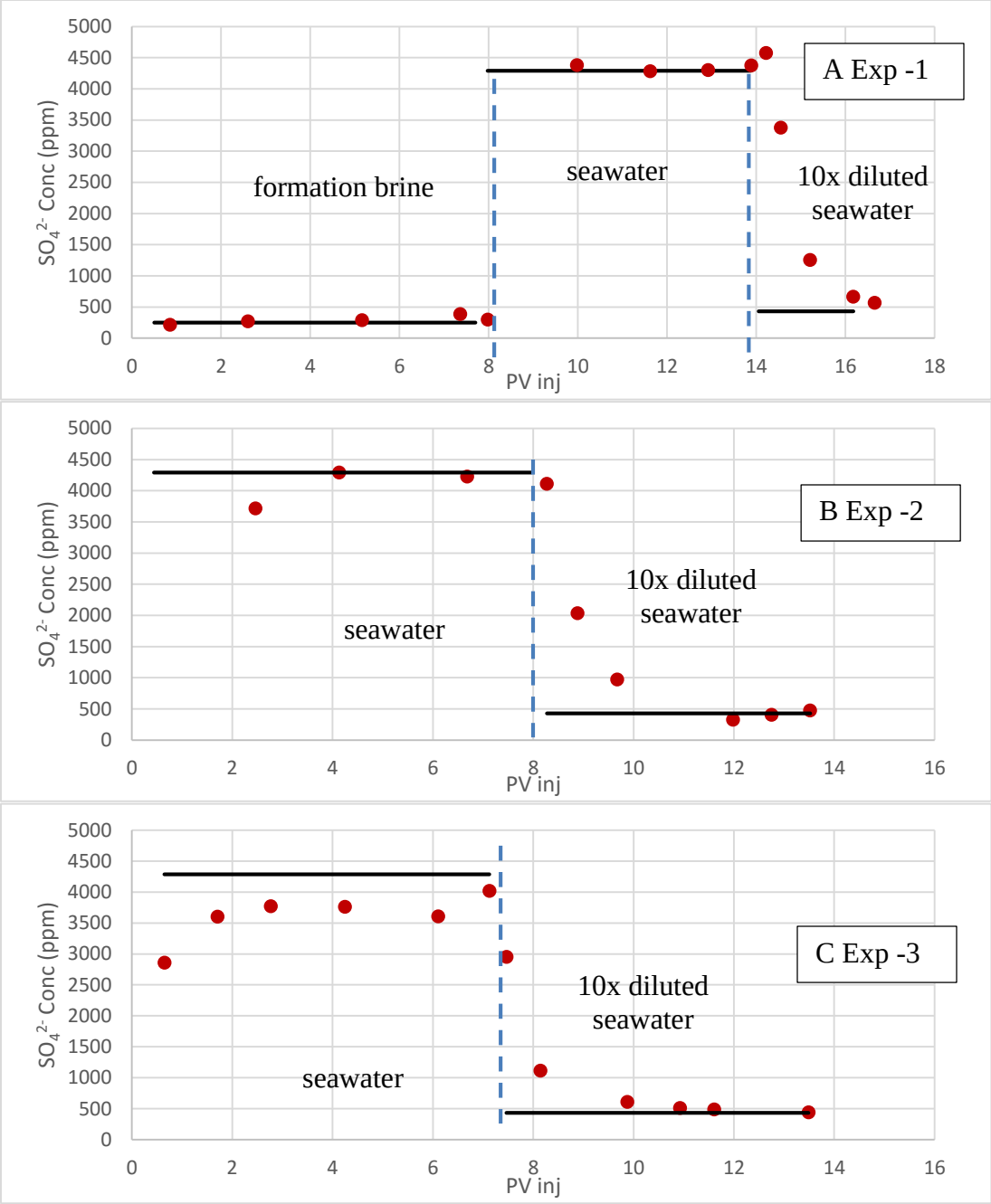

Figure 4.15 SO_4^{2+} Ion Profiles in All Experiments

SO_4^{2-} ions show that they also follow injection fluid level even during smart water flooding. It might indicate very less tendency of anhydrite dissolution (anhydrite phase is not present in mineralogy, see chapter 5) during smart water /low salinity flooding.

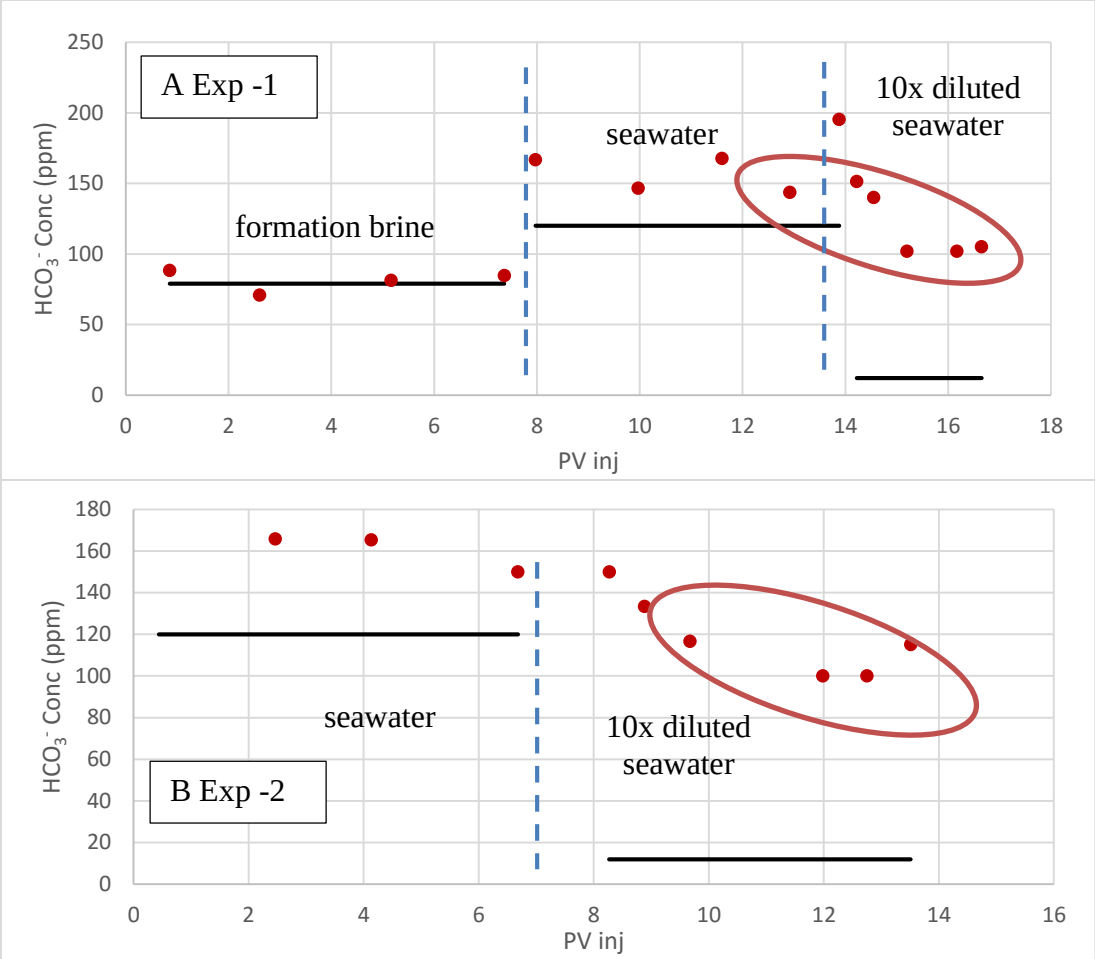

Figure 4.16 HCO_3^- Ion Profiles in All Experiments

HCO_3^- ions for experiment-1 and 2 show similar trends with Ca^{2+} ion. They show a little big gap to seawater level then relatively even bigger gap during smart water injection. This profile gives indication of the impact of smart water during coreflooding experiment.

pH and conductivity profiles

Figures 4.17 to 4.19 show the pH and conductivity/resistivity profiles during all experiments. As expected from the conductivity or resistivity profiles, as the total dissolve solid in the effluent fluid decreases, it becomes less conductive. It should be noted that, just before switching to another injection brine, the conductivity or resistivity profiles show clear stabilization period which is expected from the experimental design.

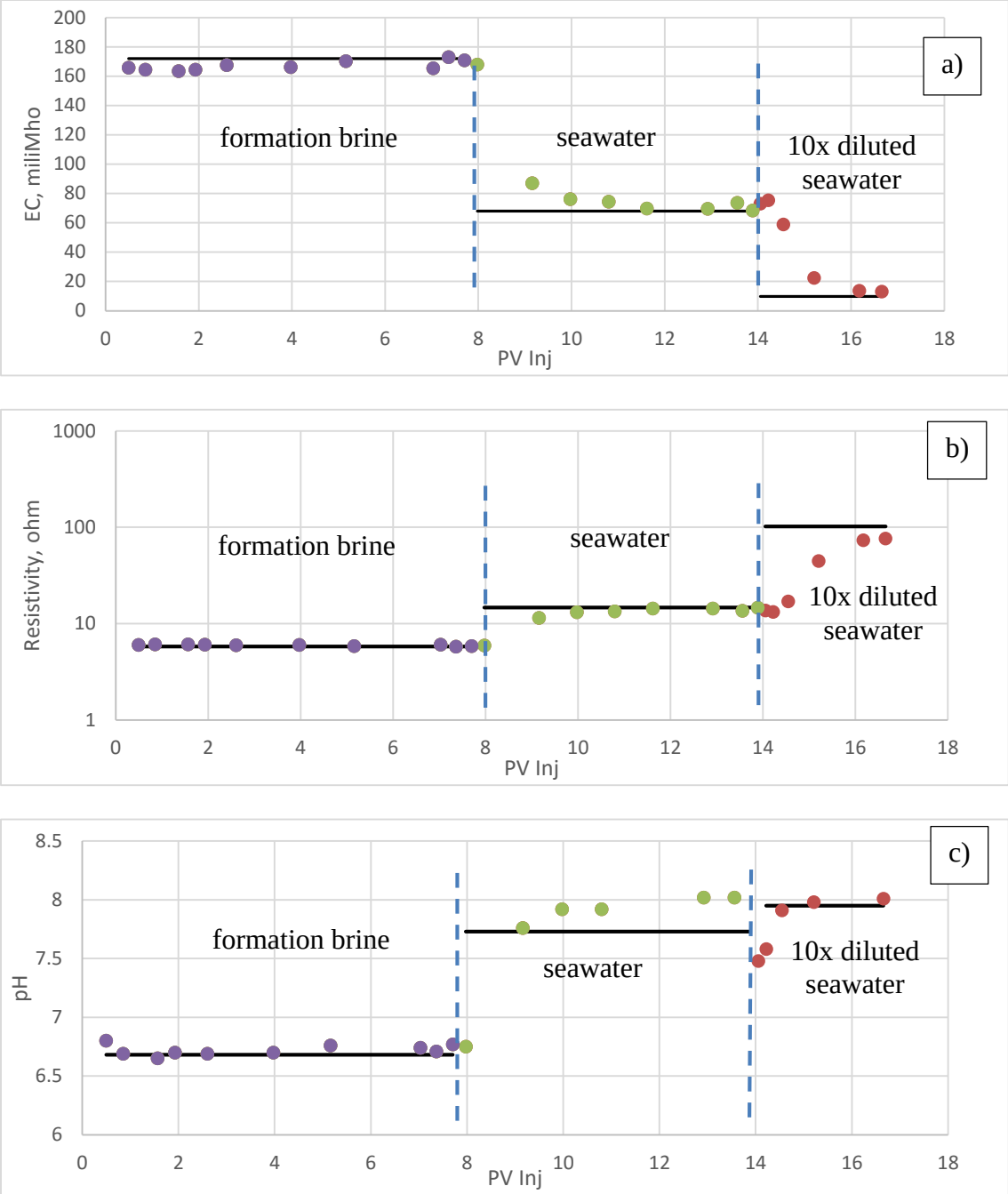

Figure 4.17 Experiment -1 Electric Conductivity (a), Resistivity (b) and pH profiles (c) , solid lines are injected fluid level

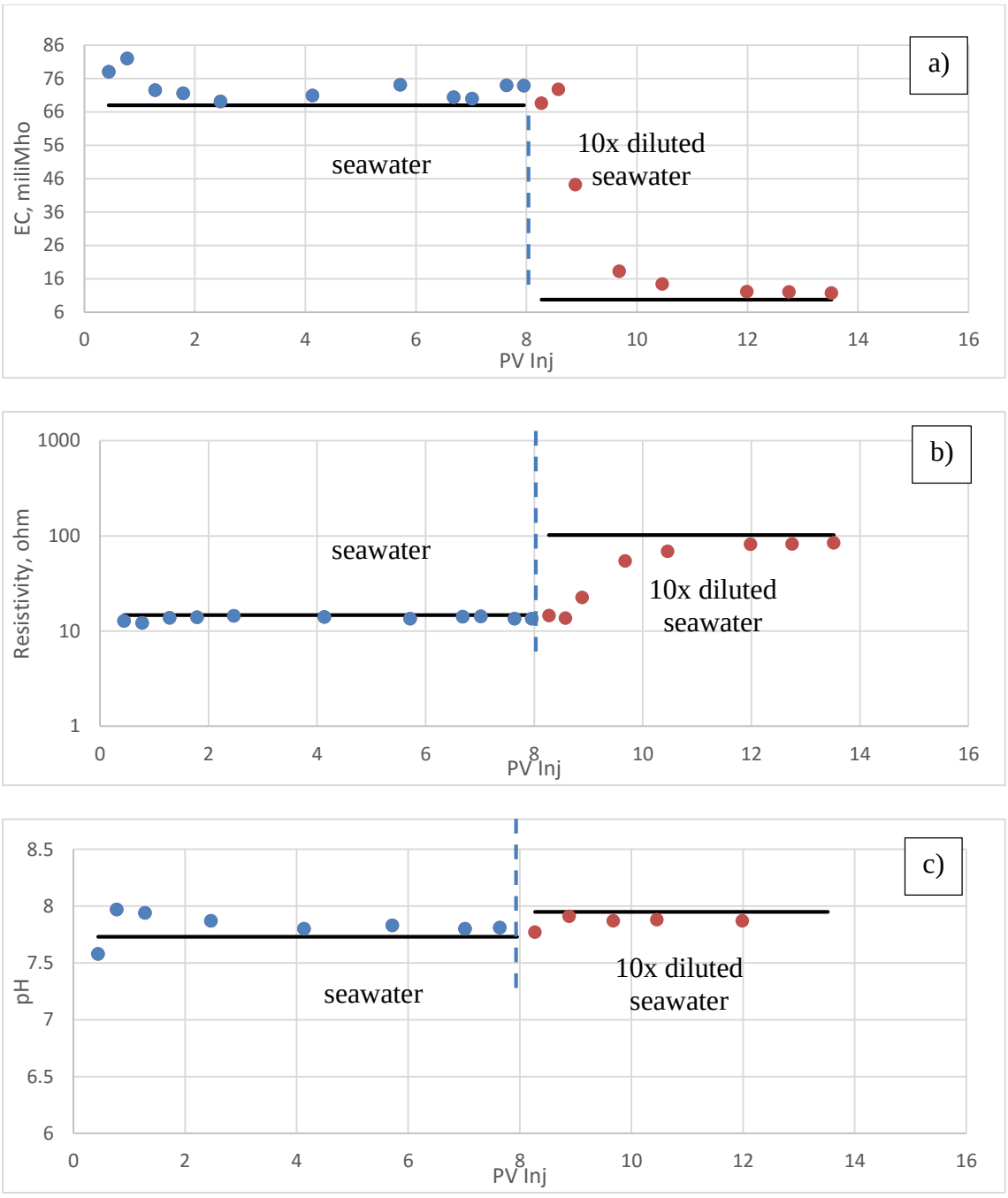

Figure 4.18 Experiment -2 Electric Conductivity (a), Resistivity (b) and pH profiles (c), solid lines are injected fluid level

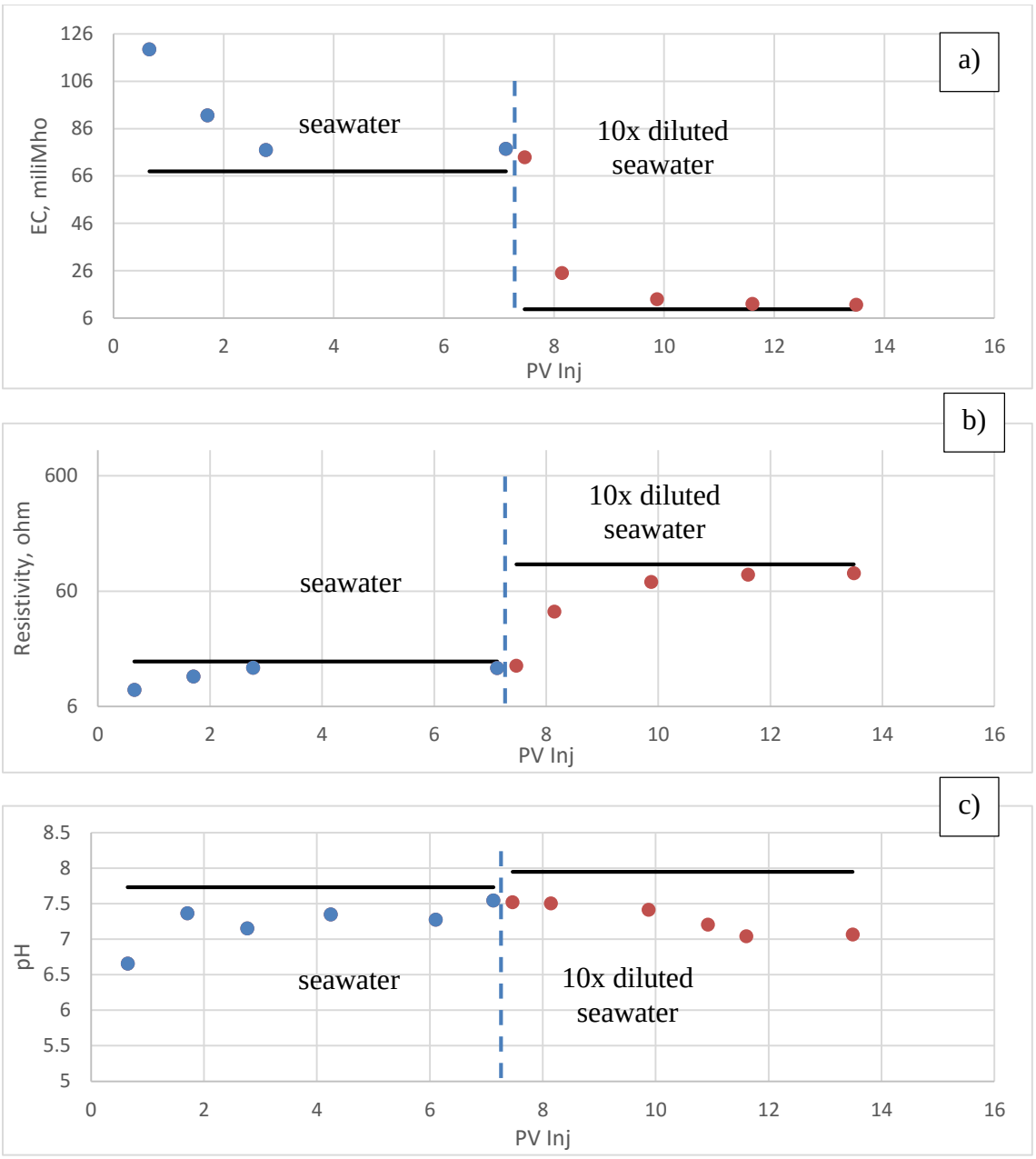

Figure 4.19 Experiment-3 Electric Conductivity (a), Resistivity (b) and pH profiles (c), solid lines are injected fluid level

While for pH profile, it shows relatively small magnitude of changing, in the range of 6 to 8. The profiles do not give clear difference during brine switching but initial changes is identified once the brine switching begin.

NMR images

NMR test before and after core flooding will give an idea about changes in the pore network distribution due to Smart water flooding. These tests are conducted at the same condition where the core is saturated with single brine fluids. Thus, after the core flooding experiments, these cores were cleaned and then re-saturated again with the same brine as preparation before core flooding. In general, there are changes but relatively not significant changes in T2 NMR profiles before and after test, which might indicate there is minor dissolution processes taking place during Smart water flooding. Figures 4.20 to 4.22 present individual comparison of each piece of core samples NMR tests in both experiments.

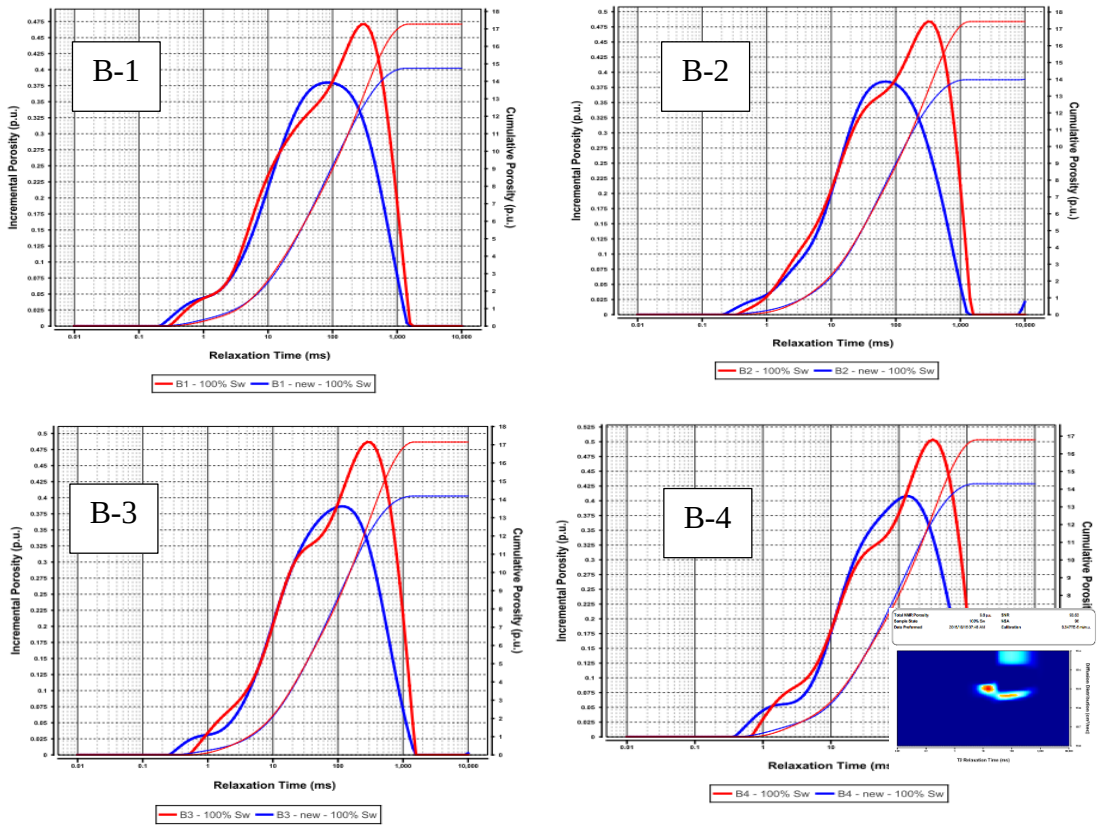

Figure 4.20 NMR profiles of Exp-1 (red = before CF and blue = after CF), small graph shows existence of remaining oil from T2 and Diffusion NMR test

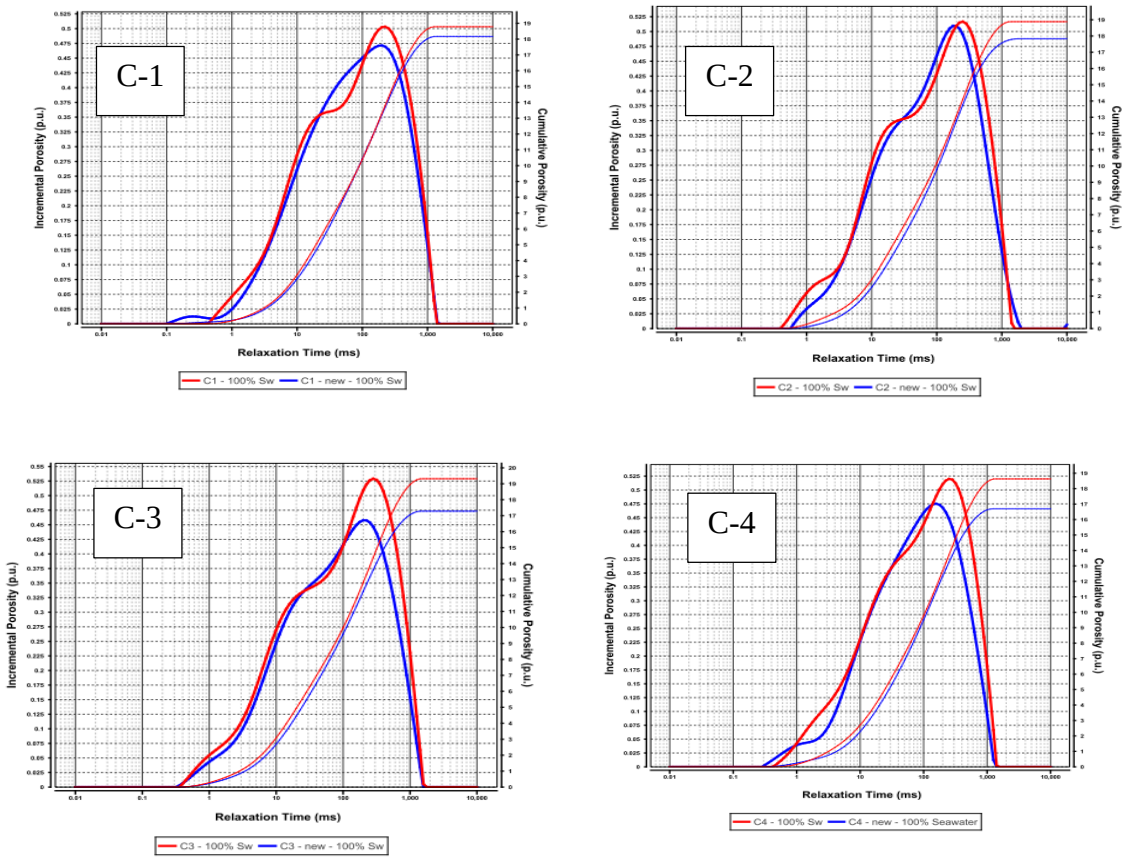

Figure 4.21 NMR Profiles Exp-2 (red = before CF and blue = after CF)

In experiment-1 there is a profound gap between T2 NMR profiles before and after the test. After further investigation using T2 and Diffusion NMR test, it shows that there is another different fluid exist in the core, most likely at the surface and inside the pores which indicates that there is certain amount of oil left after cleaning the cores. Whereas in experiment-2, the profiles show good agreement of similarity before and after core flooding. To be noted that in core B4 and C4 the NMR test difference mainly due to the trimmed section of these cores.

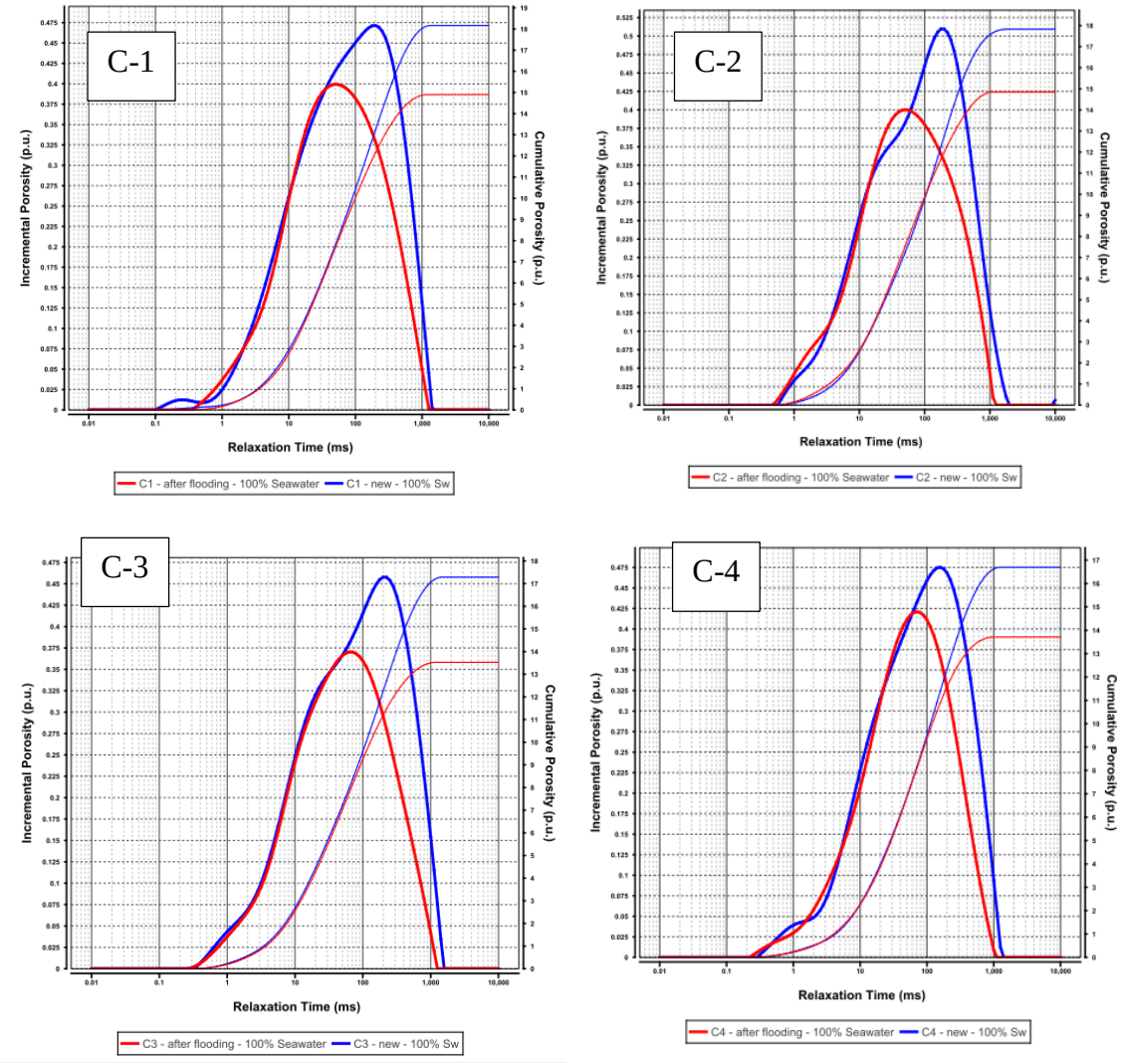

Figure 4.22 NMR Profiles Exp-3 (red = after CF and blue = before CF)

In experiment-3 there is also a profound gap between T2 NMR profiles before and after the test. The gap magnitude is similar to core set B used in experiment-1. It is suspected that certain amount of oil still remains after cleaning the cores (only a week period of cleaning). Regarding the dissolution process, close T2 NMR profiles indicate that in experiment-3 minor dissolution process might took place.

4.2 Interpretation of Experimental Results

All necessary results have been collected from the unsteady state core flooding experiments and their effluents analyses. These data show indications of the impact of Smart water flooding. This particular section will utilize pressure and production data to obtain relative permeability data by JBN Method. Moreover effluent data will be utilized as identification of Smart water brine behavior.

4.2.1 JBN Method Calculation

JBN (Johnson, Bossler, and Naumann) method is a common and reliable method to analyze production and pressure drop data from unsteady state core flooding results to obtain relative permeability. In this study the contribution of capillary pressure and capillary end effects are neglected**.** However, the rate was selected using scaling criteria to minimize the effect of capillary end effect as presented in Chapter 3.

In the unsteady state core flooding, JBN method uses the production data from the breakthrough point onwards. Then, the method begins calculation of average water saturation ($S_{w,avg}$), relative injectivity (I_r), oil fractional flow (f_o), and a derivative of I_r. Right after these calculations, water saturation at the outlet face of core ($S_{w,2}$) and relative permeabilities (k_{ro} an k_{rw}) can be obtained. To validate derived relative permeability from JBN method, back calculation of production data using Buckley Leverett is conducted to obtain oil recovery matching, while pressure drop matching will be obtained from the numerical simulation model. Figure 4.23 shows schematic of JBN method and its analytical validation.

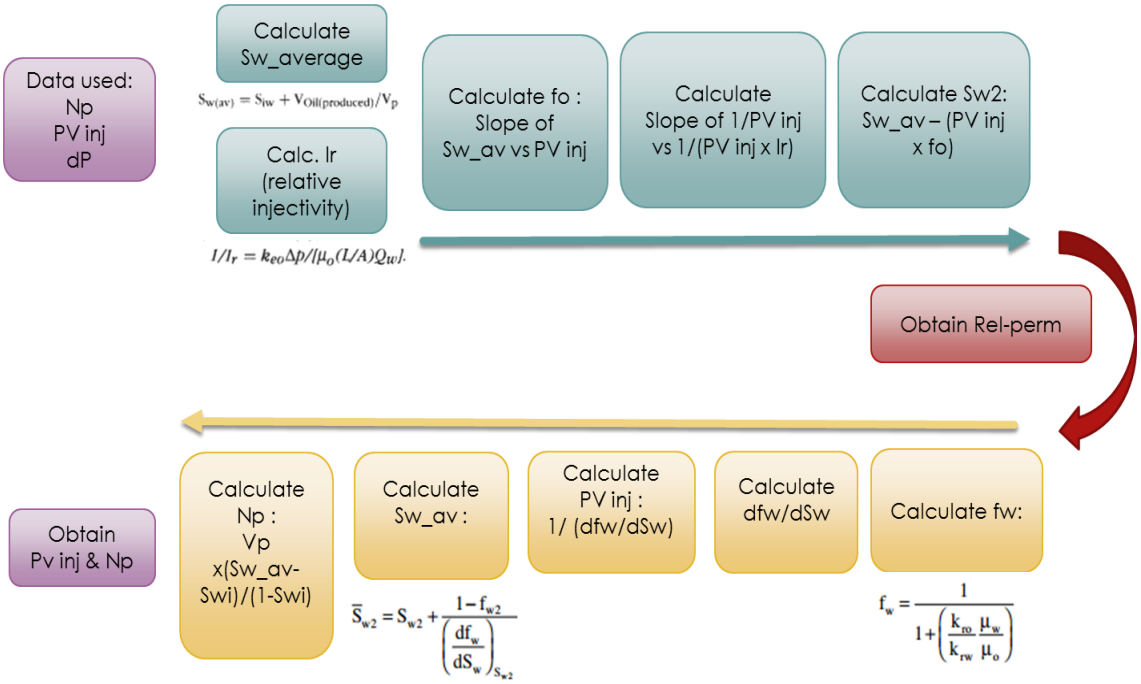

Figure 4.23 JBN Method Calculation Scheme

The procedure presented will yield single set of relative permeability. Since each experiment is sequential core flooding, thus the next injection brine will start right after last pore volume injection, and the pore volume injected in this section will start from the beginning. The quality of derived relative permeability depends on how good the trend of $S_{w,avg}$ vs PV to obtain f_o then S_w and the trend of $I/(PV*I_r)$ vs $1/PV$ to obtain k_{ro}-k_{rw} and ΔP. Another option to calculate $1/PV$ vs $I/(PV*I_r)$ is using trend of ΔP versus ln PV directly which is less sensitive, also because $1/I_r = (\Delta P / \Delta P_i)*PV$. Profiles of $S_{w,avg}$ vs PV, ΔP vs ln PV and comparison of calculated f_o from slope of $S_{w,avg}$ vs PV are presented in figures 4.24 to 4.26 for experiment-1, figures 4.29-4.30 for experiment-2 and figures 4.33-4.34 for experiment-3. In comparison of calculated f_o , the black line represent f_o calculated from the slope of $S_{w,avg}$ vs PV and blue points represent calculated data $\Delta S_{w,avg} / \Delta PV$.

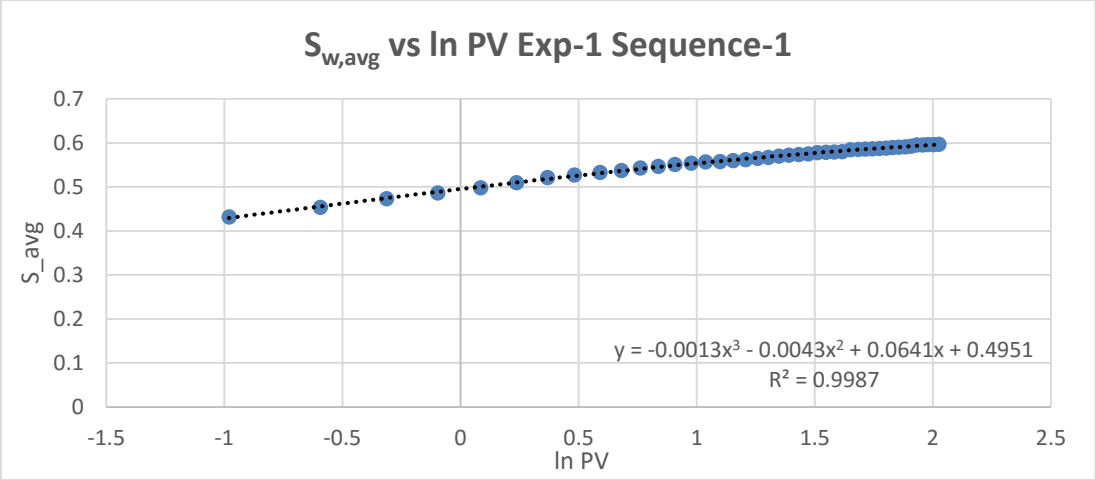

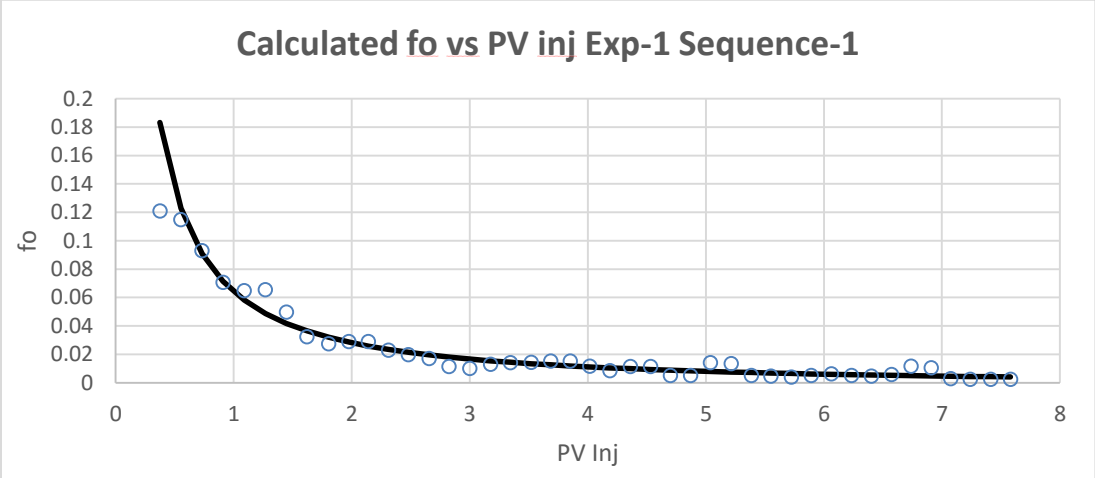

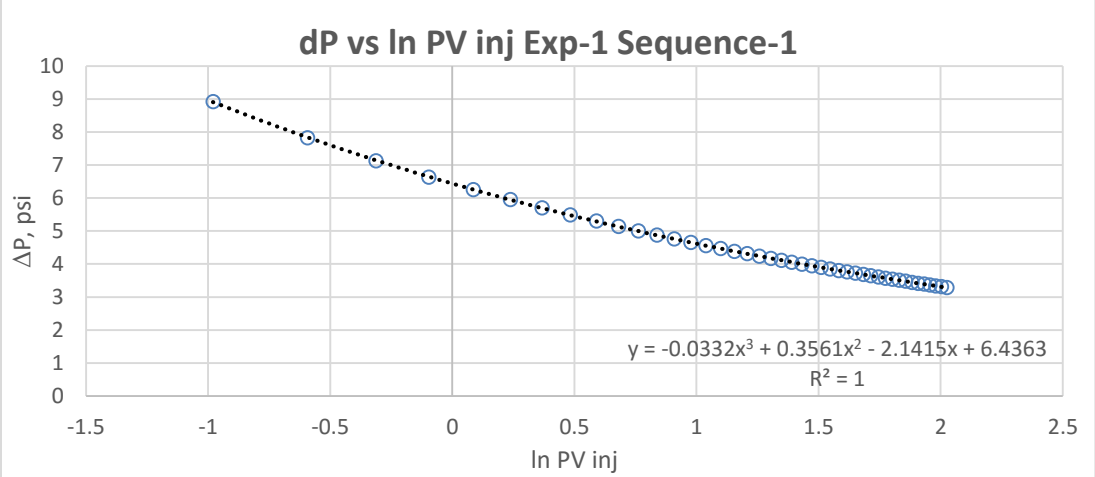

Figure 4.24 Curve fitting in JBN calculation for Exp-1 First Injected Fluid (formation brine)

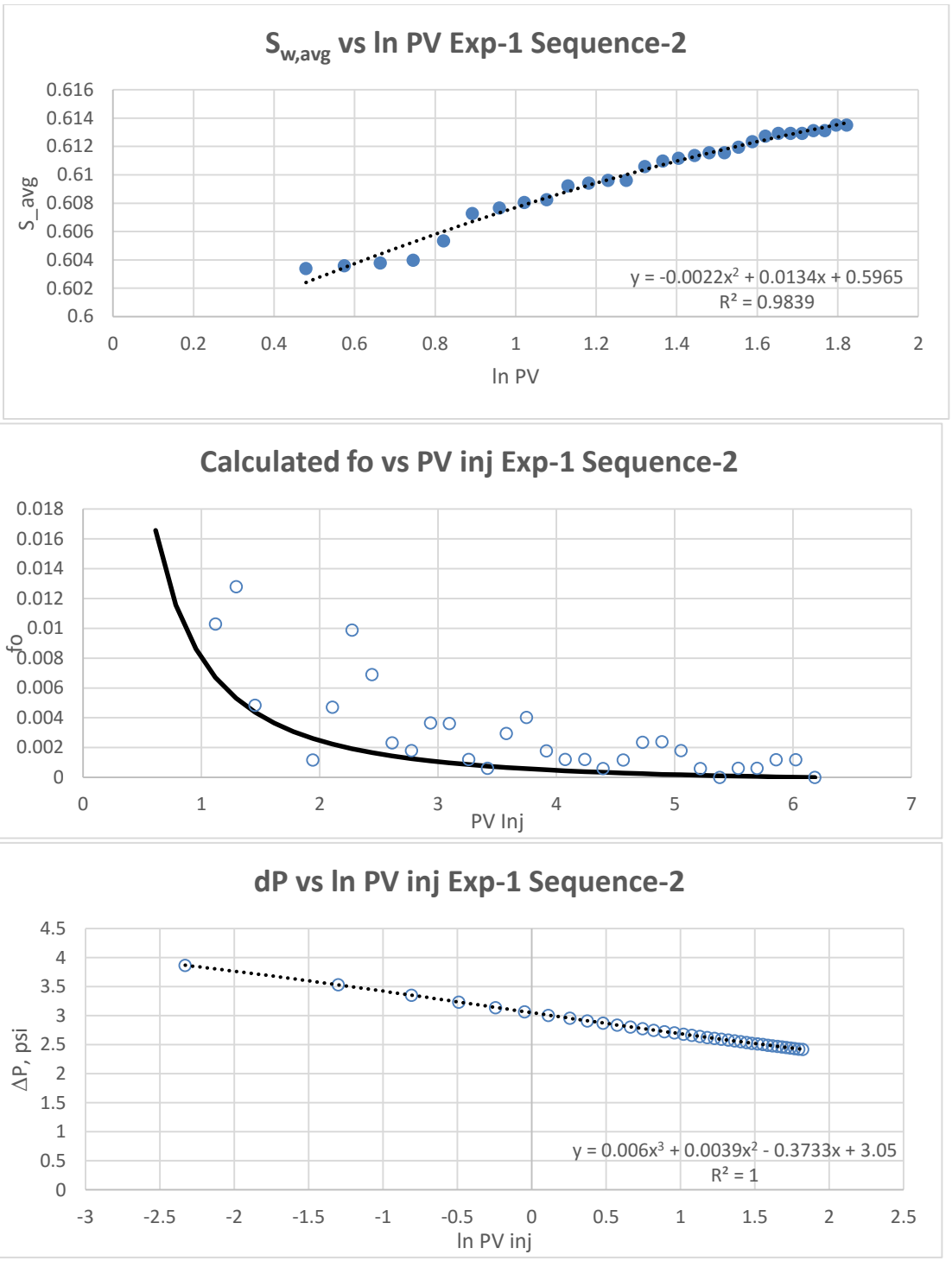

Figure 4.25 Curve fitting in JBN calculation for Exp-1 Second Injected Fluid (seawater)

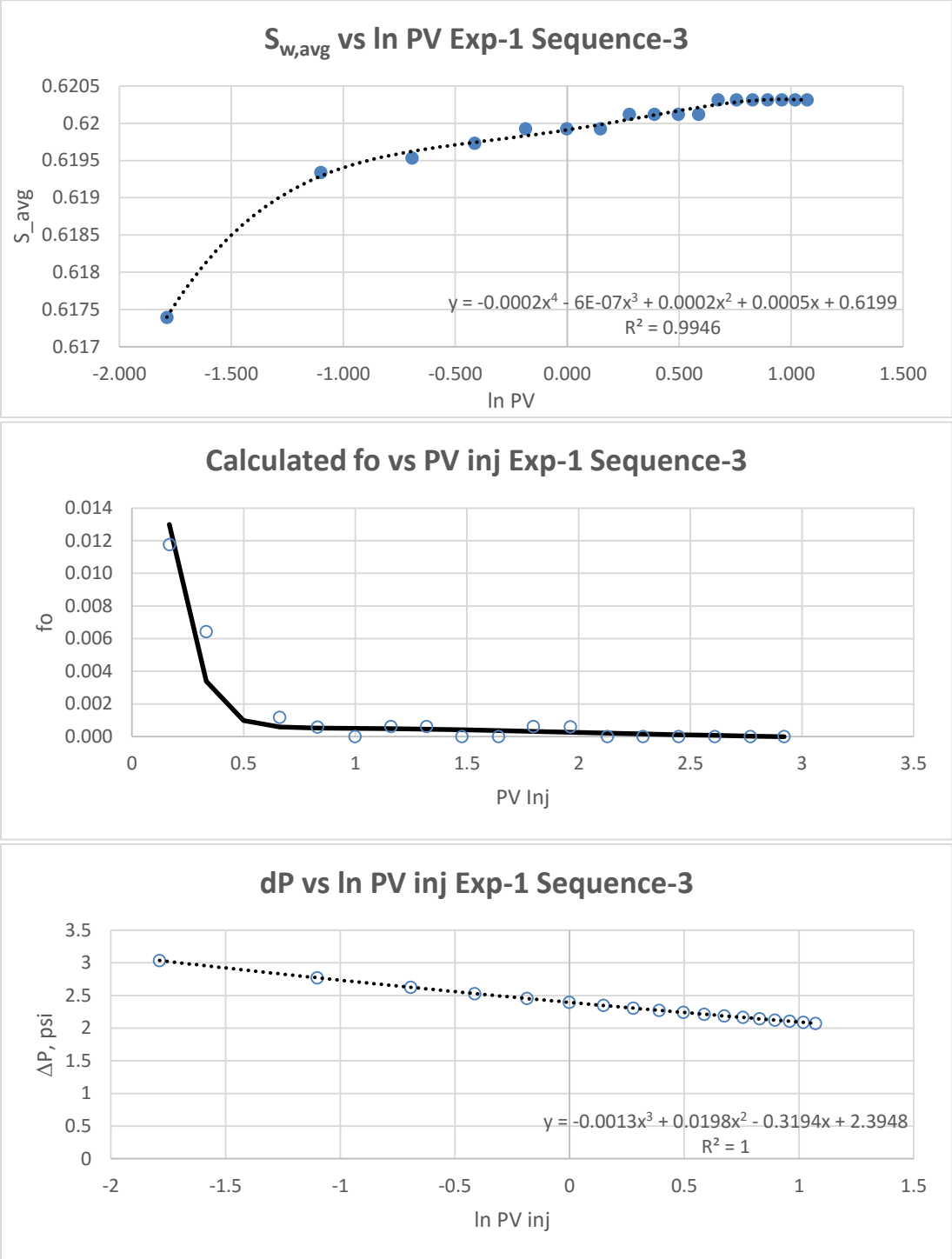

Figure 4.26 Curve fitting in JBN calculation for Exp-1 Third Injected Fluid (10x Diluted seawater)

After getting f_o and derivative of $I/(PV*I_r)$ vs $1/PV$ from its profiles, relative permeabilities of each sequence in experiment-1 can be calculated by multiplying particular fo and derivative of $I/(PV*I_r)$ vs $1/PV$, as shown in figure 4.27. Then back calculation matching using generated relative permeabilities can reproduce good match of oil recovery profile of its experiments as shown in figure 4.28.

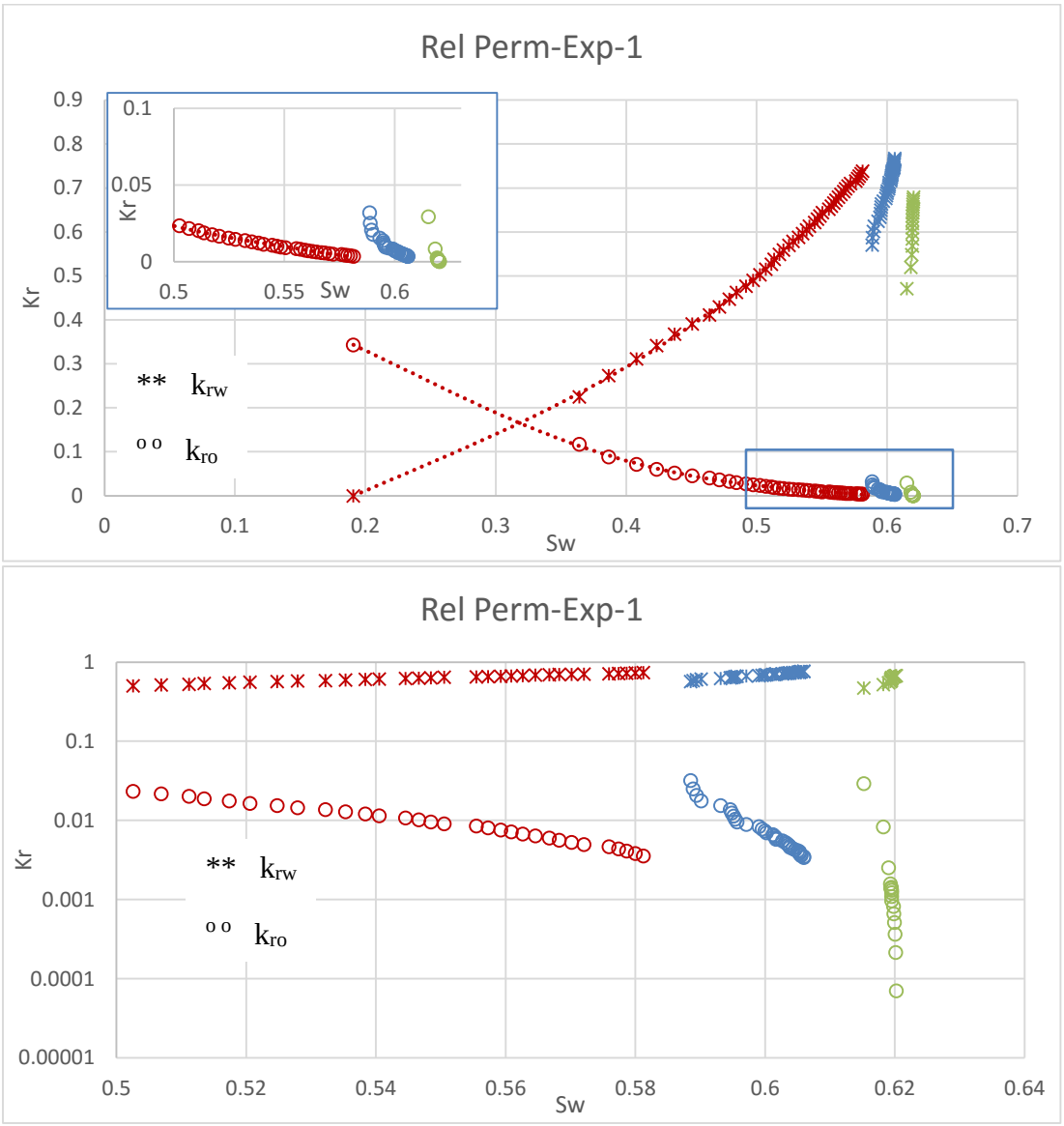

Figure 4.27 Rel Perm of Experiment-1 in normal scale (top) and semilog scale (bottom); red = formation brine, blue = seawater, green = 10x diluted seawater

Relative permeabilities of experiment-1, shows that oil relative permeabilities of seawater and 10 times diluted seawater are shifted upward after reaching Sor of last injections as shown in semilog scale in figure 4.27. It confirms that there is a potential benefit during smart water (10x diluted seawater) particularly.

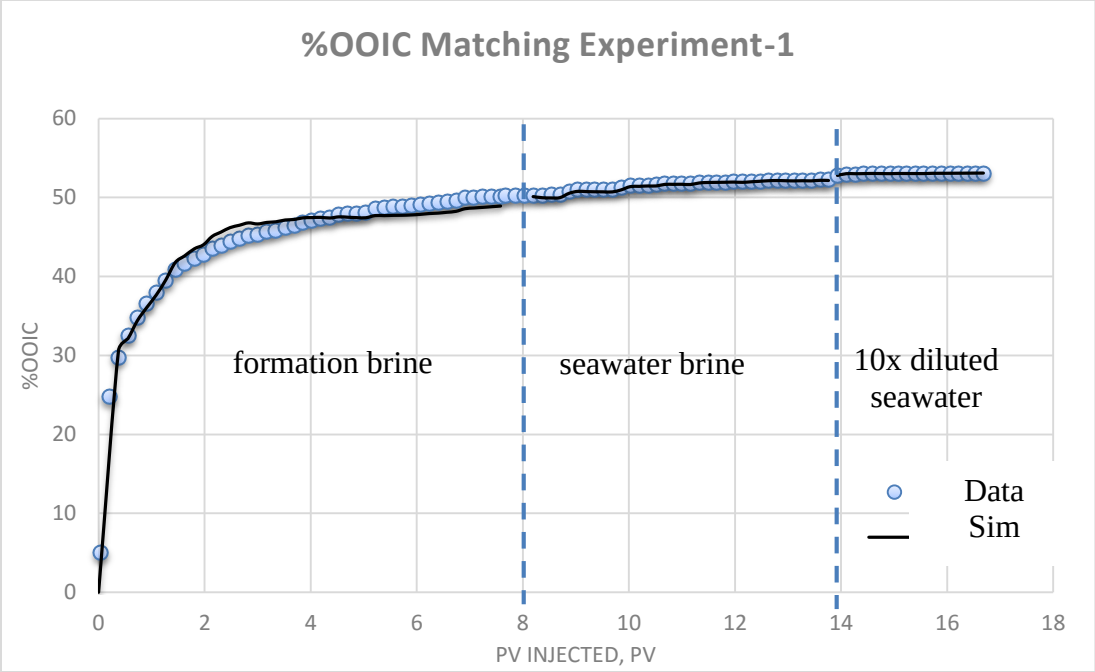

Figure 4.28 Oil Recovery Matching in Exp-1 using Rel Perm of JBN Technique

Oil recovery matching in experiment-1 using back calculation in figure 4.28 is satisfactory enough. Thus its relative permeabilities will be used to match oil recovery and pressure drop in numerical simulation of experiment-1.

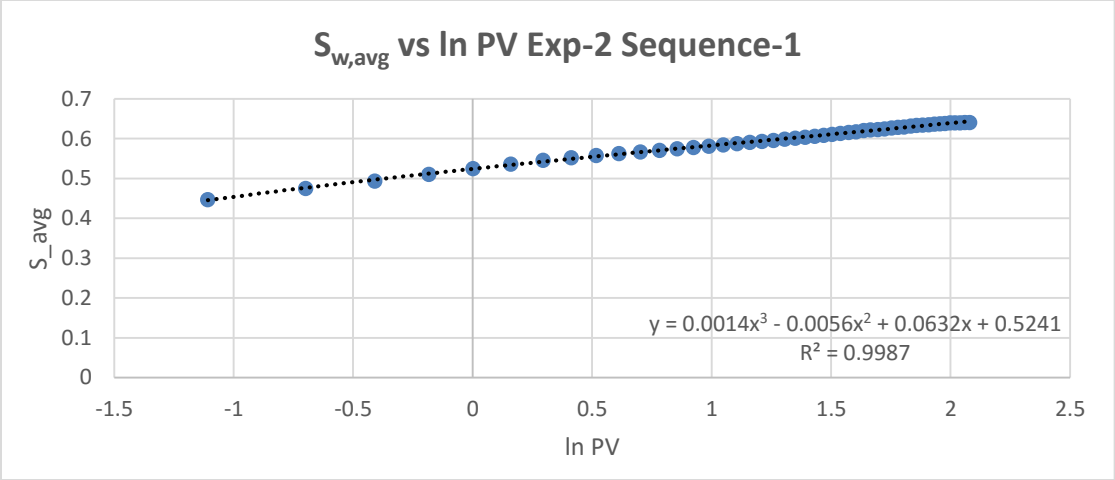

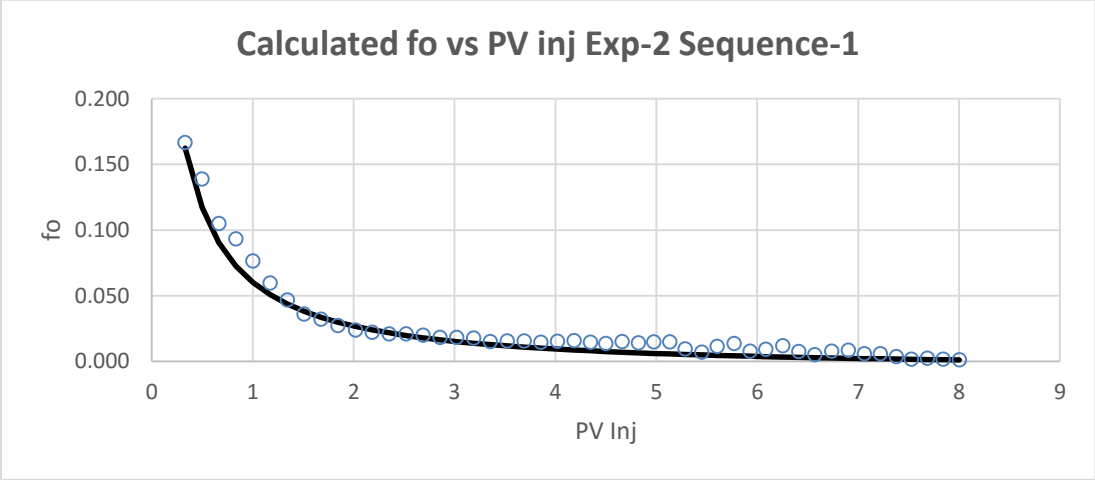

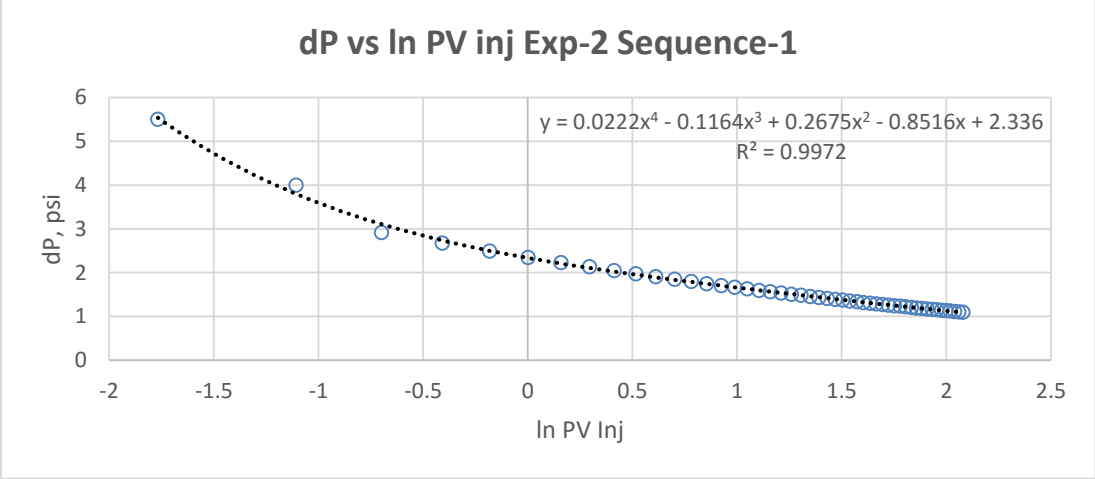

Figure 4.29 Curve fitting in JBN calculation for Exp-2 First Injected Fluid (Seawater)

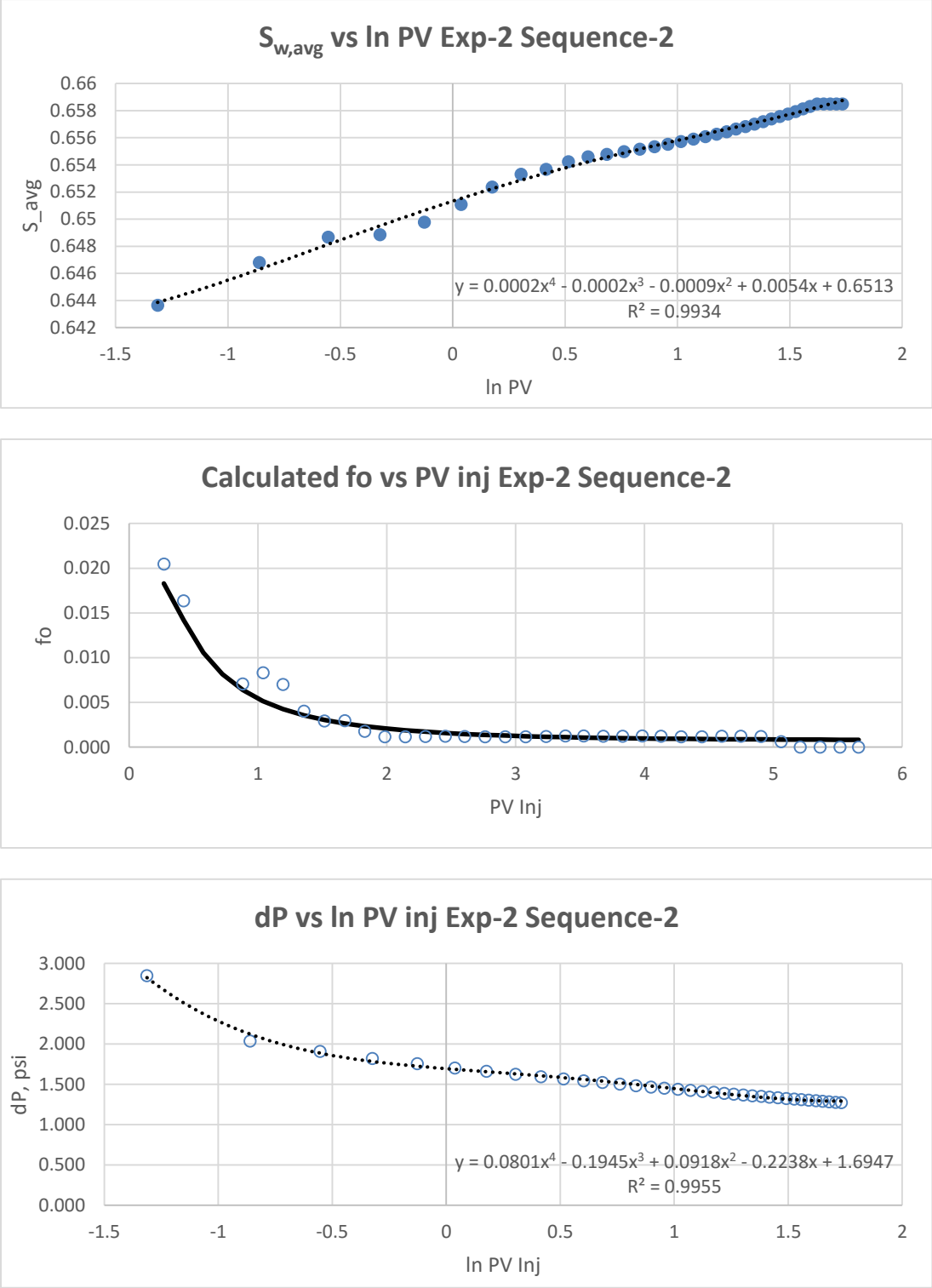

Figure 4.30 Curve fitting in JBN calculation for Exp-2 Second Injected Fluid (10x Diluted seawater)

Similar to previous step in experiment-1, relative permeabilities of each sequence in experiment-2 can be calculated by multiplying particular f_o and derivative of 1/PV vs $I/(PV*I_r)$, as shown in figure 4.31. Right after that, back calculation matching using generated relative permeabilities can reproduce good match of oil recovery profile of its experiments as shown in figure 4.32.

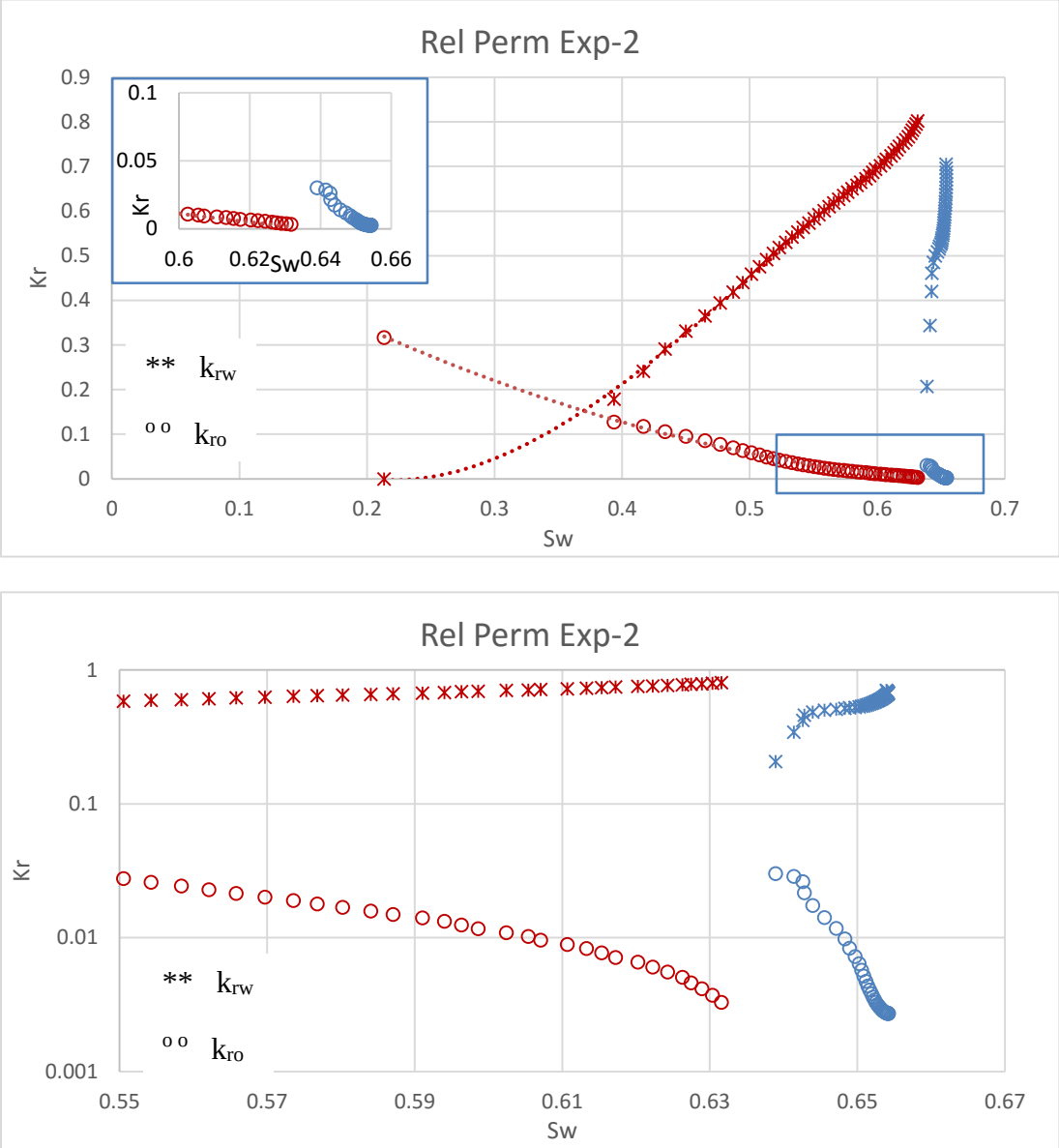

Figure 4.31 Rel Perm of Experiment-2 in normal scale (top) and semilog scale (bottom); red = seawater, blue = 10x diluted seawater

Relative permeabilities of experiment-2, show that oil relative permeabilities of 10 times diluted seawater is shifted upward after reaching S_{or} of last injections as shown in semilog scale in figure 4.31. It confirms that there is a potential benefit during smart water (10x diluted seawater) in experiment-2 as well.

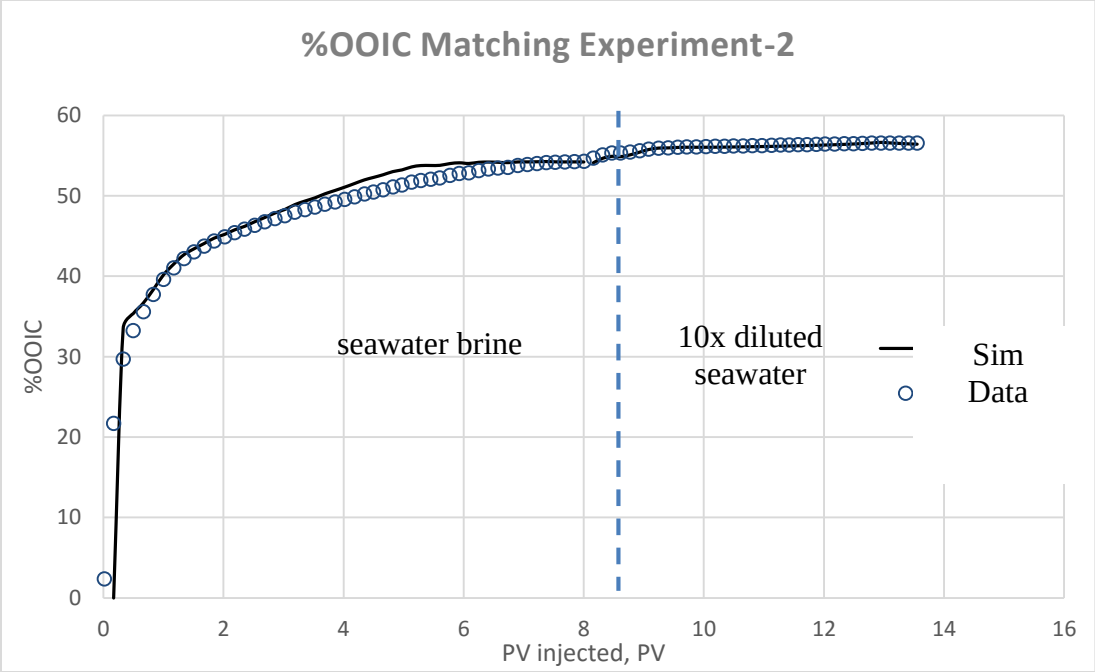

Figure 4.32 Oil Recovery Matching in Exp-2 using Rel Perm of JBN Technique

Oil recovery matching in experiment-2 using back calculation in figure 4.32 is satisfactory enough. Thus this relative permeabilities will be used to match oil recovery and pressure drop in numerical simulation of experiment-2.

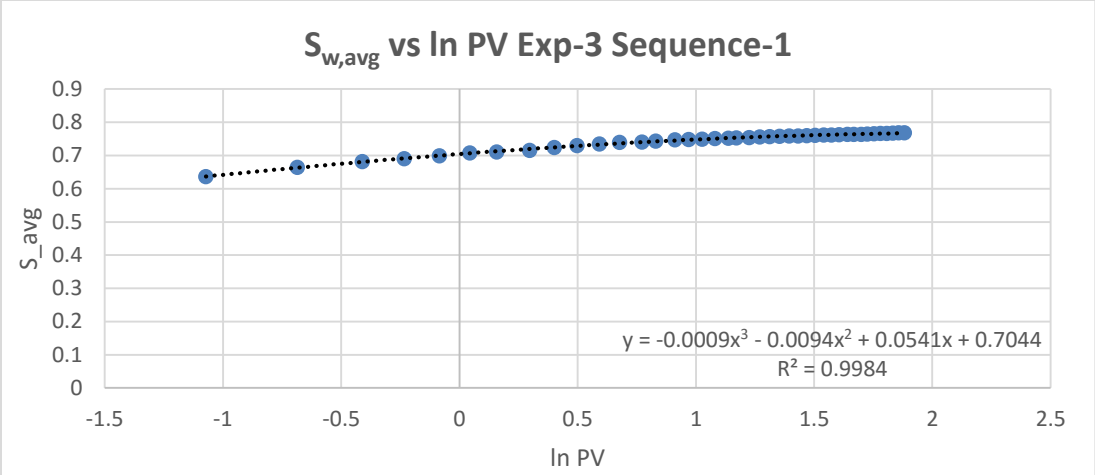

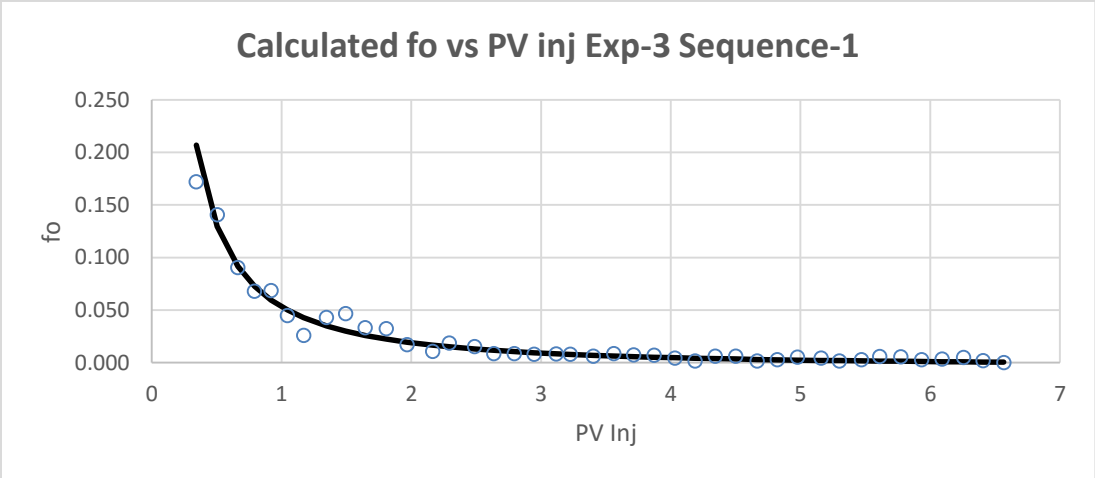

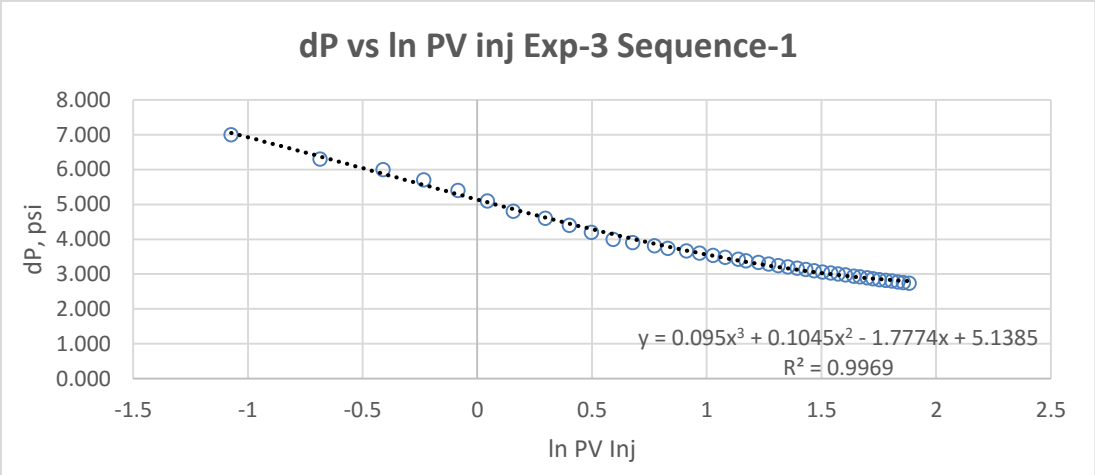

Figure 4.33 Curve fitting in JBN calculation for Exp-3 First Injected Fluid (seawater)

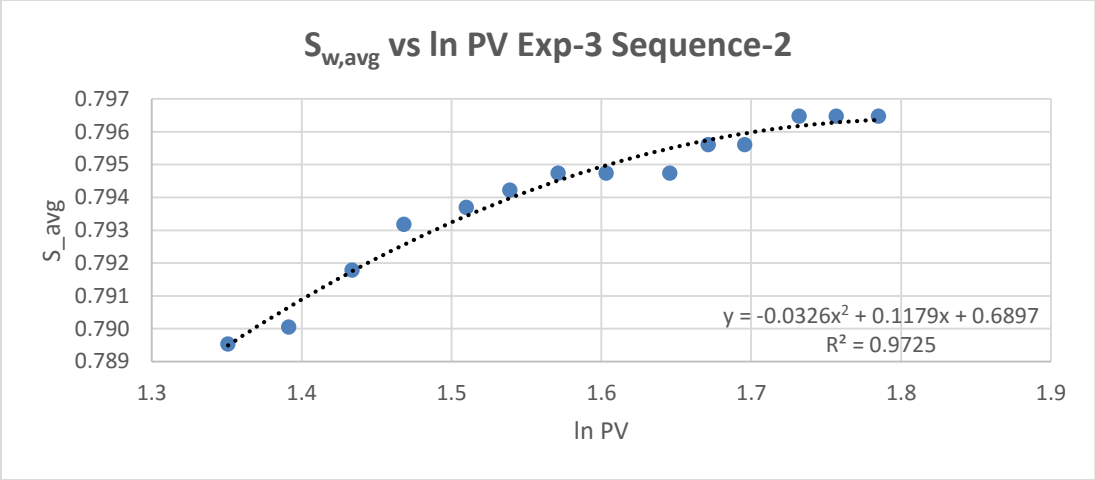

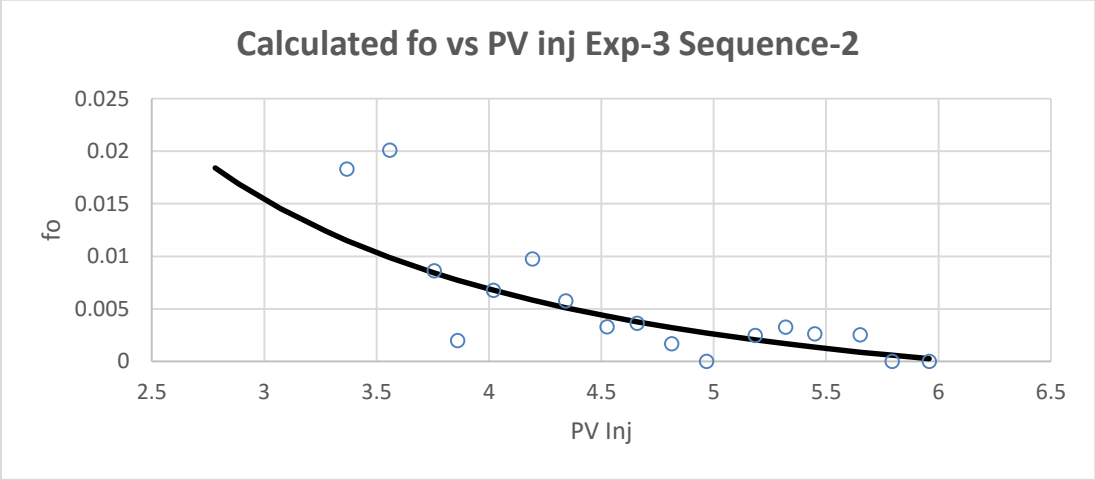

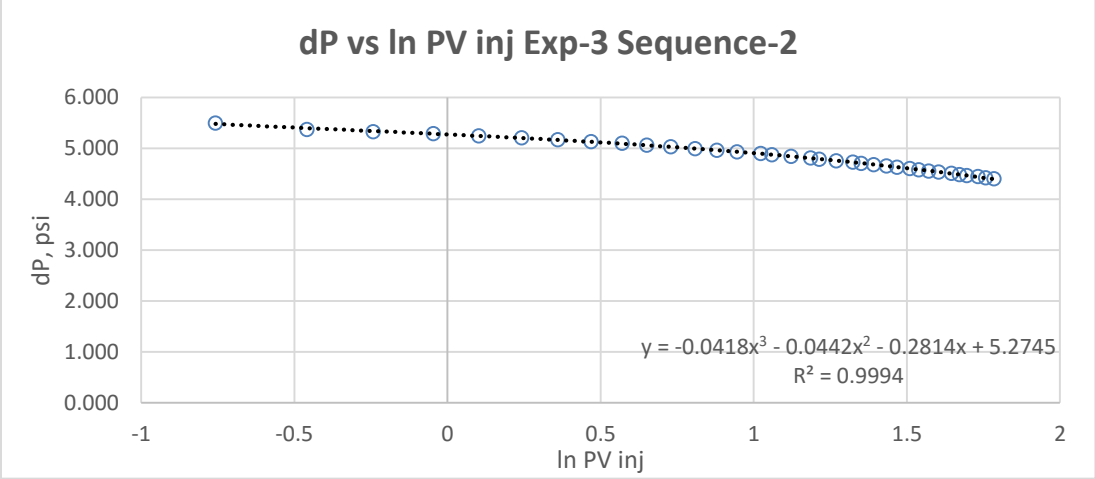

Figure 4.34 Curve fitting in JBN calculation for Exp-3 Second Injected Fluid (10x Diluted seawater)

After obtaining f_o and slope of $I/(PV*I_r)$ vs $1/PV$ for experiment-3 data, relative permeabilities of each sequence in experiment-3 can be calculated by multiplying particular fo and derivative of $I/(PV*I_r)$ vs $1/PV$ as shown in figure 4.35. Then to validate the relative permeabilities, back calculation matching using its relative permeabilities should reproduce good match of oil recovery of its experiments as shown in figure 4.36.

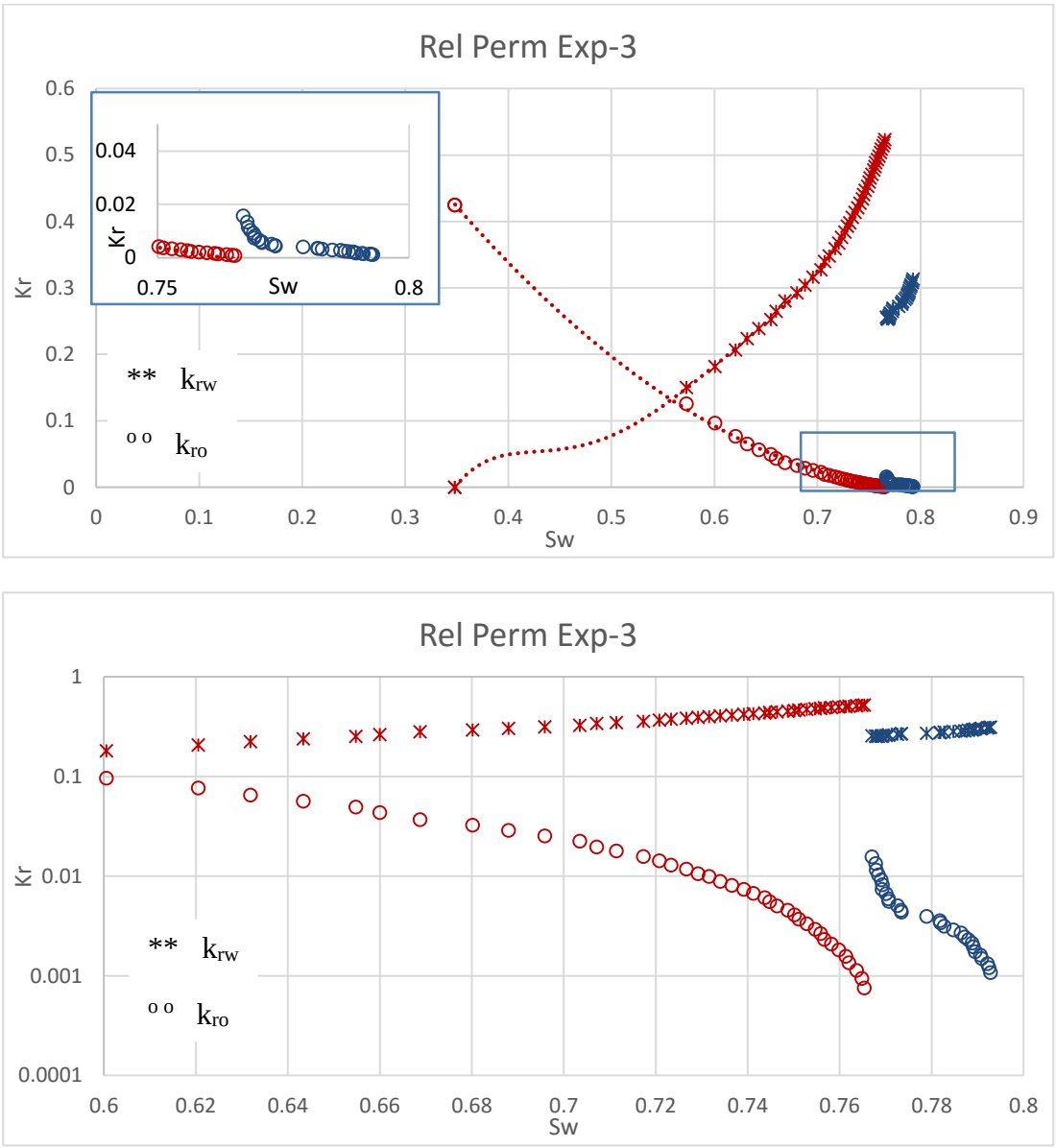

Figure 4.35 Rel Perm of Experiment-3 in normal scale (top) and semilog scale (bottom); red = seawater, blue = 10x diluted seawater

Relative permeabilities of experiment-3, also show an upward shift of oil relative permeabilities of 10x diluted seawater after last injections as shown in semilog scale figure in 4.35. It confirms that there is a potential benefit during smart water (10x diluted seawater) in experiment-3.

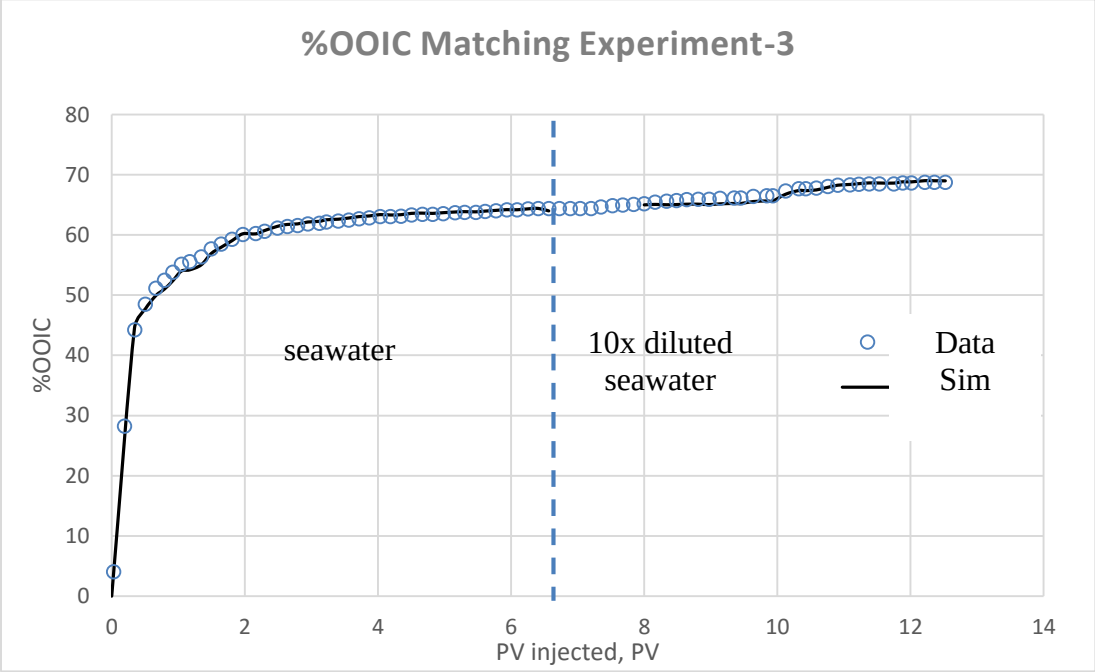

Figure 4.36 Oil Recovery Matching in Exp-3 using Rel Perm of JBN Technique

Oil recovery matching in experiment-2 using back calculation in figure 4.36 is satisfactory enough. These relative permeability will be used in the next step of simulation modeling to match oil recovery and pressure drop of experiment-3.

The relative permeability of first injection fluid show large saturation range to construct complete relative permeabilities. While next sequences of injections show narrow saturation range after last injection saturation (S_{or}). Nevertheless, to be noted in the first sequence of injections, oil relative permeability of seawater brine in experiment-2 is higher than oil relative permeability of formation brine in experiment-1, which is expected since oil recovery by seawater is higher in the first injection sequence. After repeating similar sequence of experiment-2 with conventional coreflooding in experiment-3, oil relative permeability of seawater in experiment-3 lays between oil relative permeabilities of first injection in experiment-1 and 2 as shown in its normalized scale in figure 4.37. Water relative permeability of experiment-3 is also expected to be in between of the others water relative permeabilities (experiment-1 and 2). This discrepancy is suspected due to the variation of establishment of S_{wi} in experiment-3 which cannot reproduce S_{wi} of previous experiment. Some definition of normalized relative permeabilities are:

$$S_{wn} = \frac{S_w - S_{wi}}{1 - S_{wi} - S_{or}} \tag{4.1}$$

$$k_{rwn} = \frac{k_{rw}}{k_{rw|S_{or}}} \quad and \quad k_{ron} = \frac{k_{ro}}{k_{ro|S_{wi}}} \tag{4.2}$$

This concept of lower salinity brine injection in first injection sequence is the same with smart water concept in this case low salinity injection. Where the lower salinity brine injection shifts relative permeability towards more water wet condition as also shown in normalized scale relative permeabilities in figure 4.37.

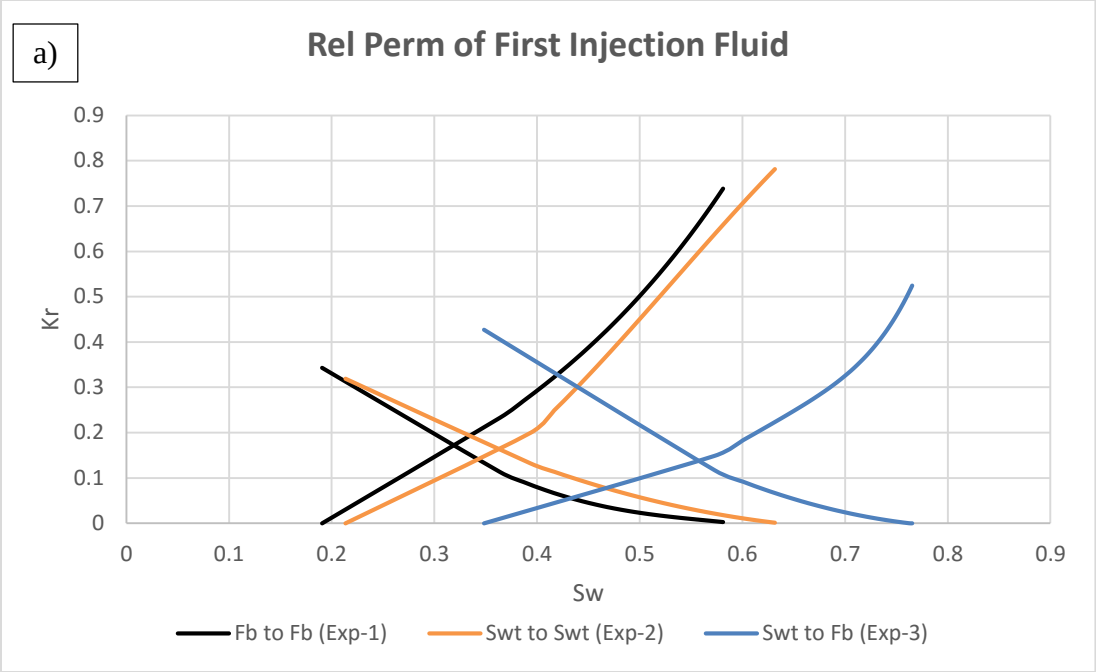

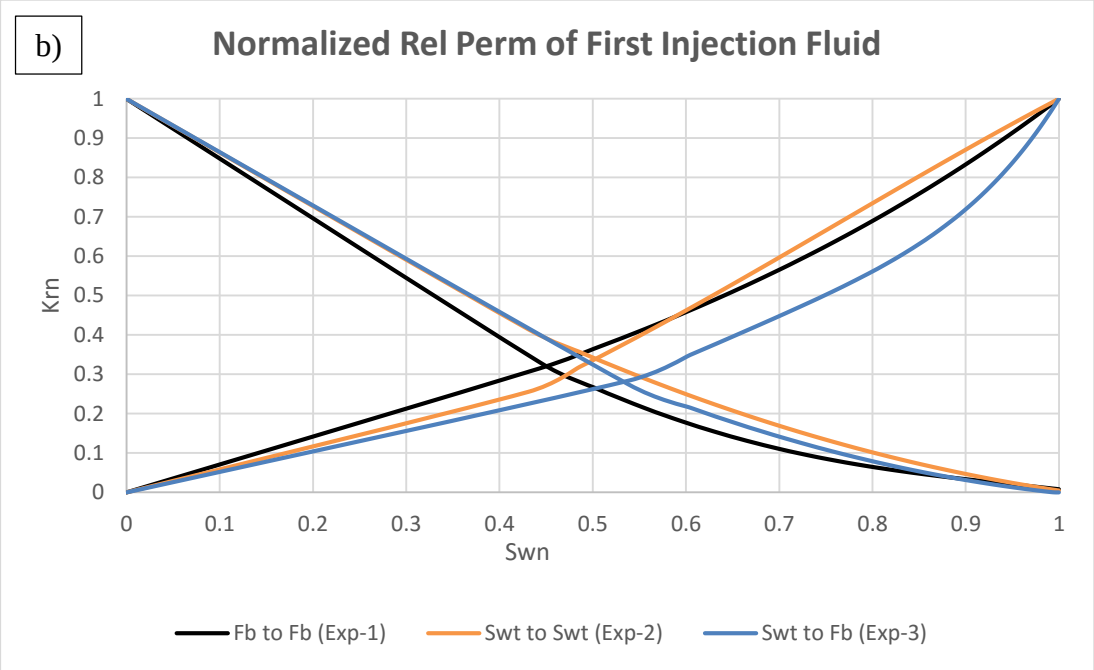

Figure 4.37 Comparison of First Injection Fluid Rel Perm in All Experiment (a), Normalized scale (b)

4.2.2 Insight of Potential Determining Ions Profiles

The examination of effluent analysis, ion profiles during each sequence shows that, most of the ions follow injection fluid level. These ions are changing in such a way that follows the ionic composition of the displacement fluid. Nonetheless, some ions reveal different behavior. Calcium ion and bicarbonate ion, both of these ions do not reach their injection fluid level, even after 3 pore volumes. Both calcium profiles measured by IC-Metrohm and ICP consistently show that after Seawater injection, calcium ion profiles do not reach but close to the level of calcium ion in Seawater fluid composition. But this phenomena is more profound after Smart water injection, where the gap between calcium ion profiles to the level of calcium in Smart water injection fluid is relatively getting bigger.

From the NMR results, minor dissolution of calcium might occur during Smart water injection process which cause additional amount of calcium ion in solution. Another possibility might be particular injection fluid, Smart water fluid, is being retarded by adsorption mechanism of surface site of carbonate rock. These geochemical reactions more likely the cause of additional oil recovery during Smart water flooding.

While in bicarbonate ions, the profiles are also showing indication of retardation process since bicarbonate ion profiles give a big gap to bicarbonate ion level in injection fluid composition. Nevertheless, these hypothesis phenomena will be confirmed in the geochemical simulation in the next chapter.

CHAPTER 5

BUCKLEY LEVERETT and PHREEQC SIMULATION

This Chapter presents an attempt to model Smart water flooding experiment considering certain aspects investigated during unsteady state core flooding experiment. This study applies Buckley-Leverett concept to build a numerical model and utilizes geochemical simulator program PHREEQC to handle complex geochemical processes. Buckley-Leverett model is specifically used in modelling the immiscible displacement process, whereas, PHREEQC is a robust program by USGS that is commonly used in modelling ground water pollution by geochemists.

5.1 Buckley-Leverett Simulation

Mathematical derivation of the Buckley-Leverett equation and its discretization will be shown in this section. Numerical scheme in this study is basically 1^{st} order accurate in time and space. Furthermore the numerical solution will be solved explicitly.

5.1.1 Model Setup

The Buckley-Leverett equation can be derived from a simple mass balance of following equation:

Mass in - mass out = rate of mass change.

$$q_w\rho_w|_x - q_w\rho_w|_{x+dx} = A\phi dx\frac{\partial}{\partial t}(\rho_w S_w) \qquad (5.1)$$

Consider an infinitesimal element of rock having porosity ϕ , an area A, and a length dx in the direction of flow. Where q_w and ρ_w denotes volume rate and density respectively. At x+dx, the mass rate of water leaving the element is $q_w\rho_w|_{x+dx}$. The mass rate of water accumulating is $A\phi dx\frac{\partial}{\partial t}(\rho_w S_w)$ where S_w is the water saturation. Due to mass balance, the mass of water entering the element in the rock, minus the mass of water leaving must be equal to the rate of water accumulation in the element. We thereby have:

$$(q_w\rho_w)_x - (q_w\rho_w)_{x+\Delta x} = A\phi\Delta x\frac{(\rho_w S_w)_{t+\Delta t} - (\rho_w S_w)_t}{\Delta t} \qquad (5.2)$$

$$-\frac{\partial(q_w\rho_w)}{\partial x} = A\phi\frac{\partial(S_w\rho_w)}{\partial t} \qquad (5.3)$$

$$\frac{\partial(q_w\rho_w)}{\partial x} + A\phi\frac{\partial(S_w\rho_w)}{\partial t} = 0 \qquad (5.4)$$

Assuming that the fluids are incompressible, the densities will be constant, both as function of time and distance. This leads us to:

$$\frac{\partial(q_w)}{\partial x} + A\phi\frac{\partial(S_w)}{\partial t} = 0 \qquad (5.5)$$

Darcy's equations for water are used to substitute for q_w, where k is the absolute permeability, and k_{rw} are the relative permeability for water, where P is the phase pressures for water and it equals to pressure in the oil phase since Buckley Leverett assumption stated that capillary pressure is negligible.

$$\frac{\partial}{\partial x}\left(-\frac{k\,k_{rw}}{\mu_w}\frac{\partial P}{\partial x}\right)+\phi\frac{\partial S_w}{\partial t}=0 \qquad (5.6)$$

$$\frac{\partial}{\partial x}\left(-\lambda_w\frac{\partial P}{\partial x}\right)+\phi\frac{\partial S_w}{\partial t}=0 \qquad (5.7)$$

Next we introduce the fluid mobility λ_w as functions of effective permeability divided by viscosity, and water fractional flow f_w as $f_w=\frac{\lambda_w}{\lambda_T}$. By Darcy law again, the total velocity of both oil and water can be written in term of the total mobility

$$u=-\lambda_T\frac{\partial P}{\partial x}\Leftrightarrow f_w u=-\lambda_w\frac{\partial P}{\partial x} \qquad (5.8)$$

$$\frac{\partial}{\partial x}\left(f_w u\right)+\phi\frac{\partial S_w}{\partial t}=0 \qquad (5.9)$$

$$u\frac{\partial f_w}{\partial x}+\phi\frac{\partial S_w}{\partial t}=0 \qquad (5.10)$$

The pressure term in the mass conservation equation for water can be eliminated and it gives the Buckley-Leverett equation.

5.1.2 Numerical Discretization

Discretization of the Buckley-Leverett equation in a one-dimensional space of length L is performed by means of a finite difference method. A mesh of J grid points x_j for j = 1-J is defined. All grid cells have width $\Delta x = L/J$ and are of the cell-centered type. Figure 5.1 shows the illustration of discretization of J+1 grid.

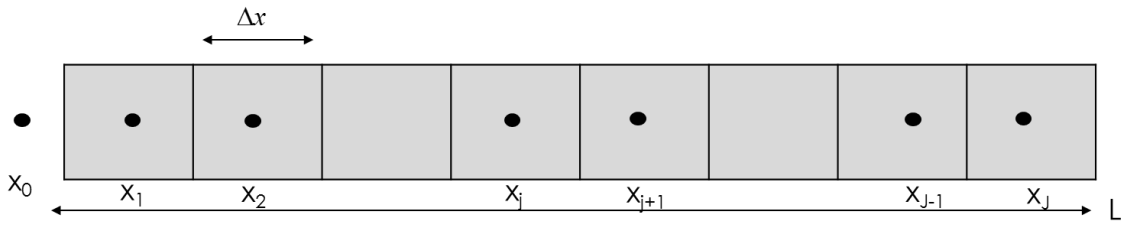

Figure 5.1 Numerical discretization J+1 grid

Recall the analytical expression of Buckley-Leverett $u\frac{\partial f_w}{\partial x}+\phi\frac{\partial S_w}{\partial t}=0$. In this study numerical scheme solution utilizes a simple explicit time stepping method with a straightforward upwind discretization (note here that flow is always from left to right). The discretization will give:

$$S_{w,j}^{n+1}=S_{w,j}^{n}+\frac{u\Delta t}{\phi\Delta x}\left(f_{w,j-1/2}^{n}-f_{w,j+1/2}^{n}\right) \qquad (5.11)$$

While for its boundary j=1, the numerical solution of Buckley Leverett can be discretized as follow:

$$S_{w,1}^{n+1}=S_{w,1}^{n}+\frac{u\Delta t}{\phi\Delta x}\left(f_{w,1/2}^{n}-f_{w,1}^{n}\right),\ f_{w,1/2}^{n}=f_{w,1}^{n}=1 \qquad (5.12)$$

As can be seen from the matrix formulation and the definition of the boundary condition j = 1, an extra point $f_{w,1/2}$ is introduced which is located a half distance of Δx in front of point x_1. At this position (x_0) the boundary condition S_w (0, t) = 1-S_{or} is extrapolated, and therefore $f_{w,1/2} = f_{w1} = 1$.

Similar to mass transport equation of Buckley leveret, ions concentration in each grid cell is modelled with the same type of advection equation as the transport water saturation. Advection equation of ion transport and discretization scheme using first order discretization in time and space are as follow:

$$u\frac{\partial}{\partial x}\left(f_w C_\gamma\right)+\phi\frac{\partial}{\partial t}\left(S_w C_\gamma\right)=0 \qquad (5.13)$$

$$C_{\gamma,j}^{n+1}=C_{\gamma,j}^{n}-\frac{u\Delta t}{2\phi\Delta x}\frac{f_{w,j}^{n}}{S_{w,j}^{n}}\left(C_{\gamma,j}^{n}-C_{\gamma,j-1}^{n}\right) \qquad (5.14)$$

Simulations for certain amounts of grid cells and time step sizes have been carried out. Sharp front is achieved with 120 grids number and 10 seconds time step. Since physical dispersion exist during brine mixing in coreflooding, numerical dispersion is honored to represent it. In this study the number of grid will be in range of 30 -70 grids and the time step is every 10 seconds. Figure 5.2 shows saturation profile from several amount of grids.

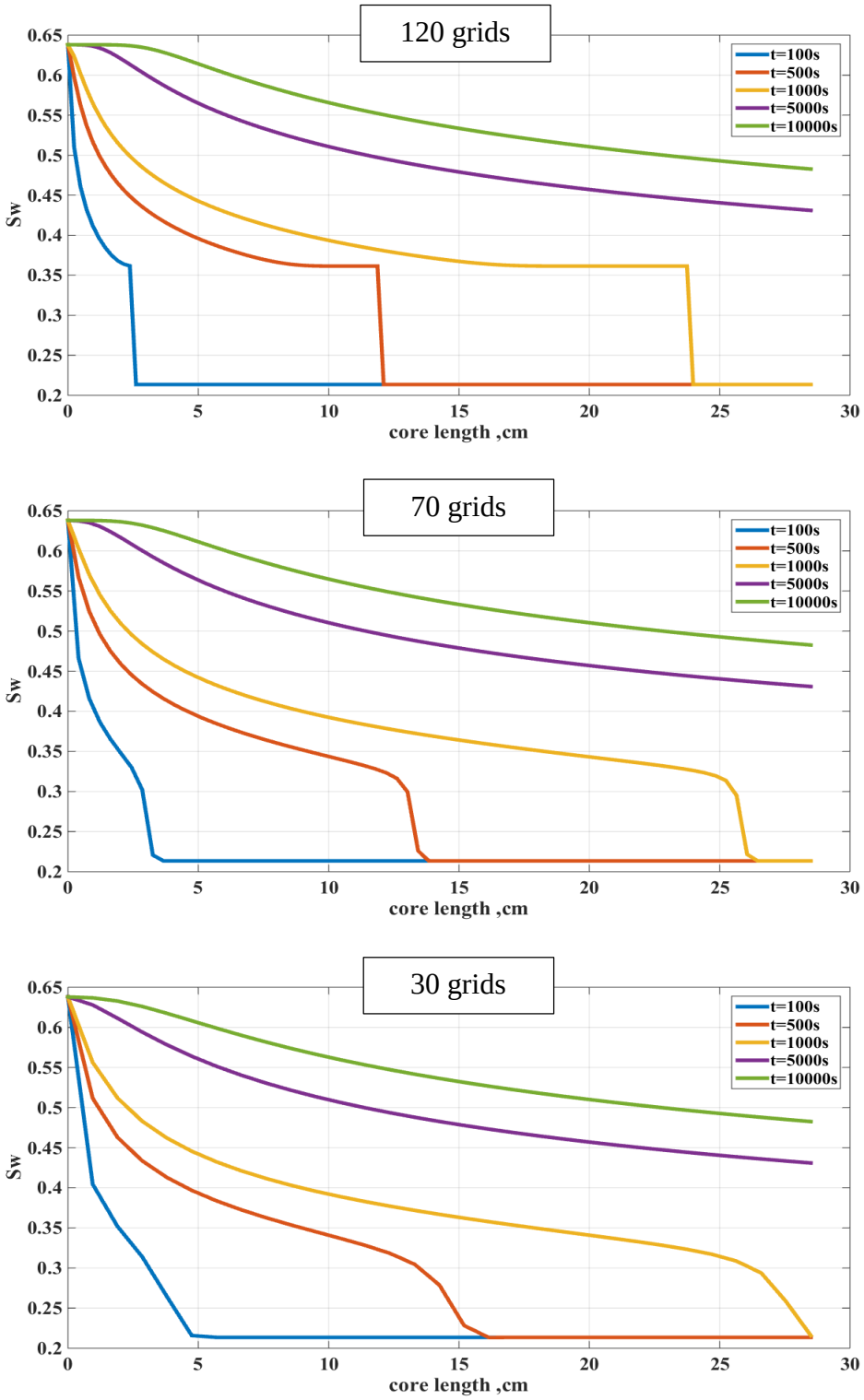

Figure 5.2 Saturation profiles of 120, 70 and 30 grids

5.2 PHREEQC Simulations

The U.S. Geological Survey (USGS) package PHREEQC is a geochemical simulator for speciation, batch-reaction, one dimensional transport and inverse geochemical calculations. A great advantage of PHREEQC is that it contains extensive general databases of geochemical data which attract many researchers in oil industries to utilize it mainly for enhanced oil recovery modelling.

Furthermore, by default in PHREEQC, batch cell calculations are based on 1 kilogram of water. All parameters are defined relative to fully saturated one kilogram of water. Based on De Bruin [13], the effect of increasing water saturation as water slowly replaces oil in the reservoir should be taken into account in the PHREEQC simulations by using the water saturation of a grid cell, as a multiplier for the amount of water used in a PHREEQC simulation. As an example, when the water saturation Sw = 0.5, the PHREEQC simulation will be carried out for 0.5 kg of water. But Korani [28, 29] stated different perspective based on his communication with D.L Parkhurst of USGS in his work. Before proceeding to the geochemistry module, total moles of the entire geochemical species and total moles of all the hydrocarbon components (if the hydrocarbon phase effect is included in the geochemical calculations) of gridblocks are divided by water mass existing in each gridblock. When UTCOMP-IPhreeqc is done with the geochemical calculation, total moles of geochemical species and hydrocarbon components (if the effect is included on the aqueous-rock geochemistry) are multiplied by water mass of gridblocks. The reason for this is the fact that IPhreeqc/PHREEQC works best if water mass is within a couple of orders of magnitude of 1 kg. It implies that 1 kg here is not necessarily related to the amount of water saturation in the rock.

This section will first introduce quick workflow of PHREEQC, its capability to handle geochemical reactions, and how the integration/couple with Buckley Leverett simulation is taking place since the programming languages of these programs are different.

5.2.1 Simulation Setups and Geochemical Databases

In order to model any geochemical reactions, PHREEQC needs some primary input for fluid and mineral compositions, as well as their properties or conditions. Reaction's type also defined in input step. Some reactions include equilibrium reaction, aqueous speciation, ion exchange, surface complexation, kinetic reaction, and inverse modeling can be modelled in PHREEQC. Moreover, user can define whether this solution will be transported using advection only and or dispersion in 1-D. All these parameters are specified by keywords which connects to geochemical database.

A further description of the input conventions and the mathematical backgrounds can be found in the program's manuals by Parkhurst and Appelo [40]. The help-file also explains the structure of the input file, the keywords, and the output. Included are new options introduced in new releases of PHREEQC. In this study, we use PHREEQC version 3.0 released with Notepad++^{TM} version.

As a glimpse, once the input parameters/keywords have been specified, PHREEQC will call its database to start determining possible species and solubility constant based on input properties. These elements have associated reactions to establish mole and charge balance equations, which are used to build Jacobian matrices of Newton Rapshon method. The Master unknowns are the activity of species, whereas, the residual are basically rearranged of those mole and charge balance equations. If these specified reactions are transported

within certain amount of grid cell, the output of each reaction will be transferred from grid to grid. General workflow of PHREEQC is presented in figure 5.3.

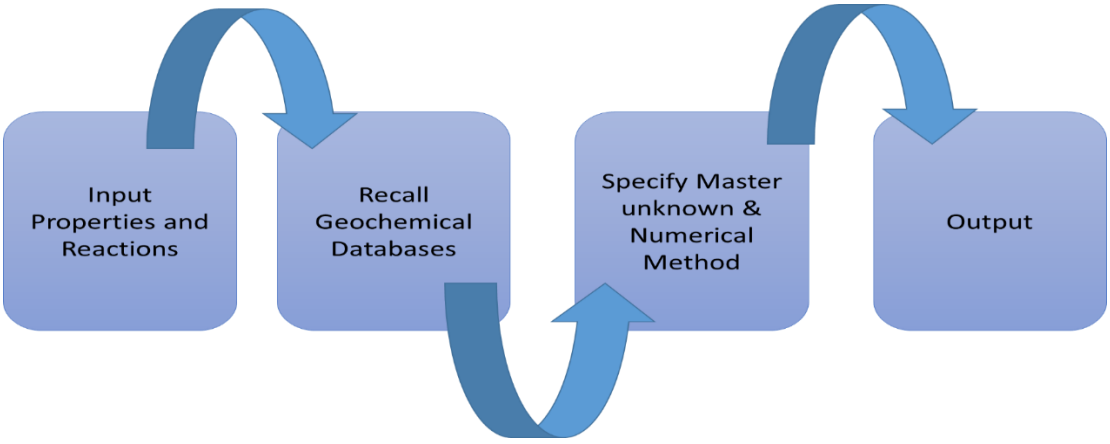

Figure 5.3 PHREEQC workflow

Furthermore, Output of any reactions generally are solution compositions after equilibrated with any fluid or minerals, distribution of its species, saturation indices of phases, etc. These output can be calculated manually but it will be very tiresome and not an easy task. For example a system of calcite mineral equilibrated with pure water. At least it needs 6 activities of species are needed [Ca^{2+}], [CO_3^{2-}], [HCO_3^-], [H_2CO_3], [OH^-] and [H^+] to be solved as master unknown. Initial guess might be activity equals to concentration, then start calculate ionic strength of mix solution, individual activity coefficients and calculate the individual activity until all species are converged. This simple case lead us to the fact that geochemical modelling is very important. PHREEQC has become the standard for doing these types of calculations. PHREEQC was developed for calculation of “real world” hydrogeochemistry and is a powerful tool for modeling data [40].

5.2.2 Geochemical Model in PHREEQC

In Smart water flooding model, Smart water brine will disturb the solubility equilibrium of calcite mineral. Calcite might dissolve to counteract the reduction in calcium ion below the calcium equilibrium concentration. The aim of the geochemical modeling here is to confirm the possible phenomena showed by core flooding experiment by matching its ion profiles.

As discussed in chapter-4, the behavior of calcium and bicarbonate ions are not aligned with the others predetermining ion profiles. During Seawater and especially Smart water flooding, these ions stay high from injection fluid level even after several pore volume injections. Some possibilities leads to dissolution and retardation/adsorption process during this process. Dissolution can be quantify by saturation indices and amount of minerals during history matching of these ions. Whereas adsorption process can be quantify by amount of calcium ions adsorbed in surface site of calcite. Unfortunately, PHREEQC database is designed for surface model of Ferrihydrite which is a widespread hydrous ferric oxyhydroxide (HFO) mineral at the Earth's surface. Thus, additional SURFACE MASTER SPECIES for mainly calcite surface site should be added in database. Another possible surface sites are analyzed in mineralogy assessment with PHREEQC.

5.2.3 Mineralogy and Geochemical Reactions

As stated in chapter-3, carbonate rock that is being used in this experiment is highly porous Indiana limestone core from set B and set C which both are quite similar in mineralogy and properties. This type of Indiana limestone outcrop consists of 98.9% calcite, 0.9% quartz and 0.2% dolomite measured by XRD test on its limestone powder as shown in figure 5.4.

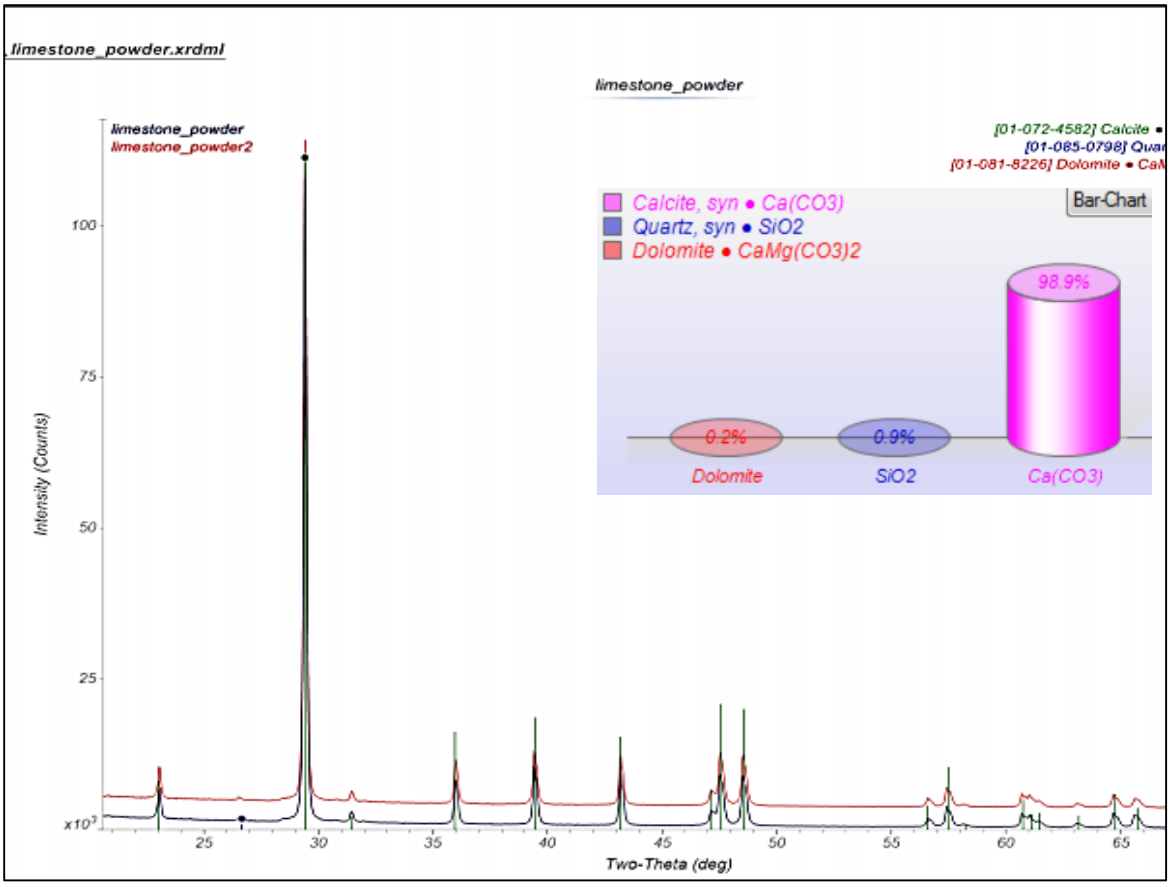

Figure 5.4 XRD Test of Indiana Limestone (after Ugul Pakoz [46])

By assuming that there is no precipitation occurred during formation brine saturation (experiment-1 and 3) and Seawater saturation (experiment 2), based on the observed effluent, we can do forced mineral equilibrium assessment using PHREEQC. This procedure was also conducted by Meling [34] to confirm which mineral that might exist in equilibrium with certain solution.

Based on XRD on Indiana limestone in figure 5.4, corresponding ions are forced equilibrated namely, calcium on calcite, magnesium on dolomite, and silica on quartz. These mineral compositions are converted to molarity in PHREEQC by assuming reported compositions as percent volume then multiplied by density and divided by molecular

weight of mineral into mole/cc. With a basis of 1 cc as a volume of grain in PHREEQC, initial water saturation volume of each experiment can be calculated. Molarity of minerals become mole of mineral divided by water saturation of each experiment in liter. For example in experiment-1, average porosity is 0.1625 and S_{wi} is 0.191; based on 1 cc of grain volume, bulk volume can be calculated as 1/(1-0.1625) =1.194 cc which results a pore volume of 0.194 cc and water saturation of (0.191x0.194)=0.037 cc. While conversion of calcite amount into mole can be calculated as (98.9% x 2.71 g/cc)/100.1 g/mole =0.027 mole/cc. Assuming 1 liter of water equals to 1 kgw, molarity of calcite is 0.027/(1000 x 0.037) = 722.55 mole/liter. Summary for all experiments is presented in table 5.1.

Table 5.1 Molarity of Minerals of all experiments

Molarity, mole/l	Experiment-1	Experiment-2	Experiment-3
Quartz	10.711	9.279	5.058
Dolomite	0.831	0.720	0.393
Calcite	722.550	625.943	341.243

Table 5.2 shows aqueous and mineral equilibration of Experiment-1 against saturating brine which is formation brine. It shows that some possible mineral phases that occurred are precipitated initially such as Talc and Chrysotile.

Table 5.2 Saturation Index of Possible Mineral Phase Saturated with Formation Brine in Experiment-1

Phase	SI	log IAP	log K (373 K, 1 atm)	
Anhydrite	-0.07	-5.34	-5.26	CaSO4
Aragonite	-0.1	-9.27	-9.17	CaCO3
Calcite	0	-9.27	-9.27	CaCO3
CH4(g)	-24.8	-27.8	-3	CH4
Chalcedony	-0.24	-3.1	-2.86	SiO2
Chrysotile	**2.97**	27.68	24.71	Mg3Si2O5(OH)4

CO2(g)	-1.99	-3.97	-1.98	CO2
Dolomite	0	-18.48	-18.48	CaMg(CO3)2
Gypsum	-0.62	-5.47	-4.85	CaSO4:2H2O
H2(g)	-10.17	-13.28	-3.1	H2
H2O(g)	-0.07	-0.07	0	H2O
H2S(g)	-23.15	-31.09	-7.94	H2S
Halite	-0.61	1.01	1.62	NaCl
O2(g)	-43.51	-46.62	-3.11	O2
Quartz	0	-3.1	-3.1	SiO2
Sepiolite	-1.04	13.14	14.18	Mg2Si3O7.5OH:3H2O
Sepiolite(d)	-5.52	13.14	18.66	Mg2Si3O7.5OH:3H2O
SiO2(a)	-0.88	-3.1	-2.22	SiO2
Sulfur	-18.19	-14.71	3.48	S
Talc	**6.98**	21.55	14.57	Mg3Si4O10(OH)2

Analysis on quartz and calcite is conducted to understand behavior of these minerals towards equilibrium. When calcite and quartz are separately immersed in seawater, calcite dissolves and reaches equilibrium of calcium ion fast, while quartz dissolves and reaches equilibrium of silica ion very slow even with high mole concentration. Figure 5.5 shows Si concentration in seawater may increase in years by kinetic dissolution of quartz, while calcite is in hours. Thus, quartz phase is not necessarily modeled and local equilibrium assumption (LEA) is relevant to be used in our geochemical model.

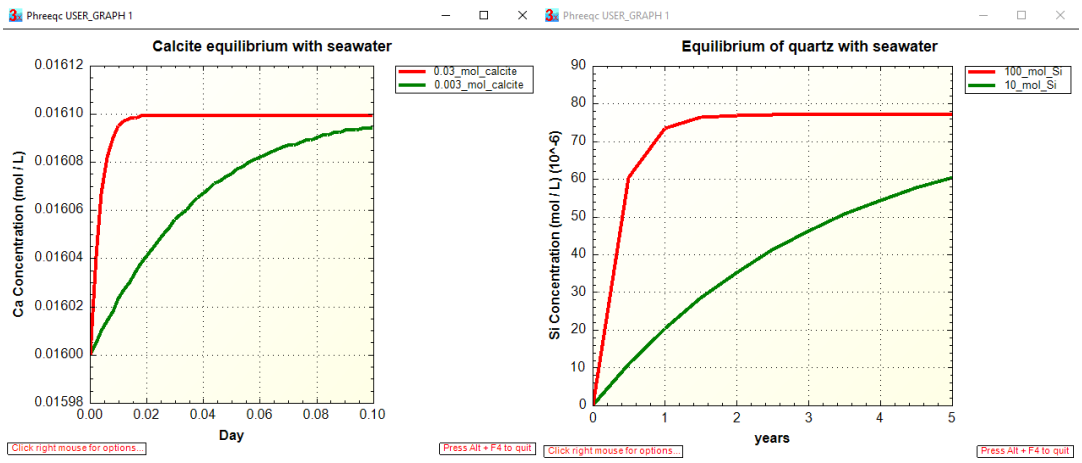

Figure 5.5 Equilibrium time for Calcite and Quartz with seawater

Tables 5.3 to 5.5 show aqueous and mineral equilibration of Experiment-1 to 3 with calcite and dolomite minerals.

Table 5.3 Saturation Index of Possible Mineral in equilibrium with formation brine in Experiment-1

Phase	SI	log IAP	log K (373 K)	
Anhydrite	-0.07	-5.34	-5.26	CaSO4
Aragonite	-0.1	-9.27	-9.17	CaCO3
Calcite	0	-9.27	-9.27	CaCO3
CH4(g)	-25.2	-28.2	-3	CH4
CO2(g)	-1.99	-3.97	-1.98	CO2
Dolomite	0	-18.48	-18.48	CaMg(CO3)2
Gypsum	-0.62	-5.47	-4.85	CaSO4:2H2O
H2(g)	-10.27	-13.38	-3.1	H2
H2O(g)	-0.07	-0.07	0	H2O
H2S(g)	-23.55	-31.49	-7.94	H2S
Halite	-0.61	1.01	1.62	NaCl
O2(g)	-43.31	-46.43	-3.11	O2
Sulfur	-18.49	-15.01	3.48	S

Table 5.4 Saturation Index of Possible Mineral in equilibrium with seawater in Experiment-2

Phase	SI	log IAP	log K(373 K)	
Anhydrite	0.47	-4.79	-5.26	CaSO4
Aragonite	-0.1	-9.27	-9.17	CaCO3
Calcite	0	-9.27	-9.27	CaCO3
CH4(g)	-89.14	-92.15	-3	CH4
CO2(g)	-1.3	-3.28	-1.98	CO2
Dolomite	0	-18.48	-18.48	CaMg(CO3)2
Gypsum	0.03	-4.82	-4.85	CaSO4:2H2O
H2(g)	-26.41	-29.51	-3.1	H2
H2O(g)	-0.02	-0.01	0	H2O
H2S(g)	-87	-94.95	-7.94	H2S
Halite	-2.13	-0.52	1.62	NaCl
O2(g)	-10.94	-14.05	-3.11	O2
Sulfur	-65.81	-62.33	3.48	S

Table 5.5 Saturation Index of Possible Mineral in equilibrium with formation brine in Experiment-3

Phase	SI	log IAP	log K(373 K)	
Anhydrite	-0.07	-5.34	-5.26	CaSO4
Aragonite	-0.1	-9.27	-9.17	CaCO3
Calcite	0	-9.27	-9.27	CaCO3
CH4(g)	-25.2	-28.2	-3	CH4
CO2(g)	-1.99	-3.97	-1.98	CO2
Dolomite	0	-18.48	-18.48	CaMg(CO3)2
Gypsum	-0.62	-5.47	-4.85	CaSO4:2H2O
H2(g)	-10.27	-13.38	-3.1	H2
H2O(g)	-0.07	-0.07	0	H2O
H2S(g)	-23.55	-31.49	-7.94	H2S
Halite	-0.61	1.01	1.62	NaCl
O2(g)	-43.31	-46.43	-3.11	O2
Sulfur	-18.49	-15.01	3.48	S

During aqueous-mineral equilibrium, precipitation and dissolution of minerals can occurred simultaneously. To observe these geochemical reactions, concentration of ions in aqueous phase could indicate whether there has been any dissolution or precipitation of

minerals. As a simple case to get an idea of dissolution and precipitation, amount of minerals (calcite and dolomite) in experiment-1 were equilibrated with injection brines. For first injection, after equilibrating formation brine with the minerals, changes of ions in aqueous phase were observed in mole/kg solution in table 5.6:

Table 5.6 Changes in Ionic composition of aqueous phase after formation brine and minerals are in equilibrium

Ions	**Formation Brine (ppm)**	**MW (g/mol)**	**Formation Brine (mol/kg)**	**Equilibrated with minerals in PHREEQC**	**difference (mol/kg)**
Na^{+}	62000	23	2.69565	2.69600	-0.00035
Ca^{2+}	23314	40	0.58285	0.38010	0.20275
Mg^{2+}	1268	24.3	0.05218	0.25460	-0.20242
Cl^{-}	120000	35.45	3.38505	3.38500	0.00005
HCO_3^{-}	79	61	0.00130	0.00072	0.00057
SO_4^{2-}	250	96.1	0.00260	0.00300	-0.00040

Through the use of equilibrium equations one can find the difference in minerals based on the difference in concentration of the ions in the water,

Calcite $CaCO_3 \rightleftharpoons CO_3^{-2} + Ca^{+2}$

Dolomite $CaMg(CO_3)_2 \rightleftharpoons Ca^{+2} + Mg^{+2} + 2CO_3^{-2}$

Changes in concentration of Ca^{2+} effect both calcite and dolomite, changes in Mg^{2+} affect dolomite mineral. Therefore the changes of minerals based on the differences of the ions:

$\Delta dolomite = \Delta Mg^{2+} = -0.20242$ mol/kg = -3.7326 wt% after multiplied by MW of dolomite (184.4 g/mole) and $\Delta calcite = \Delta Ca^{2+} - \Delta dolomite = 0.20275 – (-0.20242) = 0.40517$ mol/kg = 4.055 wt% after multiplied by MW of calcite (100.1 g/mole).

Positive sign shows additional amount of mineral which indicates precipitation, on the other hand, negative sign shows reduction of mineral amount which indicates dissolution. Similarly to other injection brines, the difference amount of minerals are presented in table 5.7, and comparison to PHREEQC calculations are presented as well. Even though, the system is not just limited to aqueous-mineral equilibrium, but the idea of initial dissolution of calcite and dolomization after seawater and 10x diluted seawater is expected.

Table 5.7 Changes in amount of minerals after aqueous mineral equilibrium

Mineral	**FB**			**SW**			**DSW**		
	Δmineral mol/kg	PHREEQC mol/kg	del wt%	Δmineral mol/kg	PHREEQC mol/kg	del wt%	Δmineral mol/kg	PHREEQC mol/kg	del wt%
Calcite	0.40517	0.40550	4.05538	-0.0627	-0.06319	-0.6282	-0.0057	-0.00574	-0.0570
Dolomite	-0.2024	-0.20260	-3.7326	0.03170	0.03187	0.58457	0.00281	0.002829	0.05186

Furthermore, calcite and dolomite are selected to be used for further analysis in this study, some properties for surface complexation model are adopted through RES³T database by Helmholtz-Zentrum Dresden-Rossendor website [22]. This database covers second model of Calcite as presented by Zhu, C., and Anderson, G. [55] in Environmental Applications of Geochemical Modeling. It stated that recent model of surface complexation model of calcite in particularly are 3 models based on calcite immersed in water system. In model 1 and 2, the calcite surface becomes immediately hydrated when immersed in water. In

model 1, however, it is assumed that the hydrolysis process that happens at the calcite/air interface are the same as those at the calcite/water interface, resulting in strongly hydrated sites of $–H^{+1/3}$ and $–OH^{-1/3}$ to which the potential determining ions sorbed independent of pH as shown in figure 5.6.

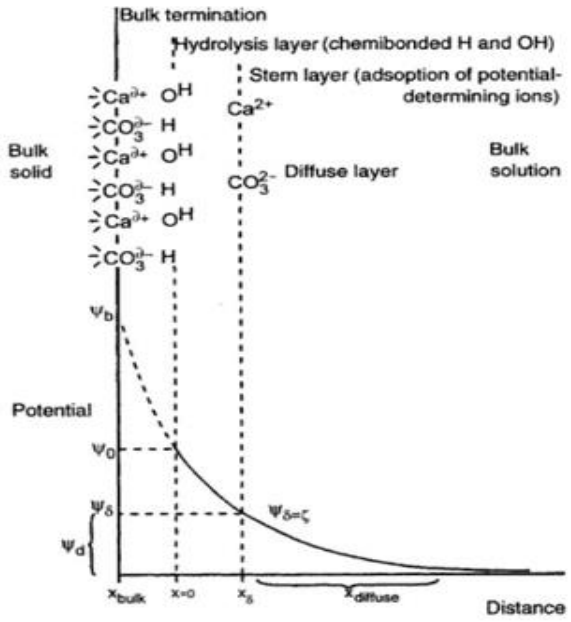

Figure 5.6 Surface Complexation model for Calcite in Model-1 (after Zhu and Anderson [55])

In model 2, the hydrolysis results in neutral sites of $–CaOH^0$ and $–CO3H^0$ which can dissociate/protonate depending on pH in the suspension. Furthermore, these neutral sites can form complexes with Ca^{2+} and $CO3^{2-}$ ions from the solution. Accordingly, the water in model 2 is more weakly bonded to the calcite surface than in model 1. In agreement with model 2, water in model 3 is not tightly bonded to the surface, as inferred from the observation of recryztalization. In model 3 (as in model 1), pH does not control the surface

charge directly, the potential determining ions tends to react directly with the surface sites $-Ca^{+1/3}$ or $-CO3^{-1/3}$.

In this study calcite surface has two surface sites that bounded with master species, Cal_aCO_3H *and* Cal_bCaOH , and dolomite surface has three surface sites that bounded with master species $Dolo\_aCO_3H, Dolo\_bCaOH$ *and* $Dolo\_cMgOH$.

Incorporating minerals and their surfaces with the brines, some geochemical reactions that might occurred, which refer to geochemical database of PHREEQC, can be grouped as aqueous species, mineral species, gas phase species and surface species, shown in table 5.8 to 5.10.

Table 5.8 Aqueous Species reactions

$H_2O \rightleftharpoons OH^- + H^+$	$Ca^{+2} + CO_3^{-2} \rightleftharpoons CaCO_3$
$2\,H_2O \rightleftharpoons O_2 + 4\,H^+ + 4\,e^-$	$Ca^{+2} + CO_3^{-2} + H^+ \rightleftharpoons CaHCO_3^+$
$2\,H^+ + 2\,e^- \rightleftharpoons H_2$	$Ca^{+2} + SO_4^{-2} \rightleftharpoons CaSO_4$
$CO_3^{-2} + H^+ \rightleftharpoons HCO3^-$	$Ca^{+2} + HSO_4^- \rightleftharpoons CaHSO_4^+$
$CO_3^{-2} + 2\,H^+ \rightleftharpoons CO_2 + H_2O$	$Mg^{+2} + H_2O \rightleftharpoons MgOH^+ + H^+$
$CO_3^{-2} + 10\,H^+ + 8\,e^- \rightleftharpoons CH_4 + 3\,H_2O$	$Mg^{+2} + CO_3^{-2} \rightleftharpoons MgCO_3$
$SO_4^{-2} + H^+ \rightleftharpoons HSO_4^-$	$Mg^{+2} + H^+ + CO_3^{-2} \rightleftharpoons MgHCO_3^+$
$HS^- \rightleftharpoons S^{-2} + H^+$	$Mg^{+2} + SO_4^{-2} \rightleftharpoons MgSO_4$
$SO_4^{-2} + 9\,H^+ + 8\,e^- \rightleftharpoons HS^- + 4\,H_2O$	$Na^+ + OH^- \rightleftharpoons NaOH$
$HS^- + H^+ \rightleftharpoons H_2S$	$Na^+ + CO_3^{-2} \rightleftharpoons NaCO_3^-$
$Ca^{+2} + H_2O \rightleftharpoons CaOH^+ + H^+$	$Na^+ + HCO_3^- \rightleftharpoons NaHCO_3$
	$Na^+ + SO_4^{-2} \rightleftharpoons NaSO_4^-$

Table 5.9 Mineral and Gas Phase reactions

Calcite	$CaCO_3 \rightleftharpoons CO_3^{-2} + Ca^{+2}$	$CO_2(g)$,	$CO_2 \rightleftharpoons CO_2$
Aragonite	$CaCO_3 \rightleftharpoons CO_3^{-2} + Ca^{+2}$	$H_2O(g)$,	$H_2O \rightleftharpoons H_2O$
Dolomite	$CaMg(CO_3)_2 \rightleftharpoons Ca^{+2} + Mg^{+2} + 2CO_3^{-2}$	$O_2(g)$,	$O_2 \rightleftharpoons O_2$
Gypsum	$CaSO_4:2H_2O \rightleftharpoons Ca^{+2} + SO_4^{-2} + 2H_2O$	$H_2(g)$,	$H_2 \rightleftharpoons H_2$
Anhydrite	$CaSO_4 \rightleftharpoons Ca^{+2} + SO_4^{-2}$	$H_2S(g)$,	$H_2S \rightleftharpoons H^+ + HS^-$
Sulfur	$S + 2H^+ + 2e^- \rightleftharpoons H_2S$	$CH_4(g)$,	$CH_4 \rightleftharpoons CH_4$
Halite	$NaCl \rightleftharpoons Cl^- + Na^+$		

Table 5.10 Surface Species reactions

SURFACE_SPECIES	
$Cal\_aCO_3H \rightleftharpoons Cal\_aCO_3H$	$-\log k$ 0.0
$Cal\_aCO_3H + Ca^{+2} \rightleftharpoons Cal\_aCO_3Ca^+ + H^+$	$-\log k$ 2.8
$Cal\_bCaOH \rightleftharpoons Cal\_bCaOH$	$-\log k$ 0.0
$Cal\_bCaOH + CO_2 \rightleftharpoons Cal\_bCaHCO_3$	$-\log k$ −0.6
$Cal\_bCaOH + CO_2 \rightleftharpoons Cal\_bCaCO_3^- + H^+$	$-\log k$ 2.6
$Cal\_bCaOH + CO_3^{-2} + H^+ \rightleftharpoons Cal\_bCaCO_3^- + H_2O$	$-\log k$ −17.1
$Cal\_bCaOH + CO_3^{-2} + 2H^+ \rightleftharpoons Cal\_bCaHCO_3 + H_2O$	$-\log k$ −23.5
$Dolo\_aCO_3H \rightleftharpoons Dolo\_aCO_3H$	$-\log k$ 0.0
$Dolo\_aCO_3H + Ca^{+2} \rightleftharpoons Dolo\_aCO_3Ca^+ + H^+$	$-\log k$ 18
$Dolo\_aCO_3H + Mg^{+2} \rightleftharpoons Dolo\_aCO_3Mg^+ + H^+$	$-\log k$ 20
$Dolo\_bCaOH \rightleftharpoons Dolo\_bCaOH$	$-\log k$ 0.0
$Dolo\_bCaOH + CO_3^{-2} + H^+ \rightleftharpoons Dolo\_bCaCO_3^- + H_2O$	$-\log k$ −16.6
$Dolo\_bCaOH + CO_3^{-2} + 2H^+ \rightleftharpoons Dolo\_bCaHCO_3 + H_2O$	$-\log k$ −24
$Dolo\_cMgOH \rightleftharpoons Dolo\_cMgOH$	$-\log k$ 0.0
$Dolo\_cMgOH + CO_3^{-2} + H^+ \rightleftharpoons Dolo\_cMgCO_3^- + H_2O$	$-\log k$ −15.4
$Dolo\_cMgOH + CO_3^{-2} + 2H^+ \rightleftharpoons Dolo\_cMgHCO_3 + H_2O$	$-\log k$ −23.5

5.3 Coupling IPhreeqc and Buckley-Leverett Simulation

PHREEQC geochemical program cannot directly coupled with another scripting language. To facilitate use of these reaction capabilities in scripting languages and other models, PHREEQC has been implemented in modules with another software. Its module namely IPhreeqc which is used to refer to the class or any PHREEQC modules.

5.3.1 IPhreeqc Module for Simulation Coupling

An IPhreeqc module is created in different ways depending on the software environment where it is used. Multiple instances of an IPhreeqc class can be created within the client program in all programming environments, such as COM server (Component Object Model), C, C++ and Fortran. Buckley Leverett simulation is conducted through MATLAB™ which allow interaction with its COM server. MATLAB™ interacts with an IPhreeqc module through a set of methods which are listed in Appendix B. These methods allow initializing the module and reading a thermodynamic database, running PHREEQC input (strings or files), and retrieving results from simulations.

After a module is created, the LoadDatabase (for clarity, all IPhreeqc method names are written in bold font) or LoadDatabaseString method reads a thermodynamic database from a file or string, respectively. When the database has been read, a module is ready to perform PHREEQC calculations. Using LoadDatabase or LoadDatabaseString a second time will re-initialize the module and remove all data stored in it. PHREEQC input can be defined and run in three different ways with an IPhreeqc module. First, the AccumulateLine method can be called sequentially to append PHREEQC input to an input buffer in IPhreeqc. When the entire input has been accumulated, it is run with the RunAccumulated method. The second way to run simulations is to define PHREEQC input in a string within the client

program. This string is then submitted and run with the RunString method. Finally, it is possible to run PHREEQC input that has been saved in a file by using the RunFile method. Because reading and writing files to disk is slow, running simulations with many calls to RunFile is expected to be slower than using RunString and RunAccumulated with internally generated strings.

IPhreeqc makes special use of the data defined by the SELECTED_OUTPUT and USER_PUNCH data blocks used in a batch PHREEQC, and allows this array of data to be returned to the client program by two methods that do not require reading or writing files. The GetSelectedOutputValue method is available in all modules and retrieves an individual data item at a given row and column from the array of selected-output results that was generated by the last call to a RunAccumulated, RunString, or RunFile method. The COM module has an additional method, GetSelectedOutputArray, which returns the entire array of the selected-output data. A data item in the selected-output array may be an integer, real, or string value. IPhreeqc implements a simple variant object, which can contain any of these three data types. The IPhreeqc module requires slightly different handling of this variant object depending on whether the module is called as a COM, or as C++, C, or Fortran program elements.

Related to transport flow model in IPhreeqc, series of input data blocks were devised that allow input of the exact contents of the data structures for solutions and other reactants. For solutions, the data block is named SOLUTION_RAW and SOLUTION_MODIFY which has the same format as SOLUTION_RAW, but does not require a complete set of data. It is expected that the SOLUTION_MODIFY will be used to update the element composition of a solution following a transport calculation, without redefining some parts

of the solution structure. Equivalent MODIFY data blocks are available for all other reactants.

5.3.2 Verification with PHREEQC

In this section Buckley Leverett 1-D simulation built in MATLAB^{TM} is coupled with IPhreeqc to test its capability in modelling geochemical reactions against PHREEQC. The way IPhreeqc is coupled is by "hard coupling" that allow calculations of geochemical reactions conducted/stored in computer memory instead of read – write output and input file during solving geochemical reaction in transport flow model. Output data stored in memory will be used to modify the parameters (concentrations, volume, etc.) of a previously defined keyword.

Korrani *et al.* [28, 29] stated that in order to obtain very good agreements between the Coupling simulator (with IPhreeqc) and PHREEQC, the geochemical elements, including the total H and O as well as the charge imbalance, must be transported with very high precision, at least by 13 digits. In MATLAB, the definition of data type is simpler than Fortran programming language used in UTCOMP/UTCHEM by Korrani et al. Instead of specifying high precision data type of each element, IPhreeqc keyword SOLUTION_MODIFY is automatically taking account of it.

One example of PHREEQC transport flow model is verified with coupling simulation MATLAB-IPhreeqc. Description of flow model is TRANSPORT data block, which simulates advection and dispersive mixing, with additional ionic exchange model. The concentrations in cell 40, which is the end cell, are plotted against pore volumes. Initially solution of Sodium and potassium are exist in column. The displacement fluids are Calcium and Chloride. Chloride is a conservative solute and arrives in the effluent after one pore

volume. The sodium initially present in the column exchanges with the incoming calcium and is eluted as long as the exchanger contains sodium. The midpoint of the breakthrough curve for sodium occurs at about 1.5 pore volumes (1 PV equals to 40 grids/cells). Because potassium exchanges more strongly than sodium (because of the larger log *K* in the exchange reaction), potassium is released after sodium. Finally, when all of the potassium has been released, the concentration of calcium increases to the steady-state concentration in the influent. Figure 5.7 shows the result performed in PHREEQC and MATLAB-IPhreeqc.

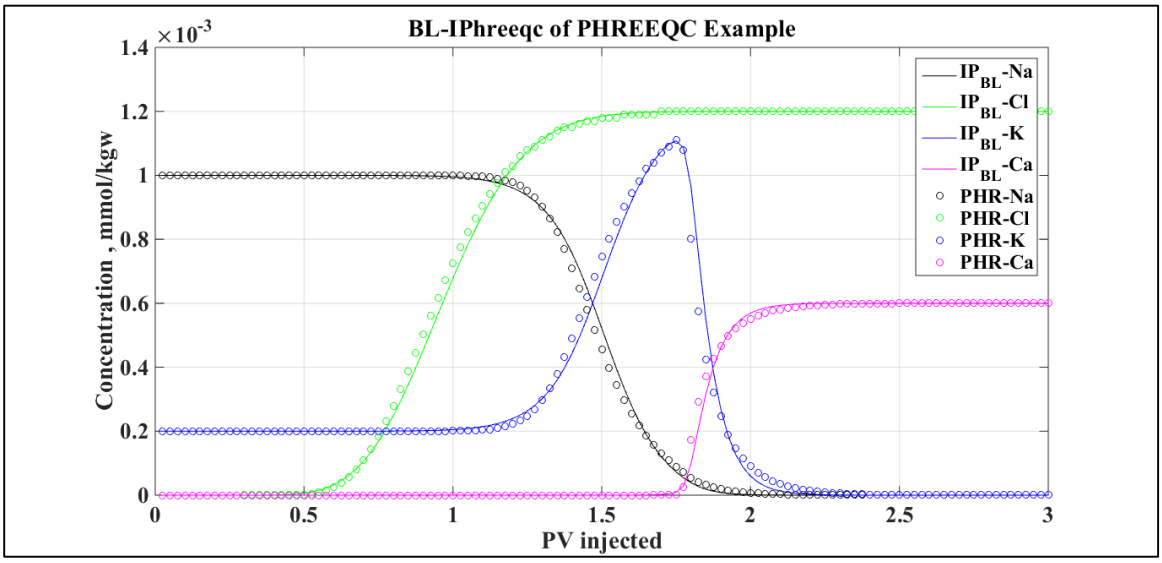

Figure 5.7 Coupled Simulator Verification to PHREEQC example

This example shows that Coupling MATLAB-IPhreeqc is able to reproduce the geochemical reaction in flow transport model in PHREEQC. The key to verify this matching is by transfer of all geochemical elements in IPhreeqc code. Table 5.11 shows Geochemistry data stored in the computer memory of only the first grid block that is retrieved from Dump file of its simulation.

Table 5.11 Dump file of Verification File, in First Grid Block

Dumpfile Transport simulation 121 Shift 1 SOLUTION_RAW 0	 Solution after simulation 1.
-temp	25
-pressure	1
-total_h	111.0124
-total_o	55.5067
-cb	5.3078e-016
-density	0.9971
-totals	
Ca	0.0006
Cl	0.0012
O(0)	0.000535
-pH	6.994914
-pe	13.63198
-mu	0.001800
-ah2o	0.999964
-mass_water	1
-soln_vol	1.002984
-total_alkalinity	7.145517e-020
-activities	
Ca	-3.30247
Cl	-2.94138
E	-13.6319
H(0)	-29.9998
O(0)	-29.9998
-gammas	

5.4 Smart water Flooding Phenomena in Coupled Simulation

Summing up experimental and simulation section, coupling a two-phase Buckley-Leverett (BL) flow simulation and geochemical simulator module IPhreeqc is conducted to confirm behavior of Smart water flooding. Core flooding results of this study clearly show that there is a production gain after switching brine to Smart water brine after no more oil production in previous injection. This indicates there is a shifting of oil relative permeability particularly for Smart water brine even after previous injection reach S_{or}. This

observation agrees with most of researcher's investigation that the general phenomena during Smart water flooding is wettability alteration. By a change in relative permeability, leading to a lower residual oil saturation and a more favorable displacement of the oil phase. Consequently, Coupled simulation BL_MATLAB-IPhreeqc accommodates this issue in its workflow shown in figure 5.8.

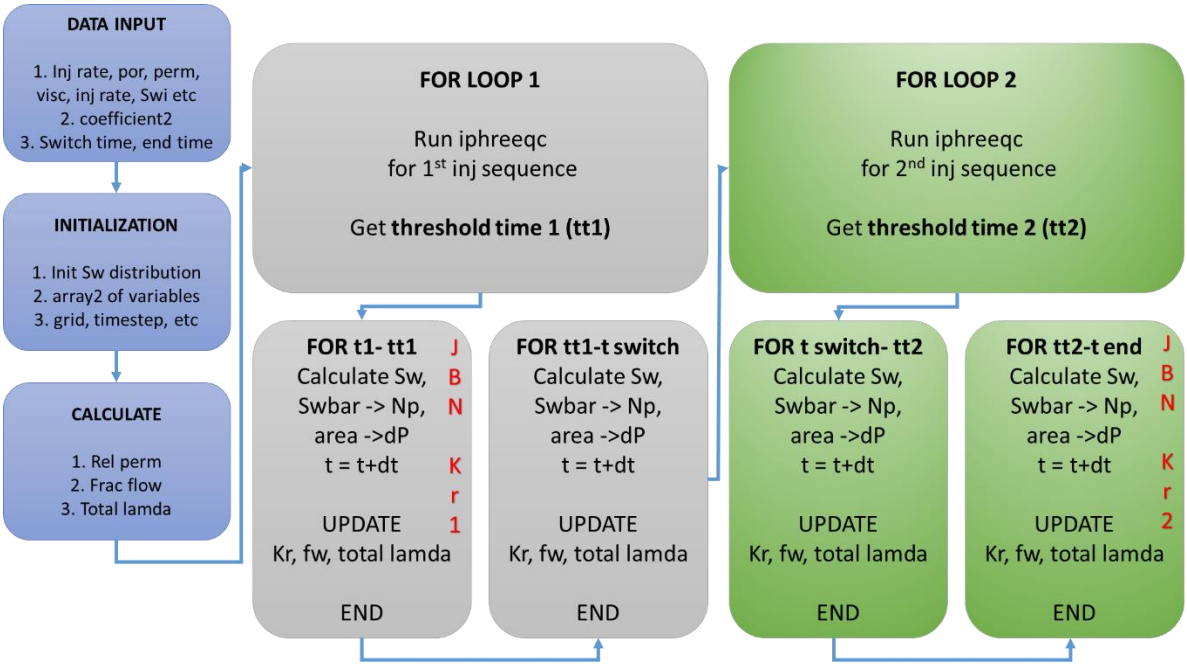

Figure 5.8 Coupling Simulation Workflow

In this scheme the mechanism of Smart water brine is taking place during brine switching (switching loop of new injection fluid). The transition during brine switching is the subject of further investigation. In this transition period, relative permeabilities of previous brine will gradually shifted to relative permeabilities of the next brine until selected threshold of the next brine is achieved. Some researchers assumed that threshold the Smart water effect can be modelled based on their proposed mechanism. For example Jerauld et al.[25] and De Bruin [13] directly used total dissolved solid or salinity level as threshold parameter

such that Rel-perm model of low salinity is used if salinity is less than certain salinity threshold whereas for high salinity is otherwise.

In this study this threshold time is being taken by investigating phenomena revealed in the core flooding experiment then being confirmed by history matching of Coupled simulation BL_MATLAB-IPhreeqc. The potential determining ions, Ca^{2+} and HCO_3^- ions, were selected as the threshold factors. Based on effluent profile of Ca^{2+} and HCO_3^- ions, the transition periods during brine switching as represented by its dispersion behavior, approximately in the range of 1 to 1.5 pore volume injection after start of brine switching. Thus, the threshold times of each sequence/loop in simulation were modeled by selecting the time just before the stabilize period of Ca^{2+} and HCO_3^- ions after switching to different brines. Then linear interpolation is conducted between relative permeabilities.

5.4.1 History Matching Experiment

BL_MATLAB-IPhreeqc coupling simulations were conducted to simulate three core flooding experiments. Input relative permeabilities for each experiment was obtained from JBN method validated with back calculation of oil recovery. The results of oil recovery, pressure drop, effluent profiles and selected geochemical elements (such as amount of minerals and saturation index of minerals) were stored in matrix for every grid and every time step. Approximate running time for 30-70 grids with 10 seconds time step in each experiment is about 1000-2000 seconds or 20 to 30 minutes.

Figures 5.9 to 5.11 present the history matching profiles of oil recovery and pressure drop from 3 experiments respectively.

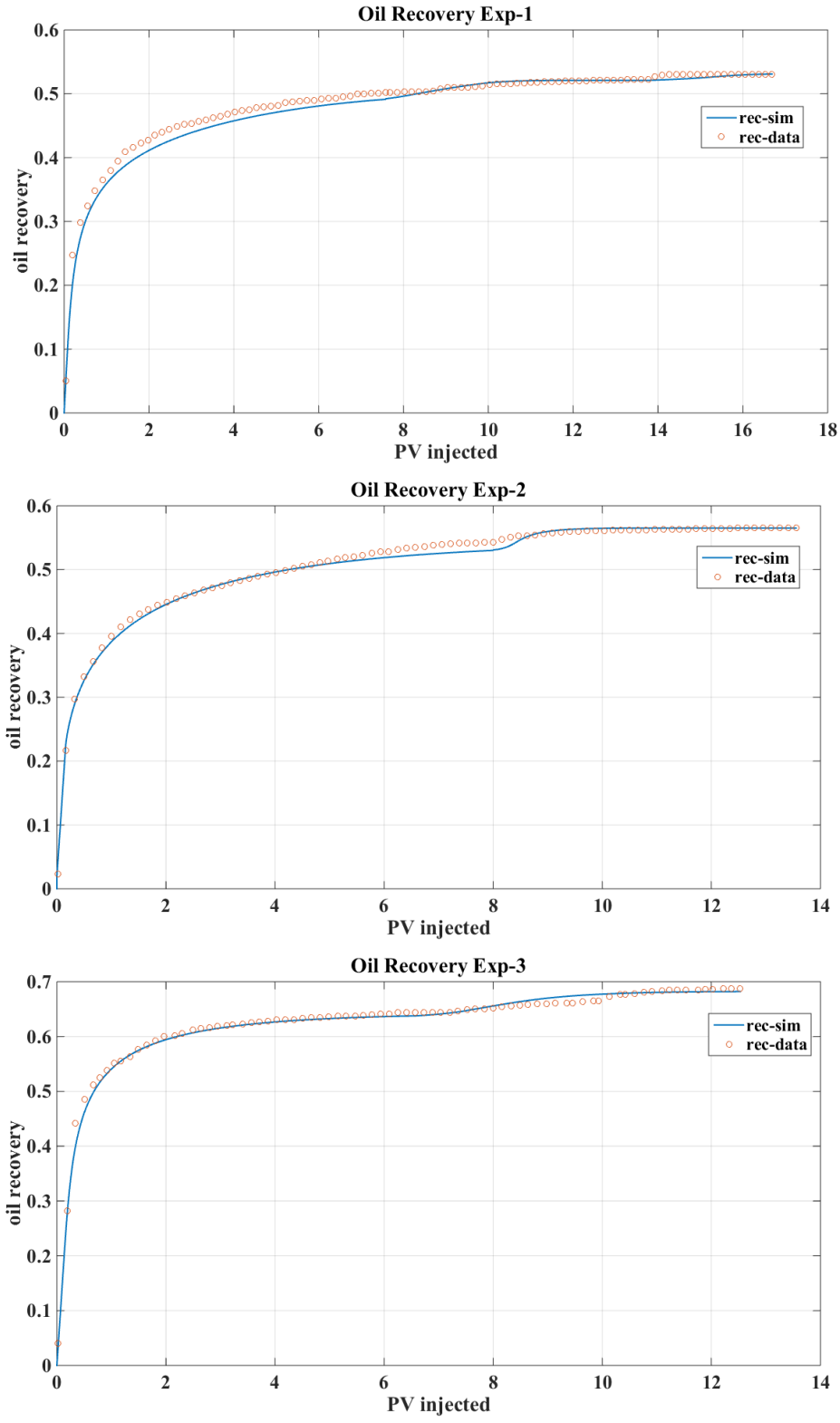

Figure 5.9 Oil recovery matching of Experiments

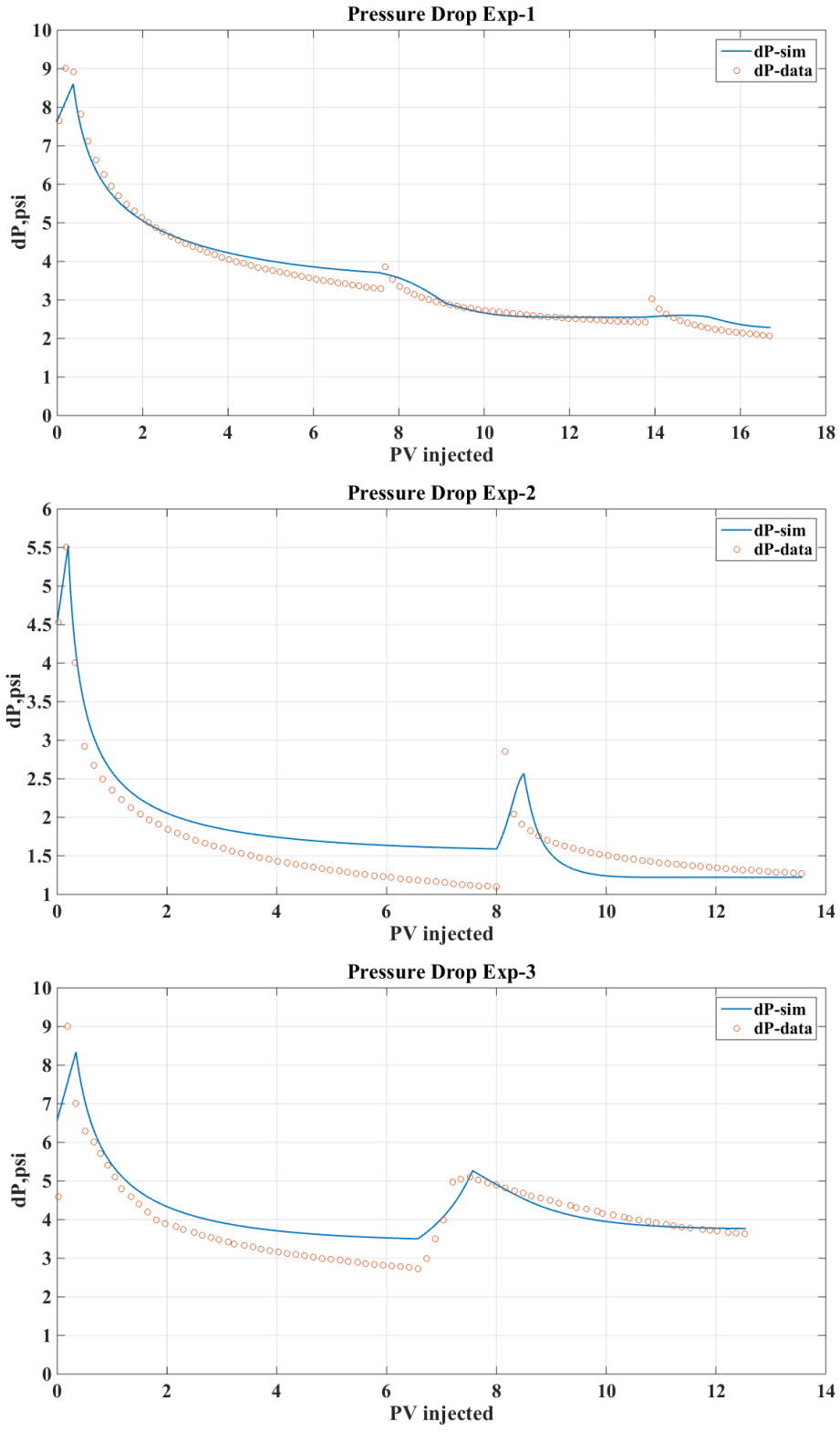

Figure 5.10 Pressure Drop matching of Experiments

Simulation of Oil recovery shows a good matched to experimental data whereas pressure drop shows a fair matched. Some difficulties during pressure drop matching occurred due to limitation to obtain a representative f_o during JBN method calculation since nature of experiment results did not show a smooth incremental oil recovery. Many attempts have been made to obtain better pressure drop matching such as selecting close curves to calculate f_o (either by $S_{w,avg}$ versus ln PV or Np versus ln PV), filtering some abrupt oil recovery data, fitting relative permeabilities, and also adjusting relative permeabilities up to 15%. Another factor that might affect pressure drop matching is the relatively high incremental pressure drop data during brine switching were suspected due to contribution of manual accumulators switching during experiments (open-close valve) since the effluents in fraction collectors show no precipitation.

Figures 5.11 to 5.17 present the history matching profiles Na^+, Cl^-, Ca^{2+}, Mg^{2+}, SO_4^{2-}, HCO_3^- ions, and pH from the three experiments respectively.

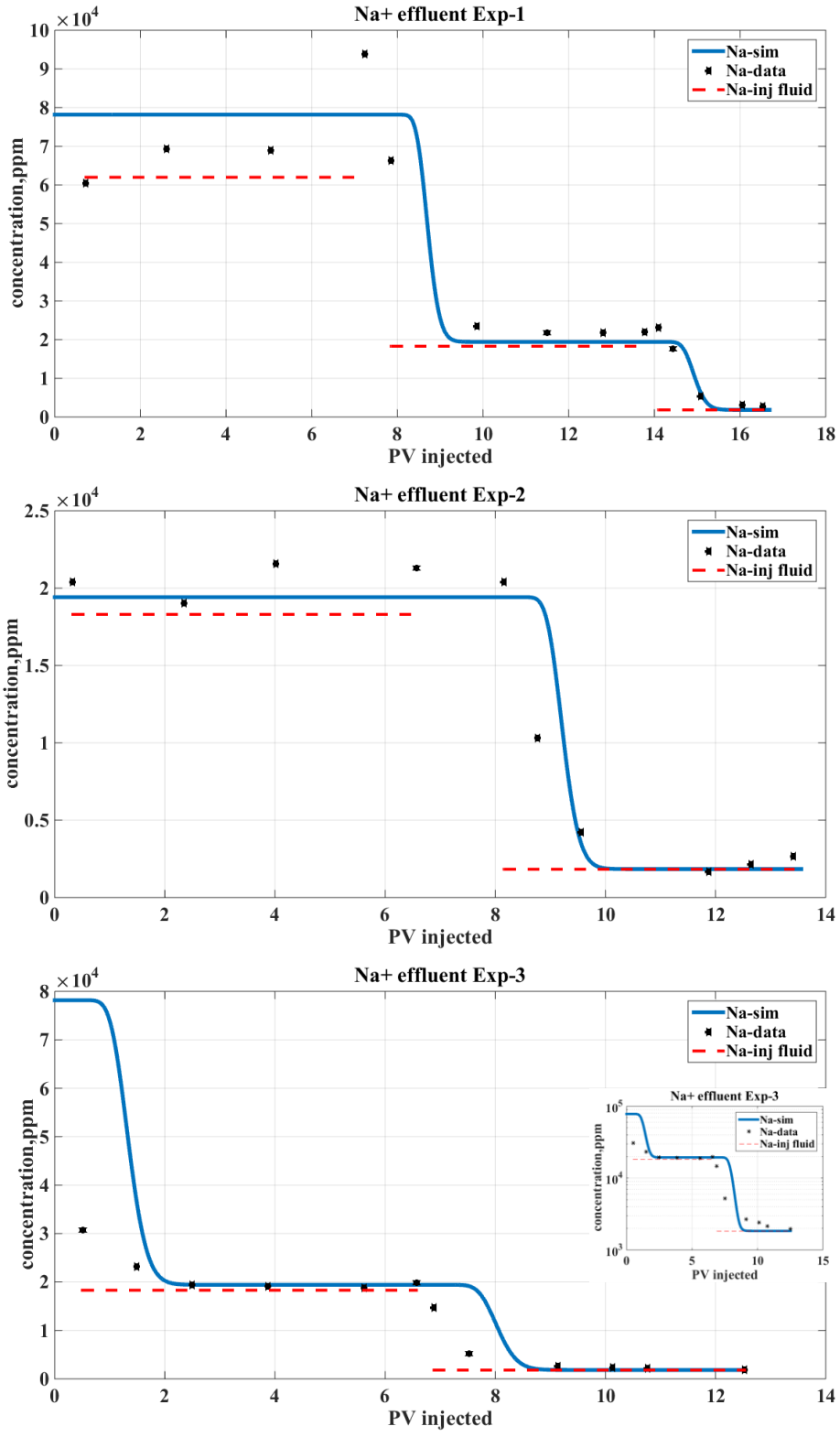

Figure 5.11 Na^+ ion matching of Experiments

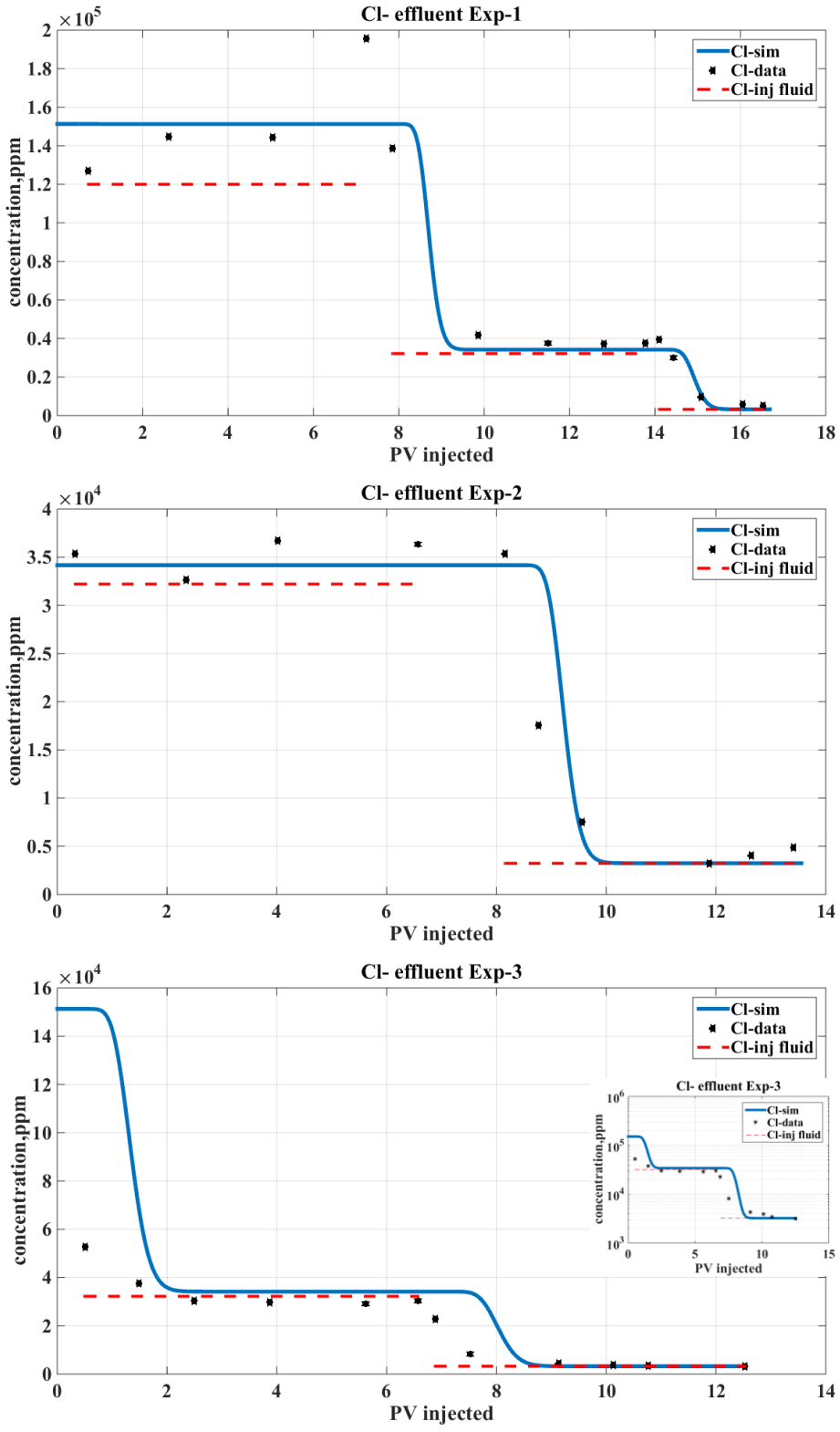

Figure 5.12 Cl^- ion matching of Experiments

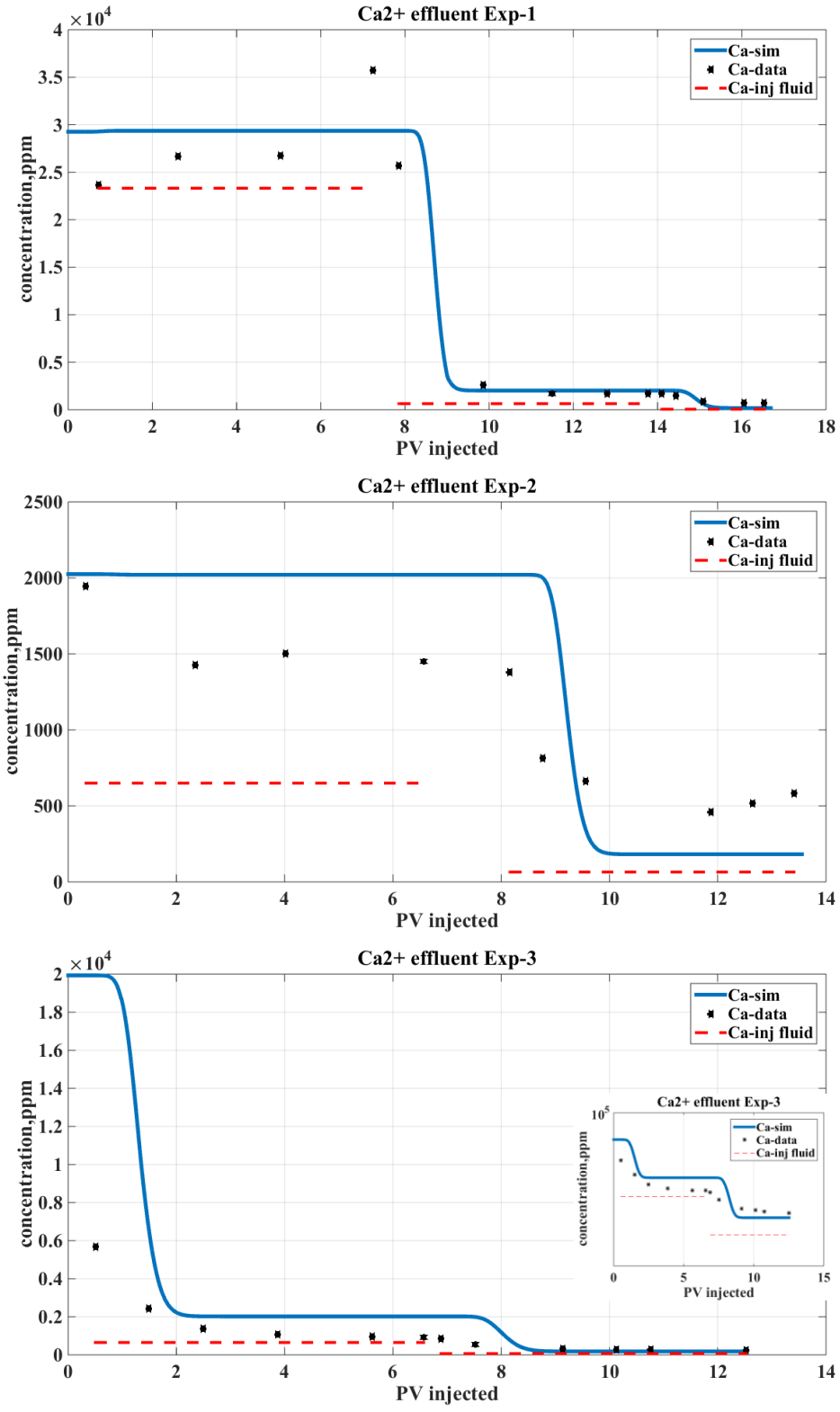

Figure 5.13 Ca^{2+} ion matching of Experiments

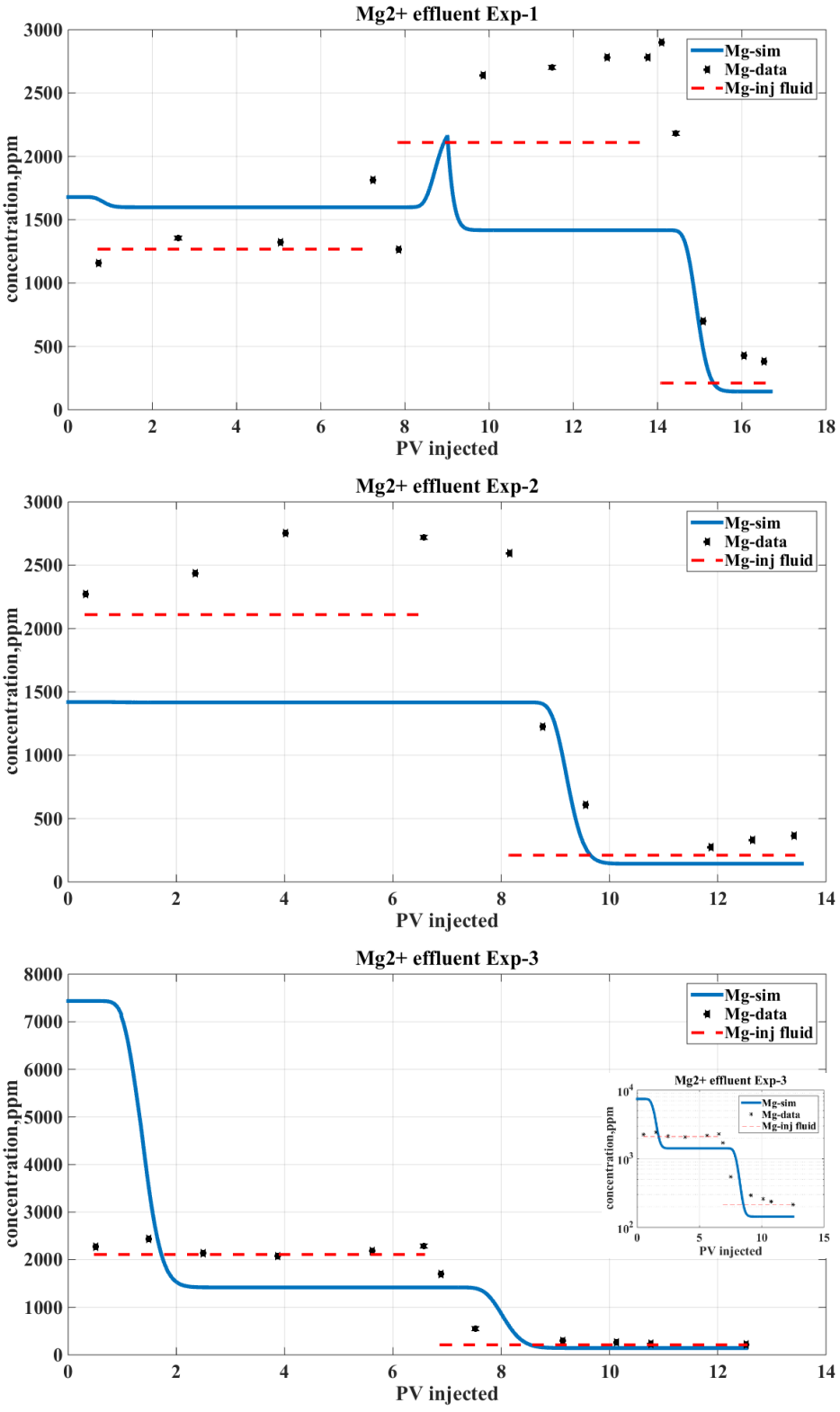

Figure 5.14 Mg2+ ion matching of Experiments

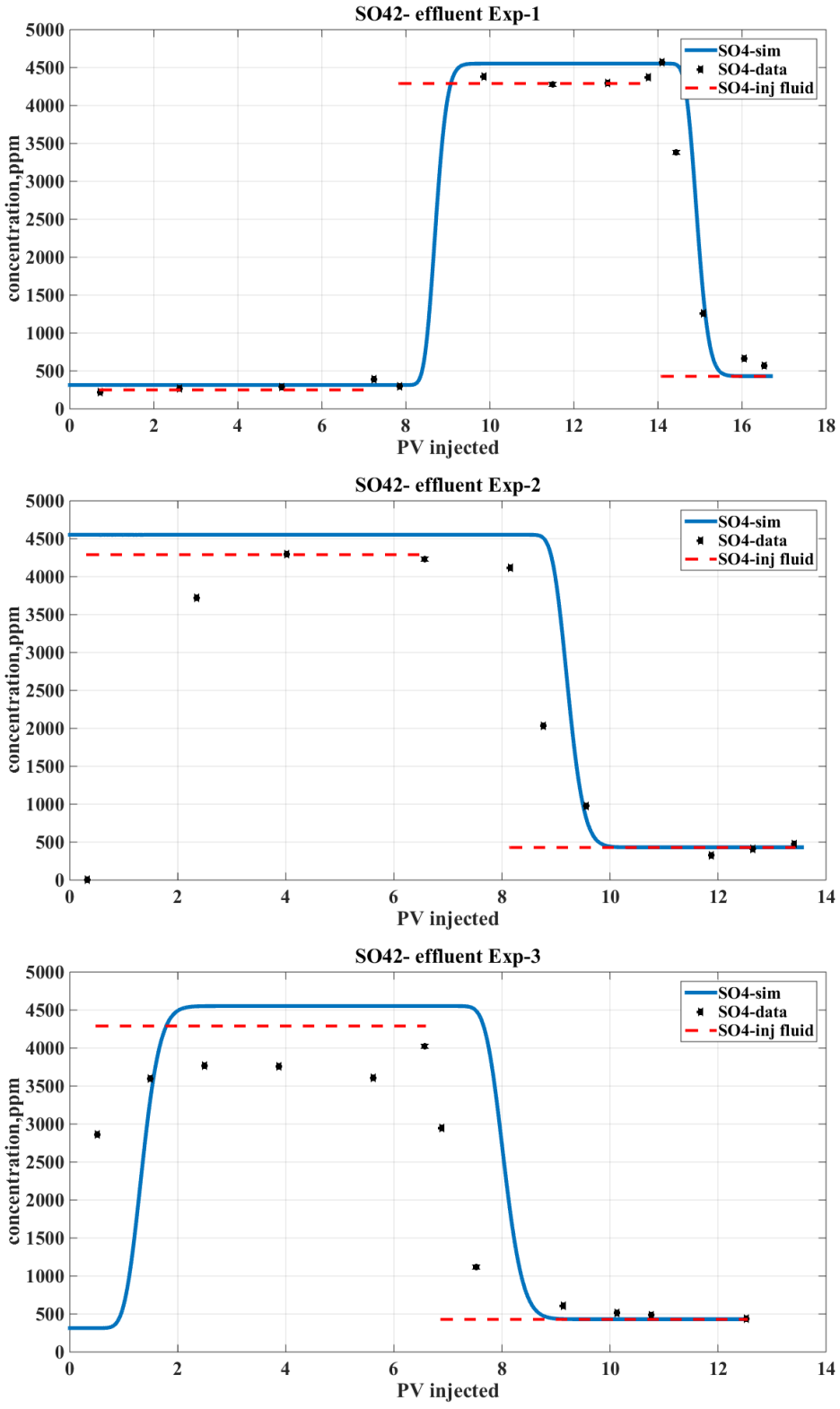

Figure 5.15 SO_4^{2-} ion matching of Experiments

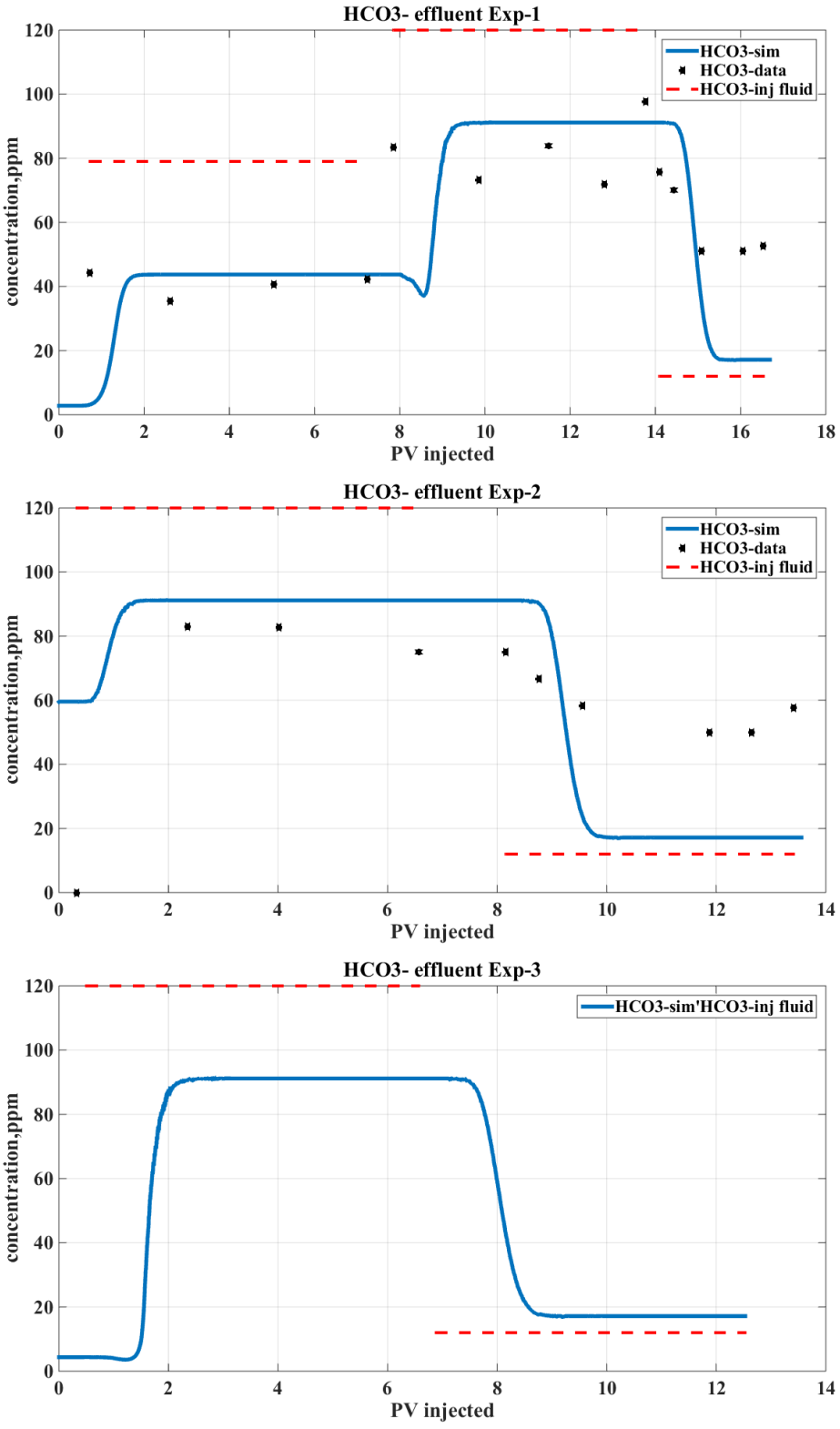

Figure 5.16 HCO_3^- ion matching of Experiments

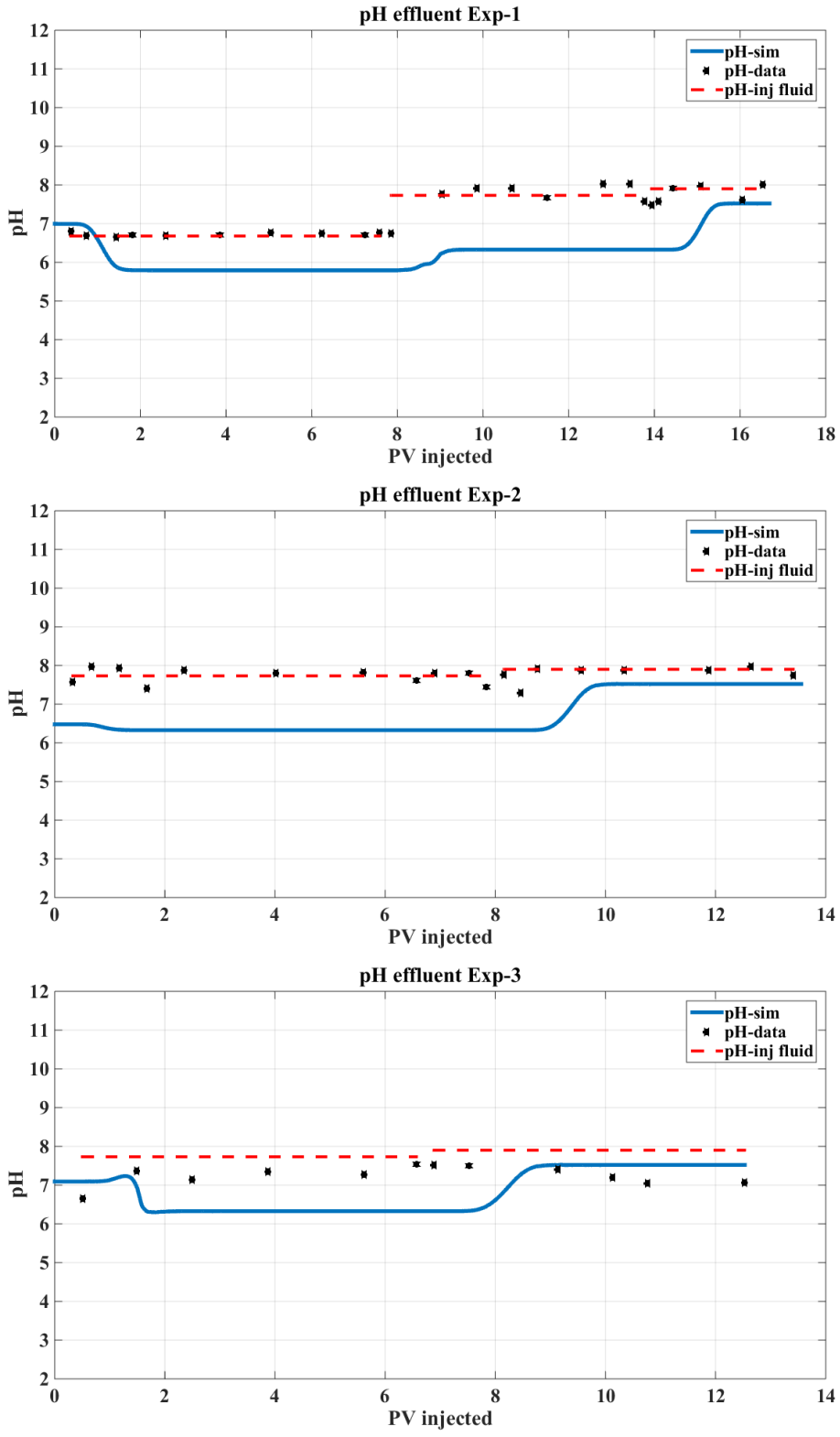

Figure 5.17 effluent pH matching of Experiments

5.4.2 Discussion on Smart water Flooding Mechanism

Based on effluent matching in coupling BL-IPhreeqc simulation, factors that contribute during Ca^{2+} and HCO_3^- ions matching are degree of mixing/ dispersivities, aqueous mineral equilibrium where dissolution and precipitation are taking place and surface adsorption model.

Dispersivities behavior occurred during fluids mixing in coreflooding experiments. Effluent profiles have shown during period of switching to different brine, that each ion is dispersed. Degree of dispersion during history matching is modeled by adjusting number of simulation grids. By doing so, numerical dispersion will represent physical dispersion due to the fluids interactions.

During aqueous-mineral equilibrium, calcite mineral dissolves in certain level to equilibrate with calcium and bicarbonate ion in the solution while dolomite mineral precipitates to equilibrate with calcium, magnesium and bicarbonate ion in the solution. Even though dissolution and precipitation are taking place, the equilibrium of aqueous and mineral are kept as indicated from level of saturation index of minerals in figure 5.18. Amount of calcite in the system of all experiments is large enough to compensate this process while amount of dolomite is not sufficient for experiment-1 which make it dissolves at early part during formation brine injection as shown in molarity of minerals in figure 5.19. Physically, the differences in the dry weight of cores before and after coreflooding that are shown in tables 4.1 to 4.3 might indicate minor dissolution during smart water flooding, although NMR tests show close result before and after experiments.

In order to maintain the ions balance during history matching especially Ca^{2+} and HCO_3^- ions, surface adsorption on minerals should be introduced in simulation model. Lowering calcium concentration during smart water/ low salinity injections causes retardation profile in calcium ion effluent that prevents this ion to follow level of calcium ion in injection fluids. Furthermore, this retardation process in Ca^{2+} and HCO_3^- ions is supported by the adjustment variable of calcite and dolomite surface site such as surface density and moles of the sites. Adsorption of bicarbonate ion onto positive surface charged.site of calcite and dolomite makes the surface sites more negatively charged, while adsorption of calcium ion into negative surface charged.site of calcite and dolomite makes the surface sites more positively charged. These variables are controlling the matching of Ca^{2+}, Mg^{2+} and HCO_3^- ions.

This adsoption process actually act as an inhibitor of calcite or dolomite dissolution. Since dissolution process most likely contributed less in these experiment, thus adsoption processes become dominant in this smart water flooding behavior particularly in these coreflooding experiments. In addition, the magnitude of adsorption is strongly depend on chemical/physical properties of organic anion present in the oil [47]. Studies at fatty acid and polycarboxilates [16, 18, 56] demonstrated that the magnitude of adsorption increases with increasing chain length because decreasing water solubility forces the molecules to escape from the water. On the other hand, a low number of functional group of the organic molecule in oil (short chain fatty acid) work against adsorption. This is relevant with the experiment results that showed less gain during smart water flooding in contact with dead oil system than live oil shown in Yousef et al. [52].

Meanwhile the other ions such as Na^+ and Cl^- behave like a passive tracer as they did not affect the results of geochemical simulation. SO_4^{2-} ion also followed the level of injection fluid as anhydrite did not present in mineralogy of carbonate cores in this study.

It can be concluded that smart water injections in Indiana limestone carbonate rock will triggers mineral dissolution and precipitation during aqueous-mineral equilibrium, and surface adsorption mechanisms.

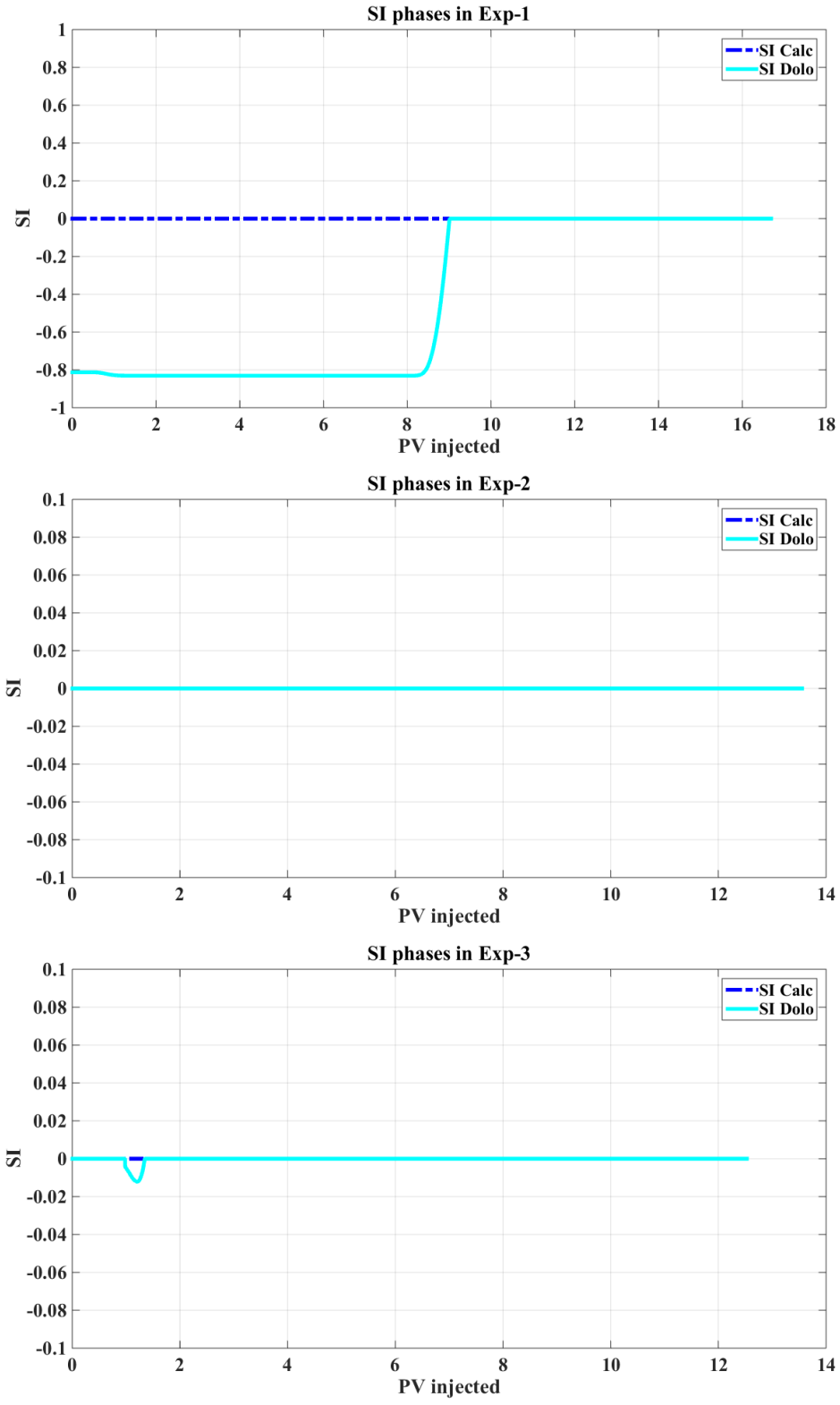

Figure 5.18 Saturation Index of Minerals of Experiments 1 to 3

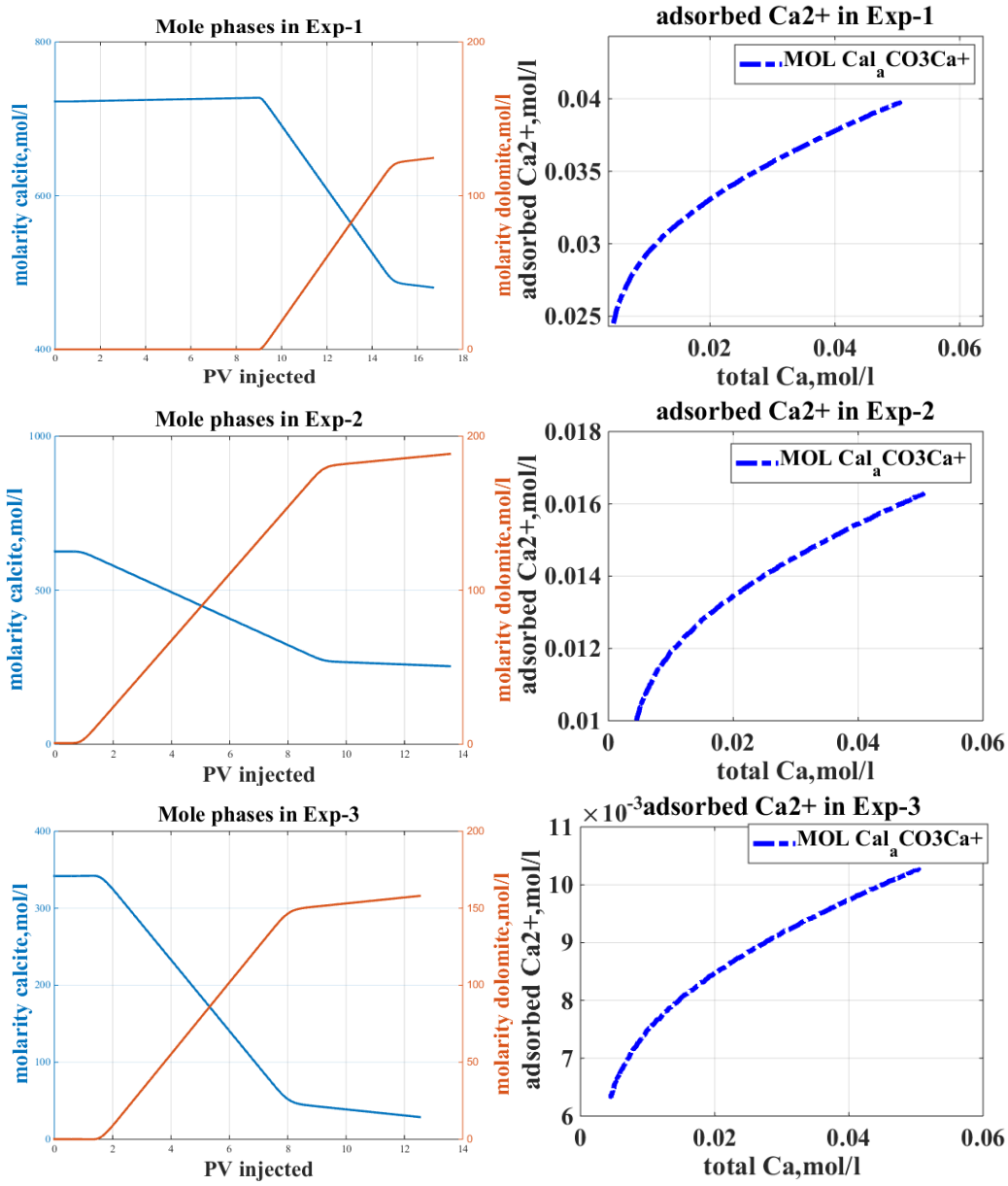

Figure 5.19 Moles of Minerals and Calcium adsorbed in Calcite site to total Calcium ion of Experiments 1 to 3

CHAPTER 6

CONCLUSIONS AND RECOMMENDATIONS

Smart water/ low salinity flooding shows additional recovery in Indiana limestone cores used in this study. Several conclusions and recommendations can be drawn from experimental and simulation model investigations are as follows.

6.1 Conclusions

Based on experimental works mainly designed unsteady state coreflooding,

- Preparations and analysis of experimental criteria show that the two sets of composite cores used in this study are quite homogenous as shown by CT Scan and Huppler criteria (F = 0.025), and rate selection of 0.5 cc/minute also fulfilled Rapoport and Leas, and Lake scaling number.
- A new approach for determining reliable relative permeabilities for smart water/low salinity brine flooding has been proposed and verified experimentally.
- Effluent profiles of core flooding experiments (pH, electric conductivity, anions and cations) show a stabilization period just before each brine switching which indicate steady behavior for reliable coreflooding results.
- Additional gain of 2-4% of oil recovery during smart water flooding (10x diluted seawater) are shown in all experiments.
- Calcium and bicarbonate ions show indication of Smart water flooding behavior since these ions showed relatively large ion profile's gap during 10x diluted seawater.

- Concept of lower salinity brine injection in first injection sequence of all experiments shows shifted relative permeabilities towards more water wet as shown by normalized scale relative permeabilities.
- Good match of oil recovery during back calculation of Buckley Leverett equation confirms relative permeabilities generated from JBN method. These relative permeabilities of each sequence of experiments are used in the simulation modeling to match oil recovery and pressure drop.

Based on simulation works of PHREEQC and coupled BL-IPhreeqc,

- Coupled BL-IPhreeqc has been built based on integration of Buckley Leverett 1-D model, Ion/concentration transport model and PHREEQC's module (IPhreeqc). It has been validated with PHREEQC in 1-D transport model.
- History matching of coreflooding experiments in oil recovery show excellent matches while the pressure drops show acceptable results confirming that reliable relative permeabilities derived from JBN method is sufficient to conduct interpretation of valid data from unsteady state coreflooding experiment.
- History matching of anions and cations are conducted in Coupled BL-IPhreeqc as well. Fair results are obtained and indicate the importance of geochemical processes during history matching, mainly mineral-aqueous equilibrium, mixing/dispersion process and surface adsorption (surface complexation model). These processes are likely the mechanism during smart water flooding in this study.

6.2 Recommendations

In order to gain further insight, some additional aspects could be considered to understand the mechanism behind smart water flooding,

- The procedures of coreflooding should be the same for all conducted experiments to minimize the source of error in laboratory works. This study used different methods for establishment of Swi which resulted in different initial condition before coreflooding, the use of the same set of cores during coreflooding experiments is also more favorable.
- Insitu saturation monitoring might give additional important information during unsteady state coreflooding experiments whether capillary end effect is significant at the end of pieces of the cores.
- Further investigation in geochemical simulation is urgently needed, since mechanisms of smart water flooding indicate complex surface complexation model, aqueous and mineral in local equilibrium or even investigation of kinetics of minerals.

References

[1] Aladasani, A., Bai Boujun, and Wu, Y. (2012). Investigating Low Salinity Waterflooding Recovery Mechanisms in Carbonate Reservoirs. Paper – SPE 155560, presented at the SPE EOR Conference at Oil and Gas West Asia held in Muscat, Oman, 16-18 April.

[2] Al-Attar, H. H., Mahmoud, M.Y., Zekri, A.Y., Almehaideb, R., and Ghannam, M.; ”Low-salinity Flooding in a Selected Carbonate Reservoir: Experimental Approach”, *J Petrol Explor Prod Technol*, vol. 3:139–149, March 2013.

[3] Al Hashim, H.S., Al Yousef, H.Y., Arshad, A., Mohammadain, A.R., “Smart Water flooding of Carbonate Reservoirs: Core flooding Tests Using a New Approach for Designing Smart Water”, Paper 172815 presented at the SPE Middle East Oil & Gas Show and Conference, Manama, Bahrain, 8–-11 March 2015

[4] Al-Shalabi, E.W., Sepehrnoori, K., and Delshad, M. (2013). Mechanisms behind Low Salinity Water Flooding in Carbonate Reservoirs. Paper – SPE 165339, presented at the SPE Western Redional and AAPG Pacific Section Meeting, held in Monterey, California, USA, 19-25 April.

[5] Alsofi, M.A., and Yousef, A.A. (2013). Insight into Smart-Water Recovery Mechanism through Detailed History Matching of Coreflood Experiments. Paper – SPE 166035, presented at the SPE Reservoir Characterization and Simulation Conference and Exhibition held in Abu Dhabi, UAE, 16-18 Sept.

[6] Austad, T et al., (2010), “Chemical Mechanism of Low salinity Water Flooding in Sandstone Reservoirs”, SPE 129767, SPE IOR Symposium, Tulsa.

[7] Austad, T, (2008), "'Smart Water' for Enhanced Oil Recovery: A Comparison of Mechanisms in Carbonates and Sandstones", presentation at the FORCE seminar on Low Salinity, NPD, Stavanger.

[8] Buckley J, (2009), "Low Salinity Waterflooding - An Overview of Likely Mechanisms", on-line presentation.

[9] Buckley, S. and Leverett, M. (1942). Mechanism of Fluid Displacement in Sands. AIME, (146):107–116.

[10] Chen, A. L., Wood, A.C.,;"Rate Effects on Water-Oil Relative Permeability", *SCA 2001-19*.

[11] Cissokho, M., Boussour, S., Cordier, P., Bertin, H., and Hamon, G.; , "Low Salinity in Oil Recovery on Clayey Sandstone: Experimental Study," *PETROPHYSICS*, vol.51, no. 5, pp. 305-313, Oct. 2010.

[12] Dang, Q.T.C., Nghiem, X.L., Chen, Z. and Nguyen, P.Q. (2013). Modelling low salinity Waterflooding: Ion Exchange, Geochemistry and Wettability Alteration. Paper – SPE 166447, presented at the SPE Annual and Technical Conference and Exhibition held in New Orleans, Lousiana, USA, 30 Sept. -2 Oct.

[13] de Bruin BSc, W. J. (2012). Simulation of Geochemical Processes during Low Salinity Water Flooding by Coupling Multiphase Buckley-Leverett Flow to the Geochemical Package PHREEQC. http://repository.tudelft.nl/assets/uuid: 2d568014-8acb-4e8e-9d39-91c76f499a46/W.J._de_Bruin_-_MSc_Thesis.pdf.

[14] Fathi, J.S., and Austad, T. (2012). Water-Based Enhanced Oil Recovery (EOR) by "Smart Water" in Carbonate Reservoirs. Paper – SPE 154570, presented at the SPE EOR Conference at Oil and Gas West Asia held in Muscat, Oman, 16-18 April.

[15] Fjelde, I., Omekeh, V.A., and Sokama-Neuyam, A.Y. (2014). Low Salinity Waterflooding: Effect of Crude Oil Composition. Paper – SPE 169090, presented at the SPE Improved Oil Recovery Symposium held in Tulsa, Oklahoma, USA, 12-16 April.

[16] Fuerstenau, M. C., & Miller, J. D. (1967). The role of the hydrocarbon chain in anionic flotation of calcite. Trans. AIME, 238(2), 153-160.

[17] Fulcher, J. R. A., Ertekin, T., Stahl, C.D.;"Effect of Capillary Number and Its Constituents on Two-Phase Relative Permeability Curves", *Journal of Petroleum Technology*, February 1985.

[18] Geffroy, C., Foissy, A., Persello, J., & Cabane, B. (1999). Surface complexation of calcite by carboxylates in water. Journal of Colloid and Interface science, 211(1), 45-53.

[19] Gomaa, E.E. (2005).Reservoir Engineering. Jakarta: P.T. EOR Teknologi, Oil and Gas Consultations and Training.

[20] Grahame, D. (1947). Electrical Double-layer and the Theory of Electro Capillary.

[21] Hassan, A. M. (2015). Optimization of In-situ Generated CO2 Using Chelating Agents for EOR from Carbonate Reservoirs. King Fahd University of Petroleum and Minerals.

[22] Helmholtz-Zentrum Dresden-Rossendorf. (2001-2016). RES³T - Rossendorf Expert System for Surface and Sorption Thermodynamics. Retrieved from https://www.hzdr.de/db/RES3T.queryData.

[23] Helvig, O. S. (2013). Models for water flooding, imbibition and coupled fracture-matrix flow in a fractured reservoir. http://brage.bibsys.no/xmlui/bitstream/handle/11250/183567/Helvig.pdf?sequence=1

[24] Huppler, J. D.;"Waterflood Relative Permeabilities in Composite Cores", *JPT Forum*. SPE-AIME Esco Production Research Co. Houston. Tex.

[25] Jerauld, G.R., Lin, C.Y., Webb, K.J., and Seccombe, J.C. (2006). Modelling Low Salinity Waterflooding. Paper – SPE 102239, presented at the SPE Annual and Technical Conference and Exhibition held in San Antonio, Texas, USA, 24-27 Sept.

[26] Kamath, J., Meyer, R. F., Nakagawa, F. M., & Others. (2001). Understanding waterflood residual oil saturation of four carbonate rock types. Paper - SPE-71505-MS, presented at SPE Annual Technical Conference and Exhibition held in New Orleans, Louisiana, 30 Sept – 3 Oct.

[27] Kassim, O.M. (2012). The Role of Potential Determining Ions in Carbonate Rock-Seawater Interactions.

[28] Korrani, A.K.N., Jerrauld, G.R., and Sepehmoori, K. (2014). Coupled Geochemical-Based Modelling of Low Salinity Waterflooding. Paper – SPE 169115, presented at the SPE Improved Oil Recovery Symposium held in Tulsa, Oklahoma, USA, 12-16 April.

[29] Korrani, A.K.N. (2014). Mechanistic Modeling of Low Salinity Water Injection. Doctor of Philosophy. http://hdl.handle.net/2152/28472

[30] Lager, A., Webb, K.J., Black, C.J.J., Singleton, M., Sorbie, K.S. (2006), "Low Salinity Oil Recovery – An Experimental Investigation", International Symposium of the Society of Core Analysts, Trondheim, Norway, 12th -16th September 2006.

[31] Lee, S.Y., Webb, K.J., Collins, I.R., Lager, A., Clarke, S.M., O'Sullivan, M., Routh, A.F., Wang, X. (2010) "Low Salinity Oil Recovery – Increasing Understanding of the Underlying Mechanisms", SPE 129722. SPE IOR Symposium, Tulsa.

[32] Ligthelm, D. et al., (2009), "Novel Waterflooding Strategy by Manipulation of Injection Brine Composition", SPE 119835, SPE EUROPEC/EAGE Annual Conference and Exhibition held in Amsterdam.

[33] Masalmeh, K.S., Sorop, G.T., Suijkerbuijk, M.J.M.B., Vermolen, M.C.E., and Douma, S. (2014). Low Salinity Flooding: Experimental Evaluation and Numerical Interpretation. Paper – IPTC 17558, presented at the IPTC held in Doha, Qatar, 20-22 January.

[34] Meling, T.T. (2013). Geochemical modeling of low salinity core flooding. University of Stavanger. http://brage.bibsys.no/xmlui/bitstream/handle/ 11250/183516/Meling.pdf ?sequence=1.

[35] Mohanty, K. K.,; ,"Impact of Capillary and Bond Numbers on Relative Permeability, " *University of Houston*, January 1999.

[36] Morrow, N.R., Zhang, Y., Thomas, C.P., Robertson, E.P.; ,"Improved Waterflooding through Injection-Brine Modification," *Idaho National Engineering and Environmental Laboratory*, EXT-02-01591, 2003.

[37] Nasralla, R.A., Batawel, M.A., Nasr-El-Din, H.A. (2011b), "Investigation of Wettability Alteration by Low Salinity Water in Sandstone", SPE 146322.

[38] Nasralla, R.A., Nasr-El-Din, H.A. (2012), "Double-layer Expansion: Is it a Primary Mechanism of Improved Oil Recovery by Low-Salinity Waterflooding?", SPE 154334.

[39] Omekeh, A., Friis, A.H., Fjelde, I., and Evje, S. (2012). Modelling of Ion-Exchange and Solubility in Low Salinity Waterflooding. Paper – SPE 154144, presented at the SPE Improved Oil Recovery Symposium held in Tulsa, Oklahoma, USA, 14-18 April.

[40] Parkhurst, D. L., and Appelo, C. A. J. 1999. User's guide to PHREEQC (Version 2): A computer program for speciation, batch-reaction, one-dimensional transport, and inverse geochemical calculations.

[41] Pu, H., Xie, X., Yin, P., Morrow, N.R. (2010), "Low Salinity Waterflooding and Mineral Dissolution", SPE 134042.

[42] Qiao, C., Johns, R.T., Li, L., and Xu, J. (2014). A Mechanistic Model for Wettability Alteration by Chemically Tuned Waterflooding in Carbonate Reservoirs. Paper – SPE 170966, presented at the SPE Annual and Technical Conference and Exhibition held in Amsterdam, Netherland, 27-29 Oct.

[43] Rapoport, L. a., & Leas, W. J. (1953). 213-G - Properties of Linear Waterfloods. Journal of Petroleum Technology, 5(5), 139–148. http://doi.org/10.2118/213-G

[44] Skauge, a, Thorsen, T., & Sylte, a. (2001). Rate selection for waterflooding of intermediate wet cores. Proceedings of the International Symposium of the Society of Core Analysts, Edinburgh, Scotland, 17, 2001–2020.

[45] Tang G and Morrow N, (1999b), "Influence of Brine Composition and Fines Migration on Crude Oil/Brine/Rock Interactions and Oil Recovery", Proceedings of the 5th International Symposium on Evaluation of Reservoir Wettability and its Effect on Oil Recovery, Trondheim, Norway, June1998, and published in J Pet. Sci. Eng, 24: 99-111.

[46] Pakoz, U. (2015). Effect of Changing Injection brine Salinity on Oil Recovery from Oil Wet Carbonate Rocks. The Pennsylvania State University. https://etda.libraries.psu.edu/paper/27292/31161.

[47] Somasundaran, P. (2006). *Encyclopedia of surface and colloid science* (Vol. 2). CRC press.

[48] Van Olphen, H. (1977). Introduction to Clay Colloid Chemistry. New York, 2nd edition.

[49] Webb, K., Lager, A., and Black, C. (2008). Comparison of High/Low Salinity Water/Oil Relative Permeability. SCA2008-39, prepared for presentation at the International Symposium of the Society of Core Analysts held in Abu Dhabi, UAE, 29 Oct-2 Nov.

[50] Wu, Y.S., and Bai, B. (2009). Efficient Simulation for Low-Salinity Waterflooding in Porous and Fractured Reservoirs. Paper – SPE 118830, presented at the SPE Reservoir Simulation Symposium held in Woodlands, Texas, USA, 2-4 Feb.

[51] Yildiz, O.H., and Morrow, R.N.; ,"Effect of Brine Composition on Recovery of Moutray Crude Oil by Waterflooding," *Journal of Petroleum Science and Engineering*, vol.14, pp.159-168, 1996.

[52] Yousef, A. A., Al-Saleh, S., Al-Kaabi, A., and Al-Jawfi, M. (2010). Laboratory Investigation of the Impact of Injection-Water Salinity and Ionic Content on Oil Recovery from Carbonate Reservoirs. Paper ―SPE 137634, presented at the SPE Canadian Unconventional Resources and International Petroleum Conference held in Calgary, Canada, 19-21 Oct.

[53] Zekri, Y.A., Nasr, M., and Al-Arabai, Z. (2011). Effect of EOR technology on Wettability and Oil Recovery of Carbonate and Sandstone Formation. Paper – IPTC 14131, presented at the IPTC held in Bangkok, Thailand, 7-8 February.

[54] Zelnijahromi, A., Borazjani, S., Bedrikovetsky, P., and Rodrigues, T. (2014). Low Salinity Fines-Assisted Water-flood: Analytical Modelling and Reservoir Simulation. Paper – SPE 1714481, presented at the SPE Asia Pacific Oil and Gas Conference and Exhibition held in Adelaide, Australia, 14-16 Oct.

[55] Zhu, C., & Anderson, G. (2002). Environmental Applications of Geochemical Modeling, 302. http://doi.org/10.1017/CBO9780511606274.

[56] Zullig, J.J.: Morse. J.W. Interaction of organic acids with mineral surfaces in seawater and related solutions: I fatty acids adsorption. Gcochim. Cosmochim. Acta 1988. 52. 1667-1678.

APPENDICES

A. All Experiments Data Results

Table A.7.1 Experiment-1 Data

Fluid Injected	PV injected	Oil Recovery,%	dP, psia	pH	Na, ppm	Ca, ppm	Mg, ppm	Cl, ppm	SO4, ppm
formation brine	0.041	5%	7.656						
	0.200	25%	9.00						
	0.375	30%	8.92	6.8					
	0.553	32%	7.83						
	0.732	35%	7.13	6.69	60484	23674	1157	126906	217
	0.909	37%	6.63						
	1.089	38%	6.26						
	1.268	39%	5.95						
	1.445	41%	5.70						
	1.621	42%	5.49						
	1.805	42%	5.30	6.7					
	1.977	43%	5.14						
	2.142	44%	5.00						
	2.311	44%	4.87						
	2.480	44%	4.76	6.69	69360	26705	1357	144737	271
	2.656	45%	4.65						
	2.825	45%	4.56						
	3.000	45%	4.47						
	3.175	46%	4.39						
	3.344	46%	4.31						
	3.519	46%	4.24						
	3.685	46%	4.17						
	3.852	47%	4.11	6.7					
	4.017	47%	4.05						
	4.187	47%	4.00						
	4.362	47%	3.95						
	4.531	48%	3.90						
	4.700	48%	3.85						
	4.870	48%	3.80						
	5.039	48%	3.76	6.76	69050	26718	1324	144485	289
	5.214	49%	3.72						
	5.387	49%	3.68						

	5.552	49%	3.64						
	5.724	49%	3.61						
	5.893	49%	3.57						
	6.064	49%	3.54						
	6.233	49%	3.51						
	6.403	49%	3.48						
	6.574	49%	3.45						
	6.739	50%	3.42						
	6.908	50%	3.39	6.74					
	7.076	50%	3.36						
	7.241	50%	3.34	6.71	93949	35712	1812	195502	389
	7.412	50%	3.31						
	7.582	50%	3.29	6.77					
seawater	7.679	50%	3.86						
	7.854	50%	3.53	6.75	66381	25664	1267	138807	297
	8.027	50%	3.35						
	8.194	50%	3.23						
	8.366	50%	3.14						
	8.535	50%	3.07						
	8.700	50%	3.01						
	8.875	51%	2.95						
	9.035	51%	2.91	7.76					
	9.196	51%	2.87						
	9.358	51%	2.84						
	9.523	51%	2.80						
	9.688	51%	2.78						
	9.854	51%	2.75	7.92	23550	2568	2639	41665	4382
	10.023	51%	2.72						
	10.192	52%	2.70						
	10.358	52%	2.68						
	10.517	52%	2.66						
	10.677	52%	2.64	7.92					
	10.840	52%	2.63						
	11.000	52%	2.61						
	11.159	52%	2.59						
	11.329	52%	2.58						
	11.498	52%	2.56	7.67	21863	1734	2702	37514	4283
	11.655	52%	2.55						
	11.821	52%	2.54						
	11.976	52%	2.53						

	12.146	52%	2.51						
	12.309	52%	2.50						
	12.474	52%	2.49						
	12.634	52%	2.48						
	12.799	52%	2.47	8.02	21796	1718	2780	37309	4300
	12.961	52%	2.46						
	13.118	52%	2.45						
	13.278	52%	2.44						
	13.437	52%	2.43	8.02					
	13.605	52%	2.43						
	13.766	52%	2.42	7.58	21901	1674	2784	37500	4374
10x Diluted seawater	13.934	53%	3.04	7.48					
	14.099	53%	2.77	7.58	23068	1682	2899	39277	4574
	14.266	53%	2.63						
	14.428	53%	2.53	7.91	17559	1449	2184	29832	3379
	14.597	53%	2.46						
	14.764	53%	2.40						
	14.926	53%	2.35						
	15.085	53%	2.31	7.98	5377.5	863	700	9561	1255.5
	15.243	53%	2.27						
	15.408	53%	2.24						
	15.564	53%	2.21						
	15.729	53%	2.19						
	15.895	53%	2.16						
	16.054	53%	2.14	7.62	3108.5	709	426	5705.5	666.5
	16.214	53%	2.12						
	16.375	53%	2.11						
	16.535	53%	2.09	8.01	2786	706	384.5	5123	569.5
	16.686	53%	2.07						

Table A.7.2 Experiment-2 Data

Fluid Injected	PV injected	Oil Recovery,%	dP, psia	pH	Na, ppm	Ca, ppm	Mg, ppm	Cl, ppm	SO4, ppm
Seawater	0.019	2%	4.53						
	0.171	22%	5.50						
	0.330	30%	4	7.58	20389	1948	2274	35328	1
	0.497	33%	2.92						
	0.664	36%	2.68	7.97					
	0.833	38%	2.49						
	1.002	40%	2.35						
	1.172	41%	2.23	7.94					
	1.343	42%	2.13						
	1.510	43%	2.05						
	1.677	44%	1.97	7.4					
	1.844	44%	1.91						
	2.018	45%	1.85						
	2.185	45%	1.80						
	2.352	46%	1.75	7.87	19025	1429	2434	32648	3717
	2.521	46%	1.70						
	2.688	47%	1.66						
	2.855	47%	1.63						
	3.022	48%	1.59						
	3.189	48%	1.56						
	3.356	48%	1.53						
	3.523	49%	1.51						
	3.689	49%	1.48						
	3.856	49%	1.46						
	4.020	50%	1.43	7.8	21586	1500	2753	36712	4295
	4.185	50%	1.41						
	4.346	50%	1.39						
	4.500	50%	1.37						
	4.660	51%	1.35						
	4.821	51%	1.34						
	4.975	51%	1.32						
	5.134	52%	1.30						
	5.287	52%	1.29						
	5.450	52%	1.27						
	5.604	52%	1.26	7.83					

	5.771	53%	1.24						
	5.928	53%	1.23						
	6.084	53%	1.22						
	6.251	53%	1.21						
	6.411	53%	1.19						
	6.570	53%	1.18	7.61	21285	1451	2717	36359	4230
	6.737	54%	1.17						
	6.904	54%	1.16	7.8					
	7.062	54%	1.15						
	7.219	54%	1.14						
	7.377	54%	1.13						
	7.527	54%	1.12	7.81					
	7.687	54%	1.11						
	7.843	54%	1.10	7.45					
	8.002	54%	1.10						
10x Diluted seawater	8.160	55%	2.85	7.77	20419	1378	2593	35367	4115
	8.314	55%	2.04						
	8.466	55%	1.91	7.3					
	8.614	55%	1.82						
	8.772	55%	1.76	7.91	10327	812.5	1228	17515.5	2036.5
	8.930	56%	1.70						
	9.084	56%	1.66						
	9.247	56%	1.63						
	9.406	56%	1.60						
	9.564	56%	1.57	7.87	4237.5	663	609	7532	975.5
	9.718	56%	1.54						
	9.876	56%	1.52						
	10.033	56%	1.50						
	10.191	56%	1.48						
	10.345	56%	1.47	7.88					
	10.495	56%	1.45						
	10.653	56%	1.44						
	10.811	56%	1.43						
	10.968	56%	1.41						
	11.126	56%	1.40						
	11.276	56%	1.39						
	11.419	56%	1.38						
	11.571	56%	1.37						
	11.721	56%	1.36						
	11.874	56%	1.35	7.87	1697.5	462	274.5	3178	329.5

	12.018	56%	1.34						
	12.176	56%	1.33						
	12.337	56%	1.33						
	12.491	57%	1.32						
	12.640	57%	1.31	7.98	2136	516.5	328.5	4054	406
	12.794	57%	1.30						
	12.952	57%	1.30						
	13.100	57%	1.29						
	13.254	57%	1.29						
	13.408	57%	1.28	7.74	2644	584.5	362.5	4856.5	477
	13.553	57%	1.27						

Table A.7.3 Experiment-3 Data

Fluid Injected	PV injected	Oil Recovery, %	dP, psia	pH	Na, ppm	Ca, ppm	Mg, ppm	Cl, ppm	SO4, ppm
Seawater	0.026	4%	4.60						
	0.189	28%	9.00						
	0.342	44%	7.00						
	0.504	48%	6.30	7.37	23110.5	2450	2435.5	37642	3603.5
	0.663	51%	6.00						
	0.792	52%	5.70						
	0.919	54%	5.40						
	1.045	55%	5.10						
	1.171	56%	4.80						
	1.346	56%	4.60						
	1.494	58%	4.40	7.37	23110.5	2450	2435.5	37642	3603.5
	1.645	58%	4.20						
	1.808	59%	3.99						
	1.968	60%	3.90						
	2.164	60%	3.82						
	2.294	61%	3.74						
	2.489	61%	3.67	7.15	19365.75	1360	2142.5	30420.5	3772.
	2.636	61%	3.60						
	2.793	62%	3.54						
	2.947	62%	3.48						
	3.117	62%	3.43						
	3.225	62%	3.38						

	3.404	62%	3.33						
	3.560	62%	3.29						
	3.715	63%	3.24						
	3.871	63%	3.20	7.35	19050.5	1062.7	2073.7	29692.2	3759.7
	4.031	63%	3.17						
	4.187	63%	3.13						
	4.343	63%	3.09						
	4.502	63%	3.06						
	4.665	63%	3.03						
	4.821	63%	3.00						
	4.977	64%	2.97						
	5.158	64%	2.94						
	5.300	64%	2.92						
	5.471	64%	2.89						
	5.611	64%	2.87	7.27	18800	950.75	2182.7	29154.5	3608.2
	5.773	64%	2.84						
	5.934	64%	2.82						
	6.091	64%	2.80						
	6.256	64%	2.78						
	6.408	64%	2.75						
	6.566	64%	2.73	7.55	19779	941	2289.5	30380.2	4021
10x Diluted seawater	6.726	64%	3.00						
	6.886	64%	3.50	7.52	14710.5	842.75	1704.5	22675.2	2950.7
	7.035	64%	4.00						
	7.199	64%	4.96						
	7.351	65%	5.05						
	7.522	65%	5.11	7.50	5246.6	536.4	547	8243.7	1114
	7.674	65%	5.03						
	7.841	65%	4.96						
	8.001	65%	4.89						
	8.164	65%	4.82						
	8.334	66%	4.75						
	8.484	66%	4.68						
	8.640	66%	4.62						
	8.810	66%	4.55						
	8.975	66%	4.49						
	9.140	66%	4.43	7.41	2696.55	314.85	292.1	4299.8	606.75
	9.349	66%	4.37						
	9.451	66%	4.32						
	9.639	66%	4.27						

	9.840	67%	4.21						
	9.934	67%	4.17						
	10.125	67%	4.12	7.21	2399.05	286.7	259.65	3885.9	510.05
	10.323	68%	4.07						
	10.427	68%	4.03						
	10.587	68%	3.99						
	10.761	68%	3.95	7.04	2136.15	267.15	236.15	3407.75	485.05
	10.908	68%	3.91						
	11.092	68%	3.87						
	11.226	68%	3.84						
	11.379	69%	3.81						
	11.535	69%	3.78						
	11.751	69%	3.75						
	11.886	69%	3.72						
	12.016	69%	3.70						
	12.218	69%	3.68						
	12.360	69%	3.66						
	12.525	69%	3.64	7.07	1953.225	239.75	215.07	3119.95	436.55

B. Key methods for IPhreeqc modules

Method	Function
LoadDatabase(*FileName*)	Reads the database from the specified file
LoadDatabaseString(*Input*)	Reads the database from the input string
AccumulateLine(*String*)	Append the input string to the input buffer for the module
RunAccumulated()	Runs PHREEQC based on the input buffer defined by calls to **AccumulateLine**
RunFile(*FileName*)	Runs PHREEQC based on the input in the specified file
RunString(*InputString*)	Runs PHREEQC based on the specified input string
GetSelectedOutputArray()	Returns an array with the selected-output results from the last run (**RunAccumulated**, **RunFile**, or **RunString**). (This method is available only in the COM module)
GetSelectedOutputValue(*Row*, *Column*)	Returns the value from the specified row and column of the selected-output array, which contains results from the last run (**RunAccumulated**, **RunFile**, or **RunString**)
GetDumpString()	Returns a string containing the output as defined by the DUMP data block of the last **RunAccumulated**, **RunFile**, or **RunString** command

C. Example Input for Matlab of Coupled BL-IPhreeqc

```
Experiment-3
#################################################################
SOLUTION 1-30 Initial formation brine solution in column
      units            ppm
      # density   1.149
      temp             100.0
      Na 62333; Cl 131303; Mg 1191; Ca 24200; S(6) 271; C(4) 52.94 as
HCO3
end
EQUILIBRIUM_PHASES 1-30
      Calcite     0     341.24
      Dolomite    0     0.3925
end

SURFACE_MASTER_SPECIES
Cal_a Cal_aCO3H
Cal_b Cal_bCaOH
Dolo_a Dolo_aCO3H
Dolo_b Dolo_bCaOH
Dolo_c Dolo_cMgOH

SURFACE_SPECIES
Cal_aCO3H  = Cal_aCO3H
-log_k 0.0
Cal_aCO3H + Ca+2 = Cal_aCO3Ca+ + H+
-log_k 2.8

Cal_bCaOH = Cal_bCaOH
-log_k 0.0
Cal_bCaOH + CO2 = Cal_bCaHCO3
-log_k -6.0
Cal_bCaOH + CO2 = Cal_bCaCO3- + H+
-log_k 2.6
Cal_bCaOH + CO3-2 + H+ = Cal_bCaCO3- + H2O
-log_k -17.1
Cal_bCaOH + CO3-2 + 2H+ = Cal_bCaHCO3 + H2O
-log_k -23.5

Dolo_aCO3H  = Dolo_aCO3H
-log_k 0.0
Dolo_aCO3H + Ca+2 = Dolo_aCO3Ca+ + H+
-log_k 1.8
Dolo_aCO3H + Mg+2 = Dolo_aCO3Mg+ + H+
-log_k 2.0

Dolo_bCaOH = Dolo_bCaOH
-log_k 0.0
Dolo_bCaOH + CO3-2 + H+ = Dolo_bCaCO3- + H2O
-log_k -16.6
Dolo_bCaOH + CO3-2 + 2H+ = Dolo_bCaHCO3 + H2O
-log_k -24.0
```

```
Dolo_cMgOH = Dolo_cMgOH
-log_k 0.0
Dolo_cMgOH + CO3-2 + H+ = Dolo_cMgCO3- + H2O
-log_k -15.4
Dolo_cMgOH + CO3-2 + 2H+ = Dolo_cMgHCO3 + H2O
-log_k -23.5

SURFACE 1-30
-equilibrate 1-30
Cal_aCO3H 5 2.4 1
Cal_bCaOH 5 1.7 1
Dolo_aCO3H 8 2.8 1
Dolo_bCaOH 8 2.8 1
Dolo_cMgOH 8 2.8 1
end
#####################################################################
SOLUTION 31 #Seawater Displacement
      units            ppm
      # density   1.037
      temp            100
      Na 18300; Cl 32200; Mg 2110; Ca 650; S(6) 4290; C(4) 120 as HCO3
END


#####################################################################
SOLUTION 32 #10xDiluted Seawater Displacement
      units            ppm
      # density   1.037
      temp            100
      Na 1830; Cl 3220; Mg 211; Ca 65; S(6) 429; C(4) 12 as HCO3
END
```

Vitae

Name	:Bramasto Cinde Adam
Nationality	:Indonesian
Date of Birth	:February 5th, 1989
Email	:adam_bramasto@yahoo.com
Address	:Diponegoro No. 55, Klaten, Central Java.
Academic Background	:M.Sc. in Petroleum Engineering, May 2016
	College of Petroleum and Geosciences
	King Fahd University of Petroleum & Minerals
	Saudi Arabia.
	B.Sc. in Petroleum Engineering, August 2009
	Department of Petroleum Engineering
	Faculty of Mining and Petroleum Engineering
	Institut Teknologi Bandung
	Indonesia.